

Brill-Noether-general Limit Root Bundles: Absence of vector-like Exotics in F-theory Standard Models

Martin Bies^{1,2}, Mirjam Cvetič^{1,2,3,4}, Ron Donagi^{2,1}, Marielle Ong²

¹*Department of Physics and Astronomy, University of Pennsylvania,
Philadelphia, PA 19104-6396, USA*

²*Department of Mathematics, University of Pennsylvania,
Philadelphia, PA 19104-6396, USA*

³*Center for Applied Mathematics and Theoretical Physics, University of Maribor,
Maribor, Slovenia*

⁴*CERN Theory Department, CH-1211 Geneva, Switzerland*

Root bundles appear prominently in studies of vector-like spectra of 4d F-theory compactifications. Of particular importance to phenomenology are the Quadrillion F-theory Standard Models (F-theory QSMs). In this work, we analyze a superset of the physical root bundles whose cohomologies encode the vector-like spectra for the matter representations $(\mathbf{3}, \mathbf{2})_{1/6}$, $(\overline{\mathbf{3}}, \mathbf{1})_{-2/3}$ and $(\mathbf{1}, \mathbf{1})_1$. For the family $B_3(\Delta_4^\circ)$ consisting of $\mathcal{O}(10^{11})$ F-theory QSM geometries, we argue that more than 99.995% of the roots in this superset have no vector-like exotics. This indicates that absence of vector-like exotics in those representations is a very likely scenario.

The QSM geometries come in families of toric 3-folds $B_3(\Delta^\circ)$ obtained from triangulations of certain 3-dimensional polytopes Δ° . The matter curves in $X_\Sigma \in B_3(\Delta^\circ)$ can be deformed to nodal curves which are the same for all spaces in $B_3(\Delta^\circ)$. Therefore, one can probe the vector-like spectra on the entire family $B_3(\Delta^\circ)$ from studies of a few nodal curves. We compute the cohomologies of all limit roots on these nodal curves.

In our applications, for the majority of limit roots the cohomologies are determined by line bundle cohomology on rational tree-like curves. For this, we present a computer algorithm. The remaining limit roots, corresponding to circuit-like graphs, are handled by hand. The cohomologies are independent of the relative position of the nodes, except for a few circuits. On these *jumping circuits*, line bundle cohomologies can jump if nodes are specially aligned. This mirrors classical Brill-Noether jumps. $B_3(\Delta_4^\circ)$ admits a jumping circuit, but the root bundle constraints pick the canonical bundle and no jump happens.

Contents

1. Introduction	3
2. Partial blowup limit root line bundles	7
2.1. Vector-like spectra in F-theory	7
2.2. Limit root bundles in the F-theory QSMs	8
2.3. Triangulation independence in the QSM geometries	9
2.4. The need for partial blowup limit root bundles	10
2.5. Beyond full blowup limit roots	11
3. Line bundle cohomology on tree-like, rational curves	14
3.1. Simplifying the tree	14
3.2. Global sections on terminal trees	16
3.3. Final algorithm	19
4. Towards Brill-Noether theory of limit root line bundles	19
4.1. The geometric multiplicity	20
4.2. Errata, corrections and immediate extensions of earlier work	21
4.3. Statistics of partial blowup limit roots in QSM geometries	22
5. $\mathcal{O}(10^{11})$ F-theory QSM without vector-like quark-doublets	25
5.1. Stationary circuits	26
5.2. Jumping circuit	28
5.3. Towards absence of vector-like exotics	31
6. Conclusion and Outlook	32
A. Speciality	38
B. Counts of partial blowup limit roots	42
B.1. Spaces with $\overline{K}_{B_3}^3 = 6$	43
B.2. Spaces with $\overline{K}_{B_3}^3 = 10$	44
C. Stationary circuits in $\mathcal{O}(10^{11})$ F-theory QSMs	51
D. Jumping circuit in $\mathcal{O}(10^{11})$ F-theory QSMs	54
D.1. Ray generators	55
D.2. Vanishing intersections and approximation of Stanley-Reisner ideal	57
D.3. The nodal curve	61
D.4. The location of the nodes	63

1. Introduction

String Theory is a leading candidate for a unified theory of quantum gravity since it elegantly couples gauge dynamics to gravity. In particular, all aspects of our physical reality, including the observed low energy particle physics, must be accounted for by String Theory. Above all, an explicit demonstration of the Standard Model from String Theory is desired.

Enormous efforts have been undertaken in this regard with perturbative String Theory such as the $E_8 \times E_8$ heterotic string [1–8] or intersecting branes models in type II [9–15] (see also [16] and references therein). These String Theory compactifications were among the first from which the Standard Model gauge sector emerged with its chiral or, in the case of [4, 5], vector-like spectrum. Typically, these perturbative models suffer from chiral and vector-like exotic matter. The first efforts to overcome this hurdle and provide a globally consistent MSSM construction from String Theory are [4, 5] (see [17, 18] for more details on the subtle global conditions for slope-stability of vector bundles).

A non-perturbative extension of type IIB String Theory must describe the gauge dynamics on 7-branes *including* their back-reactions (to all orders in the string coupling) onto the compactification geometry B_n . This is achieved elegantly in F-theory [19–21]. Namely, the back-reactions in question are encoded in the geometry of an elliptically fibered Calabi-Yau space $\pi: Y_{n+1} \rightarrow B_n$. Such a space Y_{n+1} can be investigated with well-established tools of algebraic geometry. This allows to study and satisfy the global consistency conditions of the physics in $10 - 2n$ non-compact dimension. For a modern overview of the recent developments towards connecting F-theory and the Standard Model, we point the interested reader to [22].

An important signature of the observed particle physics is the chiral fermionic spectrum. A realistic 4d $\mathcal{N} = 1$ F-theory compactifications (i.e., $n = 3$) must therefore reproduce this spectrum. From the F-theory perspective, it is uniquely determined by a background gauge flux. The latter can be conveniently specified by the internal C_3 profile in the dual M-theory geometry. Importantly, the chiral spectrum of the F-theory compactification only depends on $G_4 = dC_3 \in H^{(2,2)}(Y_4)$. In recent years, extensive toolkits have been designed to create and enumerate the primary vertical subspace of G_4 configurations [23–29]. Applications of these tools to globally consistent chiral F-theory models have been conducted in [27, 29–31]. Relatively recently, these efforts culminated in the largest currently-known class of explicit string vacua that realize the Standard Model gauge group with their exact chiral spectrum and gauge coupling unification [32] – the *Quadrillion F-theory Standard Models* (QSMs).

A 4d $\mathcal{N} = 1$ F-theory compactification contains chiral (super)fields in a representation \mathbf{R} and chiral (super)fields in the charge conjugate representation $\overline{\mathbf{R}}$. The difference between their numbers is the chiral spectrum. Accounting for these fields individually is achieved by the vector-like spectrum. This poses additional challenges as those zero modes depend on the flat directions of the potential C_3 and not only on $G_4 = dC_3$. An F-theory “gauge field” that uniquely specifies the vector-like spectrum is given by an element of the so-called *Deligne cohomology*. The program initiated in [33–35] rests on the fact that (a subset of) the Deligne cohomology can be parameterized by Chow classes. This parametrization allows one to extract line bundles $L_{\mathbf{R}}$ defined on curves $C_{\mathbf{R}}$ in B_3 . In the dual IIB picture, this can be interpreted as the localization of gauge flux on matter curves $C_{\mathbf{R}}$, which can lift vector-like pairs on these curves. Explicitly, the zero modes are counted by the sheaf cohomology groups of the line bundle $L_{\mathbf{R}}$. There are $h^0(C_{\mathbf{R}}, L_{\mathbf{R}})$ massless chiral superfields in representation \mathbf{R} . Similarly, there are $h^1(C_{\mathbf{R}}, L_{\mathbf{R}})$ massless chiral superfields in the charge conjugate representation $\overline{\mathbf{R}}$ on $C_{\mathbf{R}}$.

In theory, this procedure always works. In practice however, technical limitations arise since the line bundle cohomologies depend intricately on the complex structure of Y_4 . As a conse-

quence, even state-of-the-art algorithms, such as [36–38] (see also [34, 35]), on supercomputers specifically designed for such computations (such as Plesken at *Siegen University*) can oftentimes not perform the necessary operations in realistic compactification geometries. This is exactly the reason why the works in [33–35] focused on computationally simple geometries. Even then, these models have unrealistically large numbers of chiral fermions. Inspired by the advances in machine learning applications to String Theory [39–41] (see also [42] and references therein), the complex structure dependency of line bundle cohomologies was investigated more systematically in [43]. Inspired by the F-theory GUT models in [35] and the help of the algorithms in [36], it was possible to generate a large data set [44] of line bundle cohomologies for different complex structure moduli. This data was analyzed with data science techniques. A theoretical understanding was achieved by supplementing these data science insights by Brill-Noether theory [45] (see [46] for a modern exposition and [47] for an earlier application of Brill-Noether theory in F-theory). These insights led to a quantitative study of jumps of charged matter vector pairs as a function of the complex structure moduli of the matter curve $C_{\mathbf{R}}$.

A G_4 -flux is subject to the quantization condition $G_4 + \frac{1}{2}c_2(Y_4) \in H_{\mathbb{Z}}^4(Y_4)$. Unfortunately, this condition can often not be checked in a computationally feasible manner. The interested reader is referred to [48] for recent advances in this direction. *Quadrillion F-theory Standard Models* [32] evaluated necessary conditions for a specific G_4 -flux to satisfy the quantization condition. In this work, we proceed under the assumption that the quantization condition is satisfied. It is worth noting that the QSM G_4 -flux candidate also satisfies the D3-tadpole cancelation and masslessness of the $U(1)$ -gauge boson [32].

Therefore, the vector-like spectra in the QSMs beg to be investigated. Those modes localize on five matter curves and were first studied in [49]. It was shown that on three of these matter curves, the line bundle $L_{\mathbf{R}}$ is necessarily a fractional power $P_{\mathbf{R}}$ of the canonical bundle. On the remaining two matter curves, the line bundles are modified by contributions from the Yukawa points. Such fractional powers of line bundles are known as root bundles, which may be thought of as generalizations of spin bundles. Inspired by $P\zeta\alpha$, which is “root” in Greek, P refers to root bundles throughout this article. Similar to spin bundles, root bundles are far from unique. The mathematics of root bundles indicates that we should think of the different root bundles as being induced from inequivalent gauge potentials for a given G_4 -flux.

In general, we cannot expect that all physically relevant root bundles on the matter curve $C_{\mathbf{R}}$ are induced from F-theory gauge potentials in the Deligne cohomology. This mirrors the expectation that only some of the spin bundles on the matter curves are consistent with the F-theory geometry Y_4 . Rather, an F-theory gauge potential induces a collection $\{P_{\mathbf{R}}\}$ consisting of one root bundle on each matter curve $C_{\mathbf{R}}$. By repeating this for all physically relevant F-theory gauge potentials, we should expect that in general only a proper subset of all root bundles on $C_{\mathbf{R}}$ will be reached. Conversely, if we are given a collection of root bundles $\{P_{\mathbf{R}}\}$ – one for each matter curve – then this collection can fail to stem from an F-theory gauge potential. Namely, it is possible for one of the root bundles to not be induced at all, or not in combination with one of the other roots.

While it is of great importance for the physics to determine which roots are physical (i.e. induced from an F-theory gauge potential), this question is also extremely challenging. For this reason, this question was not investigated by [49] in favor of conducting a systematic study of all root and spin bundles on the individual matter curves. This local bottom-up analysis allowed us to name a root bundle and a spin bundle on all matter curves, except for the Higgs curve in one particular QSM geometry [32], such that their tensor product is a line bundle with the physically desired cohomologies. On a technical level, this is achieved by considering a deformation of the smooth, physical matter curves $C_{\mathbf{R}}$ into a nodal curve $C_{\mathbf{R}}^{\bullet}$. On the latter, root bundles are

described in a diagrammatic way by *limit roots* [50]. For limit root bundles on the full blowup of $C_{\mathbf{R}}^{\bullet}$, the global sections can be counted by the techniques put forward in [49].

This study was subsequently extended in [51] by a computer algorithm which enumerates all root bundles with exactly three global sections on the full blowup of $C_{\mathbf{R}}^{\bullet}$. This in turn was repeated for $\mathcal{O}(10^{15})$ different QSM geometries. The latter rests on the fact that the QSM geometries are defined by families of toric spaces $B_3(\Delta^{\circ})$ associated to the (full, regular, star) triangulations of 708 (3-dimensional, reflexive) polytopes Δ° in the Kreuzer-Skarke list [52] (see also [53]). One may think of these spaces as different desingularizations of toric K3-surfaces [54–58]. These well-known results allowed to argue that the nodal curve $C_{\mathbf{R}}^{\bullet}$ – and thus, the number of limit root bundles – only depends on the polytope Δ° . Hence, by repeating a somewhat involved computer scan for 23 different polytopes, one finds results that apply to a large fraction of the QSM geometries. This allowed, in a first approximation and statistical meaning, to find base spaces for which absence of vector-like exotics in the representation $(\mathbf{3}, \mathbf{2})_{1/6}$ is very likely.

Results In this work, we analyze a superset of all physical root bundles for the matter representations $(\mathbf{3}, \mathbf{2})_{1/6}$, $(\bar{\mathbf{3}}, \mathbf{1})_{-2/3}$ and $(\mathbf{1}, \mathbf{1})_1$ in $\mathcal{O}(10^{11})$ F-theory QSM geometries $B_3(\Delta_4^{\circ})$. We find that more than 99.995% of the roots in this superset have no vector-like exotics. We arrived at this result from a systematic study of a large fraction of QSM geometries. While our results are strongest for the family $B_3(\Delta_4^{\circ})$, this study provides statistical evidence that the absence of the vector-like exotics in $(\mathbf{3}, \mathbf{2})_{1/6}$, $(\bar{\mathbf{3}}, \mathbf{1})_{-2/3}$ and $(\mathbf{1}, \mathbf{1})_1$ is a very likely scenario for a large fraction of the QSM geometries.

As mentioned above, the vector-like spectra in the QSM geometries are necessarily counted by cohomologies of root bundles [49]. Such root bundles $P_{\mathbf{R}}$ on the matter curve $C_{\mathbf{R}}$ are by no means unique. Even more, it is not clear exactly which ones are induced top-down from F-theory gauge potentials in the Deligne cohomology. First, on one matter curve, only a subset of all mathematically allowed root bundles could be induced from all physically allowed F-theory gauge potentials. Secondly, it is conceivable that fluxes which induce a specific root bundle on matter curve C_1 , only induce a few selected root bundles on another matter curve C_2 . In this work, we have not addressed this involved question, but rather conducted a local and bottom-up analysis. Our study is bottom-up in that we study *all* root bundles that could possibly be induced from the G_4 -flux and all spin bundles on the matter curve in question. Our study is local in that we focus on one matter curve at a time. Correlations among the vector-like spectra of different matter curves are not taken into account.

A crucial step in our study is triangulation independence. Specifically, each family $B_3(\Delta^{\circ})$ of toric 3-fold QSM base spaces – obtained from the (fine, regular, star) triangulations of 708 (3-dimensional, reflexive) polytopes Δ° in the Kreuzer-Skarke list [52] admits a triangulation-independent nodal limit [51]. This observation allows one to probe the vector-like spectra on the entire family $B_3(\Delta^{\circ})$ from the vector-like spectra on just 5 nodal curves. For the family $B_3(\Delta_4^{\circ})$ – associated to the 4-th polytope in the Kreuzer-Skarke list of 3-dimensional polytopes – which consists of $\mathcal{O}(10^{11})$ different toric spaces, we argue that all limit root bundles on the nodal curves $C_{(\mathbf{3}, \mathbf{2})_{1/6}}^{\bullet}$, $C_{(\bar{\mathbf{3}}, \mathbf{1})_{-2/3}}^{\bullet}$ and $C_{(\mathbf{1}, \mathbf{1})_1}^{\bullet}$ have exactly three global sections. By upper semi-continuity, this must hold true on the corresponding smooth, irreducible matter curves in each space of $B_3(\Delta_4^{\circ})$. This rules out vector-like exotics.

Apparently, this argument relies on the ability to compute the cohomologies of all limit root bundles. This is exactly the domain of Brill-Noether theory. By following the original work in [50], we find that for some limit roots, this is equivalent to line bundle cohomology on tree-like curves. The remaining limit roots require an understanding of line bundle cohomology on

circuit-like curves. In our applications to the F-theory QSMs, the majority of limit roots arise from tree-like curves with rational irreducible components. We present a computer algorithm which counts line bundle cohomology on such curves and handle the circuit-like cases by hand. On tree-like, rational curves, the cohomologies are independent of the relative position of the nodes. While true for most circuit-like cases, special circuits admit jumps provided that the nodes are specially aligned. Such *jumping circuits* mirror classical Brill-Noether jumps. For $B_3(\Delta_4^\circ)$, one jumping circuit exists. The root bundle constraints select the canonical bundle on this jumping circuit so that we find four global sections. This leads to 99.995% instead of 100%.

In contrast to earlier works [49,51], we take the *geometric multiplicity* into account [50]. Under a deformation of a smooth to a nodal curve, distinct root bundles on the smooth curve coalesce as we approach the nodal limit. The exact number of distinct roots which coalesce is the geometric multiplicity. Alternatively, this multiplicity ensures that we count as many limit root bundles on nodal curves as root bundles on a smooth curve. This ensures comparability of the limit root counts for different QSM geometries and slightly modifies the conclusions in [51].

Outline In Section 2, we briefly recall the motivation for root bundles in F-theory vacua [49]. Subsequently, we outline the steps necessary to extend the techniques of [49, 51] to limit roots on partial blowup curves, which are compactly summarized in Figure 3, Figure 4 and Figure 5. This approach makes it natural to think about line bundle cohomology on tree-like nodal curves. We put forward an algorithm that determines these line bundle cohomologies on rational curves in Section 3. This algorithm can be optimized further to detect speciality, i.e. if a line bundle has more sections than on a smooth \mathbb{P}^1 . While this optimization currently seems not relevant for studying Brill-Noether theory of limit root bundles or for arguing the absence of vector-like exotics in $\mathcal{O}(10^{11})$ QSM geometries, we outline these steps in Appendix A. With these techniques, we return to the QSM geometries and re-analyze the setups that were originally discussed in [51]. In Section 4, we first discuss the geometric multiplicity and compare our results to [51]. Indeed, we obtain more refined results, which also identify two errors in the earlier work. We summarize our findings in Table 3 and Table 4. We propose to view these tables as a first approximation of the Brill-Noether theory of the root bundles in question. More details can be found in Appendix B. We also mention that the necessary computer implementations are available in the `gap-4`-package *QSMExplorer* as part of the `ToricVarieties_project` [36]. Many, but definitely not all, of these computations can be conducted on a simple personal computer. Finally in Section 5, we focus on the family of QSM geometries $B_3(\Delta_4^\circ)$ associated to full regular star triangulations of the 4-th polytope Δ_4° in the Kreuzer-Skarke database [52]. By hand, we analyze the global sections on a couple of circuit-like nodal curves. For most of them, the line bundle cohomologies are independent of the relative positions of the nodes (cf. Appendix C). However, there is one circuit-like nodal curve for which four nodes are located on two irreducible components. By studying the embedding of this nodal curve into each space in $B_3(\Delta_4^\circ)$, we can show that the location of all nodes is determined in terms of the input parameters to the QSMs. In particular, we argue that the root bundle constraints select the canonical bundle on this jump circuit, which leads to exactly four (and not three) global sections. The detailed study of this embedding is conducted in Appendix D. We summarize and discuss our findings in Section 6.

2. Partial blowup limit root line bundles

2.1. Vector-like spectra in F-theory

The story begins with an F-theory compactification to four dimensions given by a singular, elliptically fibered 4-fold $\pi : Y_4 \rightarrow B_3$. Suppose that Y_4 admits a smooth, crepant resolution which is a flat elliptic fibration $\widehat{\pi} : \widehat{Y}_4 \rightarrow B_3$. A G_4 -flux in $H^{(2,2)}(\widehat{Y}_4)$ satisfies the quantization condition precisely if [59]

$$G_4 + \frac{1}{2}c_2(T_{\widehat{Y}_4}) \in H_{\mathbb{Z}}^{(2,2)}(\widehat{Y}_4) := H^{(2,2)}(\widehat{Y}_4) \cap H^4(\widehat{Y}_4, \mathbb{Z}). \quad (1)$$

For F-theory compactifications on an elliptically fibered smooth Calabi-Yau 4-fold with globally defined Weierstrass model, the class $c_2(T_{\widehat{Y}_4})$ is even [60]. Consequently in such geometries, we demand $G_4 \in H_{\mathbb{Z}}^{(2,2)}(\widehat{Y}_4)$. Unfortunately, this condition can often not be checked in a computationally feasible manner. The interested reader is referred to [48] for recent advances in this direction. *Quadrillion F-theory Standard Models* [32] evaluated necessary conditions for a specific G_4 -flux to satisfy the quantization condition. In this work, we proceed under the assumption that the quantization condition is satisfied. It is worth noting that the QSM G_4 -flux candidate also satisfies the D3-tadpole cancellation and masslessness of the $U(1)$ -gauge boson [32].

There is a surjection from the Deligne cohomology group

$$\widehat{c} : H_D^4(\widehat{Y}_4, \mathbb{Z}(2)) \rightarrow H_{\mathbb{Z}}^{(2,2)}(\widehat{Y}_4), \quad (2)$$

and a G_4 -flux lifts to an F-theory gauge potential A in the Deligne cohomology group $H_D^4(\widehat{Y}_4, \mathbb{Z}(2))$. Although this group is intractable when it comes to explicit computations, we can parametrize a subset of it via the map

$$\widehat{\gamma} : \text{CH}^2(\widehat{Y}_4, \mathbb{Z}) \rightarrow H_D^4(\widehat{Y}_4, \mathbb{Z}(2)). \quad (3)$$

Thus, we turn our attention to studying $\mathcal{A} \in \text{CH}^2(\widehat{Y}_4, \mathbb{Z})$ satisfying $(\widehat{c} \circ \widehat{\gamma})(\mathcal{A}) = G_4$.

For some representation \mathbf{R} of the gauge group G of the F-theory compactification in question, let $C_{\mathbf{R}} \subseteq B_3$ be the matter curve upon which the massless matter states localize and transform in \mathbf{R} . The corresponding matter surface $S_{\mathbf{R}} \subseteq \widehat{Y}_4$ – the mathematicians will notice that $S_{\mathbf{R}}$ is actually a 2-cycle and not a surface – is a linear combination of \mathbb{P}^1 -fibration over $C_{\mathbf{R}}$ and the coefficients correspond to the weight vector \mathbf{w} of the representation \mathbf{R} (see [61] and references therein). By restricting to $S_{\mathbf{R}}$ and integrating over the fibers over $C_{\mathbf{R}}$, we can associate to each $\mathcal{A} \in \text{CH}^2(\widehat{Y}_4, \mathbb{Z})$ a divisor via the cylinder map

$$D_{\mathbf{R}} : \text{CH}^2(\widehat{Y}_4, \mathbb{Z}) \rightarrow \text{CH}^1(C_{\mathbf{R}}, \mathbb{Z}) \cong \text{Pic}(C_{\mathbf{R}}). \quad (4)$$

Specifically, we consider $\iota_{S_{\mathbf{R}}} : S_{\mathbf{R}} \hookrightarrow \widehat{Y}_4$ and $\pi_{S_{\mathbf{R}}} : S_{\mathbf{R}} \rightarrow C_{\mathbf{R}}$. Then the cylinder map is given by

$$D_{\mathbf{R}}(\mathcal{A}) = \pi_{S_{\mathbf{R}*}}(\iota_{S_{\mathbf{R}}}^*(\mathcal{A})) \in \text{Pic}(C_{\mathbf{R}}). \quad (5)$$

As explained in [33–35], the divisor $D_{\mathbf{R}}(\mathcal{A})$ gives rise to the following line bundle

$$P_{\mathbf{R}}(\mathcal{A}) = \mathcal{O}_{C_{\mathbf{R}}}(D_{\mathbf{R}}(\mathcal{A})) \otimes_{\mathcal{O}_{C_{\mathbf{R}}}} \mathcal{O}_{C_{\mathbf{R}}}^{\text{spin}}, \quad (6)$$

where $\mathcal{O}_{C_{\mathbf{R}}}^{\text{spin}}$ is a spin bundle on $C_{\mathbf{R}}$ compatible with the global structure of the F-theory compactification on \widehat{Y}_4 , whose sheaf cohomologies encode the vector-like spectrum on $C_{\mathbf{R}}$, i.e.

$$\begin{aligned} h^0(C_{\mathbf{R}}, P_{\mathbf{R}}(\mathcal{A})) &\leftrightarrow \text{chiral zero modes in representation } \mathbf{R}, \\ h^1(C_{\mathbf{R}}, P_{\mathbf{R}}(\mathcal{A})) &\leftrightarrow \text{chiral zero modes in charge conjugate representation } \overline{\mathbf{R}}. \end{aligned} \quad (7)$$

The generic case $h^0(C_{\mathbf{R}}, P_{\mathbf{R}}(\mathcal{A})) = \chi(P_{\mathbf{R}}(\mathcal{A}))$ corresponds to the absence of exotic vector-like pairs. The situation $h^0(C_{\mathbf{R}}, P_{\mathbf{R}}(\mathcal{A})) = \chi(P_{\mathbf{R}}(\mathcal{A})) + 1$, which implies the existence of exactly one Higgs pair, features prominently as the desired vector-like spectrum on the Higgs curve of an F-theory MSSM construction.

2.2. Limit root bundles in the F-theory QSMs

In [51], we followed this logic to study the vector-like spectra in the largest currently-known class of globally-consistent F-theory Standard Model constructions without chiral exotics and gauge coupling unification [32]. The geometry of the compactification space of those Quadrillion F-theory Standard Models (F-theory QSMs) determines a class $\mathcal{A}' \in \text{CH}^2(\widehat{Y}_4, \mathbb{Z})$ and an integer $\xi \in \mathbb{Z}_{>0}$ such that $D_{\mathbf{R}}(\mathcal{A}')$ is – possibly with additional contributions from the Yukawa points – expressible in terms of the canonical divisor on $C_{\mathbf{R}}$, the integer ξ divides the degree of $D_{\mathbf{R}}(\mathcal{A}')$ and \mathcal{A} is subject to two constraints

$$(\widehat{c} \circ \widehat{\gamma})(\mathcal{A}) = G_4, \quad \xi \cdot D_{\mathbf{R}}(\mathcal{A}) \sim D_{\mathbf{R}}(\mathcal{A}') \quad (8)$$

The condition on the right of Equation (8) says that $D_{\mathbf{R}}(\mathcal{A})$ is a ξ -th root divisor of $D_{\mathbf{R}}(\mathcal{A}')$ and the associated line bundle $P_{\mathbf{R}}(\mathcal{A})$ is a ξ -th root bundle on $C_{\mathbf{R}}$. To count the zero modes in the F-theory QSMs, we are therefore led to study the sheaf cohomologies of root bundles.

An important task is to find the root bundles that are induced from F-theory gauge potentials. First, on one matter curve, only a subset of all mathematically allowed root bundles could be induced from all physically allowed F-theory gauge potentials. Secondly, it is conceivable that fluxes which induce a specific root bundle on matter curve C_1 , only induce a few selected root bundles on another matter curve C_2 . The study of these questions is involved and currently beyond our abilities. While we hope to return to these questions in future work, in the current work we opt for a local and bottom-up analysis instead. In this sense, we follow the spirit of the earlier works [49, 51]. Our study is bottom-up in that we study *all* mathematically allowed root bundles. Our study covers all root bundles that could possibly be induced from the G_4 -flux and all spin bundles on the matter curve in question. Our study is local in that we focus on one matter curve at a time. Correlations among the vector-like spectra of different matter curves are therefore not taken into account.

Consequently, we study all root bundles $P_{\mathbf{R}}$ on $C_{\mathbf{R}}$ – including all spin bundles on $C_{\mathbf{R}}$. Since $C_{\mathbf{R}}$ is smooth and the integer ξ divides the degree of $D_{\mathbf{R}}(\mathcal{A}')$, there are ξ^{2g} root bundles where g is the genus of $C_{\mathbf{R}}$. Unfortunately, computing their sheaf cohomology is difficult. In particular, it is not easy to distinguish between trivial and non-trivial root bundles in general. To overcome this challenge, we consider deformations of $C_{\mathbf{R}}$ to a reducible, nodal curve $C_{\mathbf{R}}^{\bullet}$ by modifying the defining polynomials of $C_{\mathbf{R}}$ in a concrete base geometry B_3 . This comes at a double cost.

First, the deformation $C_{\mathbf{R}}^{\bullet} \rightarrow C_{\mathbf{R}}$ is, per se only subject to upper semicontinuity of global sections. This means, that we may lose global sections that exist on $C_{\mathbf{R}}^{\bullet}$ as we deform back to the smooth, irreducible $C_{\mathbf{R}}$. However, if the number of global sections match the chiral index, then it is protected by topology and cannot change. We exploited this fact in [49] and will mimic this strategy in later part of this work.

Second, the ξ -th root bundles of a line bundle L on a reducible nodal curve C do not exist if ξ does not divide the degree of the restriction of L to the irreducible components of C . Thanks to the work of [50], this is elegantly circumvented by passing to limit root bundles $P_{\mathbf{R}}^{\circ}$ on (partial) blow-ups $C_{\mathbf{R}}^{\circ}$, whose existence only requires for ξ to divide $\text{deg}(L_{\mathbf{R}})$. By properly keeping track of multiplicities, there exist ξ^{2g} limit roots, each determined by the combinatorial data associated to the dual graph of $C_{\mathbf{R}}^{\bullet}$. Fortunately, it turns out that there are less than 2×708 different dual

graphs that arise in the context of the QSMs. This observation allows us to gain insights into a large fraction of these geometries.

2.3. Triangulation independence in the QSM geometries

To understand why there are only 2×708 different dual graphs to be considered, we briefly recall the genesis of the F-theory QSM geometries, specifically the base spaces in question. These geometries are obtained from desingularizations of toric K3-surfaces. Such desingularizations were first studied in [54]. It is well-established by now that they correspond to three-dimensional, reflexive lattice polytopes $\Delta \subset M_{\mathbb{R}}$ and their polar duals $\Delta^{\circ} \subset N_{\mathbb{R}}$ defined by $\langle \Delta, \Delta^{\circ} \rangle \geq -1$. In [52], Kreuzer and Skarke listed all possible 3-dimensional polytopes [52]. Just as in [51], we consider the i -th polytope in the Kreuzer-Skarke list as subset of $N_{\mathbb{R}}$ and denote it by Δ_i° .

Recall that to each polytope $\Delta \subset M_{\mathbb{R}}$, one can associate a normal fan Σ_{Δ} . The ray generators of this fan are the facet normals of Δ and the maximal cones correspond to the vertices of Δ . Even though the toric variety $X_{\Delta} \equiv X_{\Sigma_{\Delta}}$ or the CY-hypersurface may not be smooth, we can resolve these hypersurfaces. Such resolutions were introduced in [54] as *maximal projective crepant partial* (MPCP) desingularizations. Equivalently, [56] refers to them as maximal projective subdivisions of the normal fan. MPCPs are associated to fine, regular, star triangulation (FRST) of the lattice polytope Δ° . We recall that *star* means that every simplex in the triangulation contains the origin, *fine* ensures that every lattice point of Δ° is used as ray generator¹ and that *regular* implies that $X_{\Sigma(T)}$ is projective. Together, this implies that $\Sigma(T)$ defines a *maximal projective refinement* of Σ_{Δ} . Note that in applications to toric K3-surfaces, $X_{\Sigma(T)}$ is guaranteed to be smooth. Namely, a maximal projective subdivision of Σ_{Δ} then constructs a 3-dimensional Gorenstein orbifold with terminal singularities [56] which must be smooth by proposition 11.4.19 in [63]. For more details, we refer the interested reader to [54].

708 of the 4319 polytopes in [52] satisfy $\overline{K}_{X_{\Sigma(T)}}^3 \in \{6, 10, 18, 30\}$. These are exactly the polytopes whose geometries define the base spaces for the Quadrillion F-theory Standard Models (QSMs) [32]. Just as in [51], we use $B_3(\Delta^{\circ})$ to denote the toric 3-folds obtained from FRSTs of the polytope Δ° . An instructive example is Δ_{52}° , which we display in Figure 1.

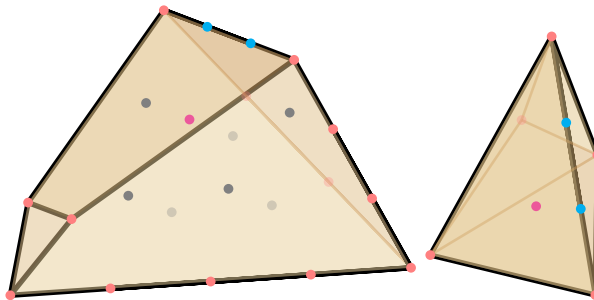


Figure 1.: $\Delta_{52}^{\circ} \subset N_{\mathbb{R}}$ on the left and $\Delta_{52} \subseteq M_{\mathbb{R}}$ on the right [52]. The magenta point is the origin. The generic K3-surface meets trivially with the gray divisors, in an irreducible curve with the pink ones, and in finite families of \mathbb{P}^1 s with the cyans. This picture is taken from [51].

For each QSM geometry, we introduced a nodal quark-doublet curve in [49]. This curve is

¹This property is also referred to as *full* [62].

canonically associated with the family $B_3(\Delta_4^\circ)$. We can write this curve as

$$C_{(\mathbf{3},\mathbf{2})_{1/6}}^\bullet = \bigcup_{a \in A} V(x_a, s_9) \cup \bigcup_{b \in B} V(y_b, s_9) \cup \bigcup_{c \in C} V(z_c, s_9). \quad (9)$$

We explained the rationale behind this notation in [51]. Namely, one can show that $V(x_a, s_9)$ is irreducible, $V(y_b, s_9)$ a finite collection of \mathbb{P}^1 s and $V(z_c, s_9) = \emptyset$. This rests on arguments originally presented in [54–57, 64].

This classification is directly related to the geometry of the polytope Δ° . Namely, the homogeneous coordinates are one-to-one with the lattice points of Δ° (minus the origin) since we use these as rays of the refined fan. A homogeneous coordinate associated to a facet interior point of Δ° is denoted by z_c . For a lattice point in the interior of an edge $\Theta \subset \Delta^\circ$, two facets F_1, F_2 of Δ° meet at Θ . In the dual polytope Δ , they correspond to vertices m_1, m_2 and the dual edge Θ is the edge connecting m_1 and m_2 . If Θ has interior points, we denote the homogeneous coordinate by y_b . All remaining coordinates are indicated as x_a . In Figure 1, distinct types of lattice points are marked in different colors.

Consequently, all irreducible components of $C_{(\mathbf{3},\mathbf{2})_{1/6}}^\bullet$ are smooth, irreducible curves embedded into a smooth and projective K3-surface. This alone implies, and equivalently follows from [54–57, 64], that the pairwise topological intersection numbers are non-negative. Furthermore, we can restrict to open subsets near intersection points. Since an open subset of an irreducible topological space is irreducible, it follows that the multiplicity of intersection at each intersection point is non-negative. Consequently, for generic s_9 , the number of pairwise intersection points among the irreducible components of $C_{(\mathbf{3},\mathbf{2})_{1/6}}^\bullet$ matches the topological intersection number. This is how we concluded in [51] that the dual graph of $C_{(\mathbf{3},\mathbf{2})_{1/6}}^\bullet$ is the same for all FRSTs of Δ° . This leads to at most 708 distinct dual graphs. In fact, one finds that distinct polytopes in the QSM database can lead to identically the same dual graphs. So, there are strictly less than 708 distinct dual graphs for the canonical nodal quark-doublet curve $C_{(\mathbf{3},\mathbf{2})_{1/6}}^\bullet$ in the QSMs. There are two matter curves with distinct topology, namely the Higgs curve $C_{(\mathbf{1},\mathbf{2})_{-1/2}}^\bullet$ and a curve supporting right-handed quarks $C_{(\mathbf{3},\mathbf{1})_{1/3}}^\bullet$. However, their topologies are identical, contributing to at most 708 more distinct dual graphs. In this work, we will ignore those two curves and focus on the curve with dual graph identical to that of $C_{(\mathbf{3},\mathbf{2})_{1/6}}^\bullet$.

In Appendix D, we refine this result for the polytope Δ_4° . We will explain in Section 2.5, that the counting of limit root bundles on $C_{(\mathbf{3},\mathbf{2})_{1/6}}^\bullet$ only depends on some irreducible components and the nodes on these components. For Δ_4° , we therefore focus on four components C_0, C_1, C_2, C_3 . Our arguments show that there are homogeneous coordinates for these four irreducible components such that, in these coordinates, the location of the nodes is the same for all FRSTs of Δ_4° . This in turn is critical for our analysis in Section 5.2, where we study the one jumping circuit associated to Δ_4° . To the best of our knowledge, this FRSTs independence of the location of the nodes does not follow from earlier works [54–57, 64]. At this point, our argument rests on a detailed computational analysis which can, in principle, be extended to all QSM spaces. One can speculate that such an extension would lead to the very same conclusion, namely triangulation independent positions of the relevant nodes. This extension is beyond the scope of the current work and we leave this study for future investigation.

2.4. The need for partial blowup limit root bundles

In order to approximate physical root bundle on the smooth matter curve $C_{(\mathbf{3},\mathbf{2})_{1/6}}$, we thus employ limit root bundles on the nodal curve $C_{(\mathbf{3},\mathbf{2})_{1/6}}^\bullet$. As we explained before, the dual graph

of $C_{(\mathbf{3},\mathbf{2})_{1/6}}^\bullet$ is independent of the FRSTs. This extends to certain topological intersection numbers and implies that the operations performed on basis of [50], which construct and count limit root line bundles $P_{\mathbf{R}}^\bullet$ on (partial) blow-ups of $C_{\mathbf{R}}^\bullet$ from combinatorial data, are independent of the FRSTs.

In [49], we compute the zeroth sheaf cohomology of all limit root bundles that arise from the full blow-up of $C_{\mathbf{R}}^\bullet$. We refer to this work for additional background for the application of limit root bundles towards F-theory QSMs. In particular, we explained that the sheaf cohomology of such limit root bundles is given by the following formula,

$$h^0(C_{\mathbf{R}}^\circ, P_{\mathbf{R}}^\circ) = \sum_Z h^0(Z, P_{\mathbf{R}}^\circ|_Z), \quad (10)$$

where Z is an irreducible component of $C_{\mathbf{R}}^\bullet$. Since the pushforward of the limit roots $P_{\mathbf{R}}^\circ$ along the blow-up map $\pi : C_{\mathbf{R}}^\circ \rightarrow C_{\mathbf{R}}^\bullet$ preserves the number of global sections, we also have that

$$h^0(C_{\mathbf{R}}^\circ, P_{\mathbf{R}}^\circ) = h^0(C_{\mathbf{R}}^\bullet, \pi_* P_{\mathbf{R}}^\circ). \quad (11)$$

Along the deformation of $C_{\mathbf{R}}^\bullet$ back to the original curve $C_{\mathbf{R}}$, the number of sections either decreases or remains constant as the dimension of the zeroth cohomology is an upper semi-continuous function, i.e.

$$h^0(C_{\mathbf{R}}, P_{\mathbf{R}}) \leq h^0(C_{\mathbf{R}}^\bullet, \pi_* P_{\mathbf{R}}^\circ). \quad (12)$$

In this work, we aim to establish the absence of vector-like exotics for *physical* roots. Since we cannot yet tell which roots are physical, we cover all (mathematical) roots and identify their sheaf cohomologies. With an eye towards the nodal quark-doublet curve $C_{(\mathbf{3},\mathbf{2})_{1/6}}^\bullet$, we would ideally find that all of its roots have exactly three global sections. Then, by upper semicontinuity this remains true as we deform back to the smooth, irreducible (and physical) curve $C_{(\mathbf{3},\mathbf{2})_{1/6}}$. But for this argument to work, we need to extend to all roots, including those on partial blowups. This requires an extension of the techniques in [51]. As a side effect of these extensions, we shall present – what we believe are the very first – results on Brill-Noether theory of limit root bundles.

2.5. Beyond full blowup limit roots

We show the generalizations necessary to go from full to partial blowups in an example that will be relevant in later part of this work. Namely, we focus on the family of F-theory QSMs defined in terms of the fourth polytope Δ_4° in the Kreuzer-Skarke database [52]. There are $\mathcal{O}(10^{11})$ such geometries [53] and by following [49, 51], each contains a canonical nodal curve $C_{(\mathbf{3},\mathbf{2})_{1/6}}^\bullet$ with dual graph displayed in Figure 2a. The edges in this graph represent nodal singularities and the vertices are irreducible components of $C_{(\mathbf{3},\mathbf{2})_{1/6}}^\bullet$. The four curves C_i each are smooth \mathbb{P}^1 , which are marked in pink in the graph. In addition, L_{i_1, \dots, i_k} represents a chain of k smooth genus zero curves C_{i_j} such that C_{i_j} and $C_{i_{j+1}}$ intersect each other at a single node. Hence, as dual graph, L_{i_1, \dots, i_k} corresponds to a chain or link of k vertices. It is ordered so that C_{i_1} intersects the \mathbb{P}^1 on the left and C_{i_k} intersects the \mathbb{P}^1 on the right. For $L_{21,27}$, we have that C_{21} intersects C_3 while C_{27} intersects C_1 .

Simplifying the dual graph On this curve, we are looking for 12-th roots P^\bullet of the 12-th power of the canonical bundle $K_{(\mathbf{3},\mathbf{2})_{1/6}}^\bullet$. To this end, we can replace the above dual graph by another

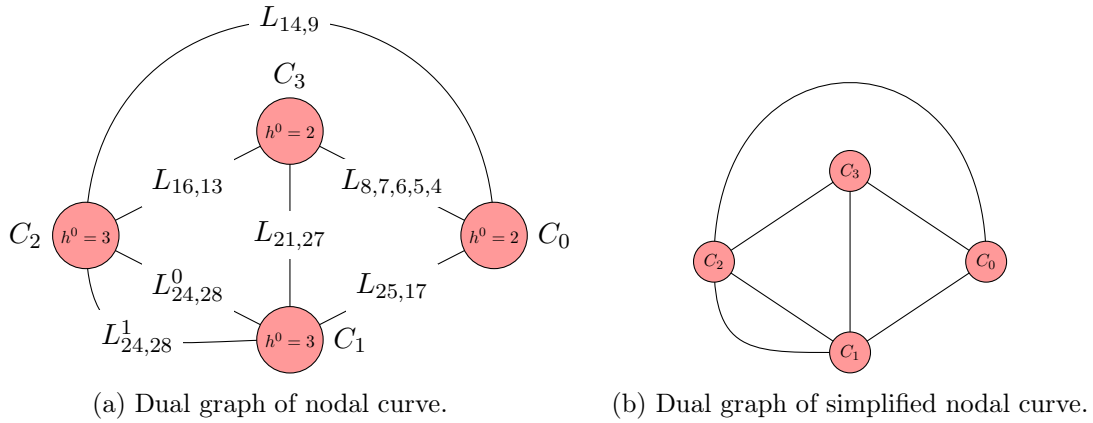


Figure 2.: Dual graph of (simplified) nodal curve $C_{(\mathbf{3},\mathbf{2})_{1/6}}^\bullet$ in the QSM spaces $B_3(\Delta_4^\circ)$.

graph, for which the combinatorics task of enumerating the limit root bundles is simpler. To see this, we consider the following:

$$\textcircled{C_0} \text{---} \textcircled{C_1} \text{---} \dots \text{---} \textcircled{C_{n-1}} \text{---} \textcircled{C_n} \quad (13)$$

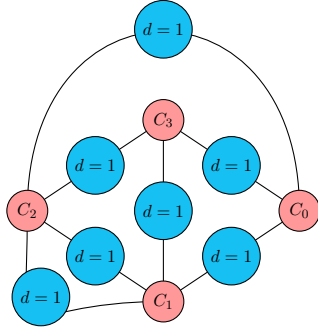
In [51], we argued that when constructing limit roots on the full blow-up of a chain of curves, the weights along the chain in the weighted subgraph are uniquely fixed. Thus, we were able to replace these chains by a single edge and we would still count the same number of weighted subgraphs and hence, limit root bundles. Indeed, this is the only weighted subgraph which satisfies the rules (C1) and (C2) in [50]. Namely, a curve C with dual graph Γ_C has $r^{b_1(\Gamma_C)}$ weighted subgraphs satisfying (C1) and (C2). If C is a chain of rational curves, then

$$b_1(\Gamma_C) = \#(\text{edges}) + \#(\text{connected components}) - \#(\text{vertices}) = 0. \quad (14)$$

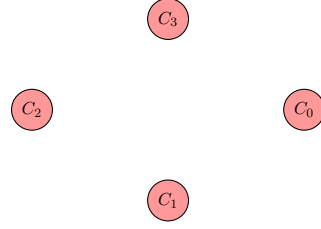
Hence, there is only $1 = r^0$ weighted subgraph, which corresponds to the full blow-up. Consequently, we can transition to the simpler dual graph displayed in Figure 2b.

Global section counting of partial blowup limit roots In order to find 12-th roots P^\bullet of the 12-th power of the canonical bundle $K_{(\mathbf{3},\mathbf{2})_{1/6}}^\bullet$ and count their global sections, we blew up every node in our earlier works [49, 51]. In following [49–51] we first focus on limit roots P^\bullet that correspond to a certain line bundle on the full blowup curve of $C_{(\mathbf{3},\mathbf{2})_{1/6}}^\bullet$. This full blowup curve is a curve $C_{(\mathbf{3},\mathbf{2})_{1/6}}^\circ$ in which each node is replaced by an exceptional \mathbb{P}^1 . Its dual graph is therefore of the form displayed in Figure 3a. In this diagram, we have marked the exceptional \mathbb{P}^1 s in blue color. Furthermore, it holds $P|_{E_i} \cong \mathcal{O}_{\mathbb{P}^1}(1)$ for each exceptional \mathbb{P}^1 by [50]. The (local) sections on the exceptional \mathbb{P}^1 s are uniquely fixed by the demand to bridge between the sections on the components C_i of $C_{(\mathbf{3},\mathbf{2})_{1/6}}^\bullet$. Therefore, we called these sections *bridging sections* in [49]. The number of global sections of P^\bullet is therefore identical to those of the restriction of P^\bullet to the completely disconnected curve in Figure 3b. In particular, it holds

$$h^0(C^\bullet, P^\bullet) = \sum_{i=0}^3 h^0(C_i, P^\bullet|_{C_i}). \quad (15)$$

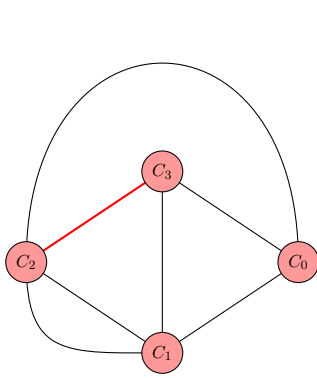


(a) Full blowup of nodal curve.

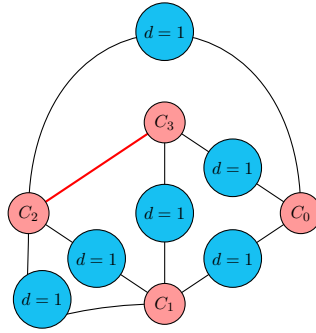


(b) Disconnected curve from removing nodes.

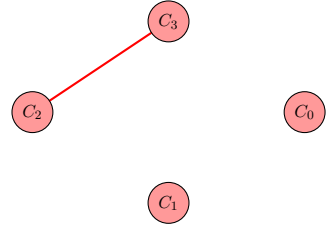
Figure 3.: For full blowup limit roots, each node is replaced by an exceptional \mathbb{P}^1 . The global sections are isomorphic to those of a line bundle on the disconnected curve.



(a) No blowup on red edge.



(b) Partial blowup.



(c) Tree-like nodal curve.

Figure 4.: For partial blowup limit roots, some nodes are not replaced by an exceptional \mathbb{P}^1 . In some cases, global sections are then counted on tree-like nodal curves.

Tree-like and circuit-like graphs In order to generalize this procedure to partial blowups, let us first look at the situation in which we decide not to blow up the edge marked in red in Figure 4a. It is in general not guaranteed that such a partial blowup admits limit roots. However, if limit roots P^\bullet exist, then they correspond to line bundles on the nodal curve in Figure 4b. Again, the sections on the exceptional \mathbb{P}^1 s bridge between the sections on neighboring components C_i . However, since one node – namely the one corresponding to the red edge – has not been blown up, the number of global sections of P^\bullet match that of the restriction of P^\bullet to the nodal curve with dual graph displayed in Figure 4c. There, $C_2 \cup C_3$ is a nodal, tree-like curve. If we are able to compute its line bundle cohomology, then we have

$$h^0(C^\bullet, P^\bullet) = h^0(C_0, P^\bullet|_{C_0}) + h^0(C_1, P^\bullet|_{C_1}) + h^0(C_2 \cup C_3, P^\bullet|_{C_2 \cup C_3}). \quad (16)$$

Apparently, this generalizes Equation (15).

In our applications, we find that for the majority of limit roots, the number of global sections is the same as the number of global sections of a line bundle on a rational, tree-like nodal curve. For example, 99% of the limit root bundles on Δ_4° arise in this way. Consequently, in order to

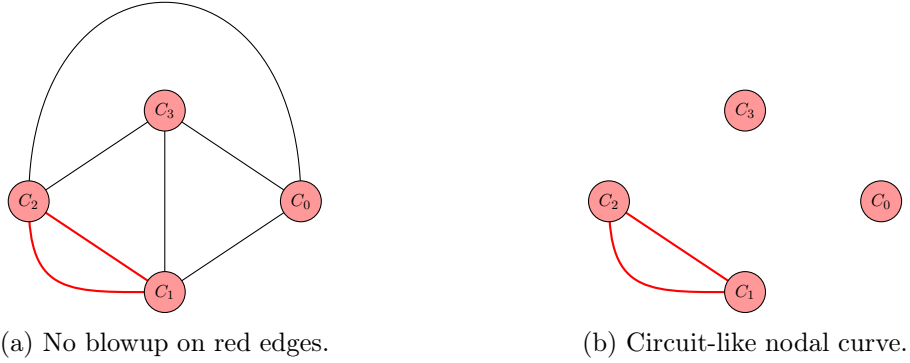


Figure 5.: Some choices of partial blowups lead to limit roots whose cohomologies are counted by line bundles on circuit-like nodal curves.

classify the limit root bundles with regard to their number of global sections, it becomes rather important for us to compute line bundle cohomology of line bundles on tree-like nodal curves. We will therefore discuss this at length in Section 3.

All remaining root bundles stem from circuit-like graphs. For example, suppose that we do not blow-up the two nodes marked in red in Figure 5a, then this leads to the computation of line bundle cohomology on the nodal curve with dual graph displayed in Figure 5b. This curve has a circuit-like component $C_1 \cup C_2$, which we cannot yet treat systematically.

Fortunately, in our current applications, these circuits account for very few limit root bundles. The reason why seems related to the fact that we are looking for 12-th and even 20-th roots of the canonical bundle. If instead, we were looking at second roots, one should expect equal contributions from tree-like and circuit-like graphs. It would be even conceivable that the circuits would dominate. However, in our applications, this is not the case. Therefore, we can conduct a case-by-case study for those few circuit-like curves that we encounter. We will come back to this in Section 5.1 and Section 5.2 and distinguish two types of circuits. First, there are circuits for which the number of global sections is the same irrespective of the position of the nodes. We call them *stationary circuits*. On the other hand, circuits for which the number of global sections depends on the (relative) location of the nodes are called *jumping circuits*. For these, it is possible to achieve more than the minimal number of global sections upon rearranging the position of the nodes.

3. Line bundle cohomology on tree-like, rational curves

3.1. Simplifying the tree

Consider a connected rational nodal curve $C := \bigcup_{i \in I} C_i$ and a line bundle L on it. Then, I is a simply connected graph and all components C_i are \mathbb{P}^1 's.

Definition 3.1. Let $d_i = \deg(L|_{C_i})$. Write $I = I_+ \cup I_-$, where

$$I_- := \{i \in I \mid d_i < 0\}, \quad I_+ := \{i \in I \mid d_i \geq 0\}. \quad (17)$$

Let

$$C_+ := \bigcup_{i \in I_+} C_i, \quad C_- := \bigcup_{i \in I_-} C_i. \quad (18)$$

Note that the curves C_+ , C_- could be disconnected. Let e_i be the intersection number of C_i with C_- and let L_+ be the line bundle on C_+ with $\deg(L_+|_{C_i}) = d_i - e_i$.

Proposition 3.2. $h^0(C, L) = h^0(C_+, L_+)$.

Proof

Consider a connected component $Y = \cup Y_i$ of C_+ . Suppose that e_i connected components Z_j of C_- intersect Y_i . Since C is connected and rational, Y_i intersects each Z_j at exactly one point n_j . Hence, e_i is exactly the number of connected components of C_- that meet Y_i . The connected components of C_- support only the trivial section, which automatically glues across the intersections between the components of Z_j . Hence, after choosing local coordinates, we can parametrize the local sections as follows:

Curve	Coordinates	Sections	
Y_i	$[x : y]$	$\text{Span}_{\mathbb{C}}(x^{d_i}, x^{d_i-1}y, \dots, y^{d_i})$	(19)
Z_j	$[u_j : v_j]$	0	

Without loss of generality, we can assume that the nodes are at the following positions:

Label	Coordinates in Y_i	Coordinates in Z_j	
n_j	$[x : y] = [a_j : b_j]$	$[u_j : v_j] = [0 : 1]$	(20)

Each intersection between Y_i and Z_j forces the local sections on Y_i to vanish at n_j . This amounts to exactly one equation of linear dependence on $h^0(Y_i, L|_{Y_i})$, namely

$$\sum_{k=0}^{d_i} \alpha_k a_j^k b_j^{d_i-k} = 0, \quad (21)$$

If $d_i \geq e_i$, then

$$h^0\left(Y_i \cup \left(\bigcup_{j=1}^{e_i} Z_j\right), L\right) = h^0(Y_i, L|_{Y_i}) - e_i = h^0(\mathbb{P}^1, \mathcal{O}_{\mathbb{P}^1}(d_i - e_i)) = h^0(Y_i, L_+|_{Y_i}). \quad (22)$$

If $d_i < e_i$, then the number of equations of linear dependence imposed by the e_i intersections exceeds $h^0(Y_i, L|_{Y_i})$. Hence,

$$h^0\left(Y_i \cup \left(\bigcup_{j=1}^{e_i} Z_j\right), L\right) = 0, \quad (23)$$

which coincides with $h^0(Y_i, L_+|_{Y_i}) = h^0(\mathbb{P}^1, \mathcal{O}_{\mathbb{P}^1}(d_i - e_i))$. Counting the sections of L over C is the same as counting the sections over C_+ and then, enforcing the gluing conditions at $C_+ \cap C_-$. Hence, $h^0(C, L) = h^0(C_+, L_+)$. ■

Note. By iterating this process we have

$$h^0(C, L) = h^0(C_+, L_+) = \dots = h^0(C_+^{(n)}, L_+^{(n)}), \quad (24)$$

In fact, since (C_+, L_+) has at most as many components as C this process must eventually become “constant”. Let us illustrate this with two examples.

Example 3.3. We first perform the following simplification:

$$\begin{array}{c}
 \begin{array}{c}
 \textcircled{-2} \text{---} \textcircled{1} \text{---} \textcircled{2} \\
 \text{-----} \\
 \textcircled{0} \text{---} \textcircled{2}
 \end{array}
 \end{array}
 \tag{25}$$

The latter cannot be simplified further.

Example 3.4. We perform the following simplifications:

$$\begin{array}{c}
 \begin{array}{c}
 \begin{array}{c}
 \textcircled{1} \text{---} \textcircled{1} \text{---} \textcircled{1} \\
 \textcircled{-2} \text{---} \textcircled{1} \text{---} \textcircled{-1} \quad \textcircled{-1} \text{---} \textcircled{1} \text{---} \textcircled{-1} \\
 \text{-----} \\
 \textcircled{-1} \text{---} \textcircled{-1} \text{---} \textcircled{1} \\
 \text{-----} \\
 \textcircled{0}
 \end{array}
 \end{array}
 \end{array}
 \tag{26}$$

The latter cannot be simplified further.

Definition 3.5. Let C be a tree-like nodal (but not necessarily connected) curve and $L \in \text{Pic}(C)$. We call a pair (C, L) *terminal* iff $C_+ \cap C_- = \emptyset$.

Consequence. Once we know how to compute global sections on a terminal tree-like pair (C, L) , we can employ the following algorithm to compute the global sections on a connected nodal pair (C, L) :

1. By iterating the simplification process, we have:

$$h^0(C, L) = h^0(C_+, L_+) = \cdots = h^0(C_+^{(n)}, L_+^{(n)}), \tag{27}$$

with terminal $(C_+^{(n)}, L_+^{(n)})$.

2. Compute $h^0(C_+^{(n)}, L_+^{(n)})$.

3.2. Global sections on terminal trees

We will now turn to line bundle cohomology on terminal trees. Recall that such terminal trees have $C_+ \cap C_- = \emptyset$. Since C_- does not support global sections, we can focus on just C_+ . We begin with the following lemma.

Lemma 1. Consider a curve $C = \mathbb{P}_a^1 \cup \mathbb{P}_b^1$ with $\mathbb{P}_a^1 \cap \mathbb{P}_b^1 = \{n\}$ a nodal singularity:

$$\begin{array}{c}
 \textcircled{\mathbb{P}_a^1} \text{---} \textcircled{\mathbb{P}_b^1}
 \end{array}
 \tag{28}$$

On this curve, consider the line bundle

$$\mathcal{L} = \mathcal{O}_C(d_a, d_b) \in \text{Pic}(C). \tag{29}$$

That is, we consider $\mathcal{O}_{\mathbb{P}_a^1}(d_a) \in \text{Pic}(\mathbb{P}_a^1)$ and $\mathcal{O}_{\mathbb{P}_b^1}(d_b) \in \text{Pic}(\mathbb{P}_b^1)$ subject to gluing at the node n . Assume $d_a, d_b \geq 0$. Then

$$h^0(C, L) = h^0(\mathbb{P}_a^1, \mathcal{O}_{\mathbb{P}_a^1}(d_a)) + h^0(\mathbb{P}_b^1, \mathcal{O}_{\mathbb{P}_b^1}(d_b)) - 1 = d_a + d_b + 1. \quad (30)$$

Proof

We pick the following local coordinates and parametrize the local sections by $\alpha_i, \beta_i \in \mathbb{C}$:

Curve	Coordinates	Sections
C_1	$[x : y]$	$\sum_{i=0}^{d_a} \alpha_i \cdot x^{d_a-i} \cdot y^i$
C_2	$[w : z]$	$\sum_{i=0}^{d_b} \beta_i \cdot w^{d_b-i} \cdot z^i$

(31)

Without loss of generality, we can assume that the node is at the following position:

Label	Superset	Coordinates in C_1	Coordinates in C_2
n	$\mathbb{P}_a^1 \cap \mathbb{P}_b^1$	$[x : y] = [0 : 1]$	$[w : z] = [0 : 1]$

(32)

Enforcing gluing at n_1 is equivalent to $\alpha_{d_a} = \beta_{d_b}$. Hence it follows:

$$h^0(C, L) = h^0(\mathbb{P}_a^1, \mathcal{O}_{\mathbb{P}_a^1}(d_a)) + h^0(\mathbb{P}_b^1, \mathcal{O}_{\mathbb{P}_b^1}(d_b)) - 1 = d_a + d_b + 1. \quad (33)$$

This completes the argument. ■

It is not too hard to generalize this result.

Lemma 2. Consider a *connected* rational nodal curve $C := \bigcup_{i \in I} C_i$ and L a line bundle on it. (This means that I is a simply connected graph and the C_i are \mathbb{P}^1 's.) Let d_i be the degree of the restriction of L to C_i . Suppose that $d_i \geq 0$ for all $i \in I$. Then

$$h^0(C, L) = d + 1, \quad d = \sum_{i \in I} d_i. \quad (34)$$

Proof

We prove this statement by induction on $|I|$. If $|I| = 1$, then the statement is obviously true.

For the induction step, consider a connected, rational curve C with n components. Assume that our statement is true for C . By adding one component C_{n+1} to C , we obtain a new curve C' . Assume that C' is tree-like, i.e. C_{n+1} intersects exactly one component of C in exactly one point. Without loss of generality, let us denote this component as C_n and $p = C_n \cap C_{n+1}$.

The global sections on C_n correspond to a subset $S \subseteq H^0(C_n, \mathcal{O}_{C_n}(d_n))$ on C_n . Let us glue these sections to $H^0(C_{n+1}, \mathcal{O}_{C_{n+1}}(d_{n+1}))$ at p . Without loss of generality, we make the following choices:

Curve	Coordinates	Sections
C_n	$[x : y]$	$S \subseteq \text{Span}_{\mathbb{C}}(x^{d_n}, x^{d_n-1}y, \dots, y^{d_n})$
C_{n+1}	$[u : v]$	$\text{Span}_{\mathbb{C}}(u^{d_{n+1}}, u^{d_{n+1}-1}v, \dots, v^{d_{n+1}})$

(35)

Choose $p = V(x)$ on C_n and $p = V(u)$ on C_{n+1} . Let us now assume that no gluing condition in p was required. This would mean that for any $\varphi \in S$ and $\psi \in H^0(C_{n+1}, \mathcal{O}_{C_{n+1}}(d_{n+1}))$, they satisfy

$$\varphi(p) = \psi(p). \quad (36)$$

However, since $u^{d_{n+1}}, v^{d_{n+1}} \in H^0(C_{n+1}, \mathcal{O}_{C_{n+1}}(d_{n+1}))$, this would imply that any $\varphi \in S$ satisfies

$$\varphi(p) = u^{d_{n+1}}(p) = 0, \quad \varphi(p) = v^{d_{n+1}}(p) = 1. \quad (37)$$

This cannot be satisfied in \mathbb{C} . Hence, there is at least one condition to be imposed at p . However, since p imposes at most one condition, it imposes exactly one condition. Recall that by assumption,

$$h^0(C, L) = d + 1, \quad d = \sum_{i \in I} d_i. \quad (38)$$

Consequently, we find for C' that:

$$h^0(C', L) = h^0(C, L) + h^0(C_{n+1}, L) - 1 = d + 1 + (d_{n+1} + 1) - 1 = (d + d_{n+1}) + 1. \quad (39)$$

This completes the argument. ■

Corollary 3.6. Consider a rational nodal curve $C := \bigcup_{i \in I} C_i$ and a line bundle L on it. Suppose that C has k connected components and the restrictions of L to C_i have degrees $d_i \geq 0$. Then

$$h^0(C, L) = \left(\sum_{i \in I} d_i \right) + k. \quad (40)$$

We are now in the position to formulate the result which allows one to count the global sections on any terminal tree.

Proposition 3.7. Let (C, L) be terminal and C_+ have k connected components. Then,

$$h^0(C, L) = \left(\sum_{i \in I_+} d_i \right) + k. \quad (41)$$

Proof

Since (C, L) is terminal, $C_+ \cap C_- = \emptyset$ and

$$h^0(C, L) = h^0(C_+, L|_{C_+}) + h^0(C_-, L|_{C_-}) = h^0(C_+, L|_{C_+}). \quad (42)$$

Now, let e be the number of intersections between curves in C_+ . Then, $e = |I_+| - k$ and

$$h^0(C, L) = \left(\sum_{i \in I_+} (d_i + 1) \right) - e = \left(\sum_{i \in I_+} d_i \right) + |I_+| - e = \left(\sum_{i \in I_+} d_i \right) + k. \quad (43)$$

This completes the argument. ■

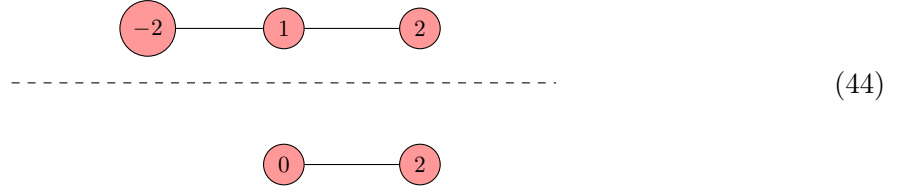
3.3. Final algorithm

Algorithm 1. Consider a connected, rational nodal curve $C := \bigcup_{i \in I} C_i$ and a line bundle L on it. Then, the following algorithm computes $h^0(C, L)$.

1. Simplify $(C, L) \rightarrow (C_+, L_+) \rightarrow \dots (C_+^{(n)}, L_+^{(n)})$ with terminal $(C_+^{(n)}, L_+^{(n)})$.
2. Then $h^0(C, L) = d_+(L_+^{(n)}) + c_+(C_+^{(n)})$, where
 - $d_+(L_+^{(n)}) = \sum_{i \in I_+(C_+^{(n)})} d_i$.
 - $c_+(C_+^{(n)})$ is the number of connected components of $C_+^{(n)}$.

Note. Since C_+ has less or as many components as C , this algorithm must terminate after a finite number of iterations. Let us illustrate this algorithm in a couple of examples.

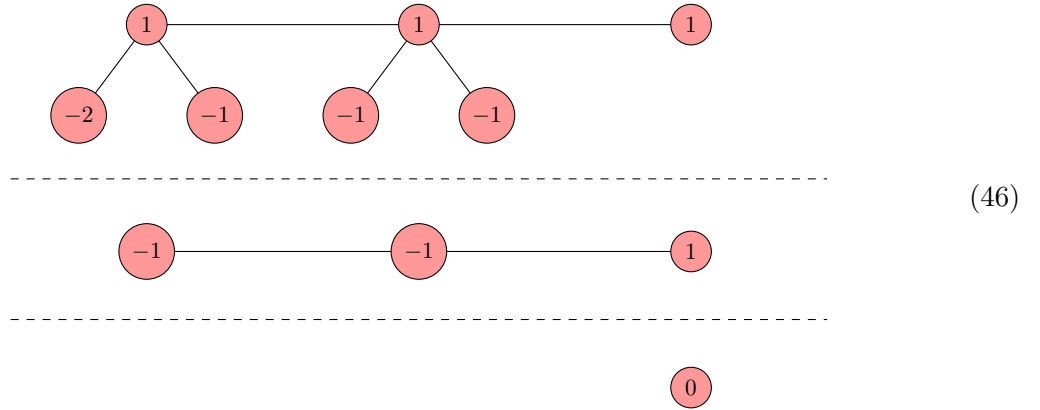
Example 3.8. We first perform the following simplification:



The latter is terminal and we have

$$h^0(C, L) = (0 + 2) + 1 = 3. \quad (45)$$

Example 3.9. We perform the following simplifications:



The latter is terminal and we have $h^0(C, L) = 0 + 1 = 1$.

4. Towards Brill-Noether theory of limit root line bundles

We now turn back to the QSM geometries. Our task is to enumerate all physically relevant limit root bundles on the nodal quark-doublet curve of the QSM geometries. Subsequently, we want to identify their number of global sections. To this end, we first briefly explain the geometric multiplicity (see [50] for more details) and then turn towards the counts relevant for the QSMs.

4.1. The geometric multiplicity

Recall that every line bundle L with degree divisible by r has r^{2g} roots on a smooth curve of genus g . For a nodal curve C^\bullet , the root bundle construction in [50] yields less than r^{2g} limit roots. Indeed, let Γ_C be the dual graph of C^\bullet with edge set $E(\Delta)$ and vertex set $V(\Delta)$. Fix a weighted subgraph Δ^w . Its edges are the nodes at which we blow up and so, it determines a partial normalization $\tilde{\pi}_{\Delta^w} : \tilde{C}_{\Delta^w} \rightarrow C^\bullet$ with dual graph $\Gamma_C \setminus E(\Delta^w)$ and partial blow-up $C_{\Delta^w}^\circ$. Its weights u_i, v_i determine a line bundle $\tilde{\pi}_{\Delta^w}^*(L)(-\sum_i(u_i p_i + v_i q_i))$ on \tilde{C}_{Δ^w} of which we can take the r th root $\tilde{P}_{\Delta^w} \in \text{Pic}(\tilde{C}_{\Delta^w})$, i.e.

$$(\tilde{P}_{\Delta^w})^{\otimes r} \cong \tilde{\pi}_{\Delta^w}^*(L)\left(-\sum_{n_i \in E(\Delta^w)} (u_i p_i + v_i q_i)\right). \quad (47)$$

Degree 1 line bundles on the exceptional components are then glued to \tilde{P}_{Δ^w} to obtain a limit root $P_{\Delta^w}^\circ$ on $C_{\Delta^w}^\circ$. To count the limit roots associated to Δ^w , consider the tower of normalizations:

$$\nu : C^\nu \xrightarrow{\nu_{\Delta^w}} \tilde{C}_{\Delta^w} \xrightarrow{\tilde{\pi}_{\Delta^w}} C^\bullet, \quad (48)$$

where ν_{Δ^w} is the normalization of \tilde{C}_{Δ^w} and C^ν is the full normalization of C^\bullet with geometric genus g^ν and arithmetic genus $g(C^\nu) = g^\nu + 1 - |V(\Delta)|$. The other arithmetic genera can be expressed in terms of g^ν as:

$$g(C^\bullet) = g(C^\nu) + |E(\Delta)| = g^\nu + b_1(\Gamma_C). \quad (49)$$

$$g(\tilde{C}_{\Delta^w}) = g(C^\nu) + |E(\Delta) \setminus E(\Delta^w)| = g^\nu + b_1(\Gamma_C \setminus E(\Delta^w)). \quad (50)$$

The two genera above are related to each other as

$$g(C^\bullet) = g(\tilde{C}_{\Delta^w}) + |E(\Delta^w)| = \sum_{i \in I} g(X_i) + b_1(\Sigma_C), \quad (51)$$

where X_i is a *connected* component of \tilde{C}_{Δ^w} and Σ_C is the dual graph whose vertices are X_i and whose edges are the exceptional components. Taking pullbacks induces the composition

$$\nu^* : \text{Pic}(C^\bullet) \xrightarrow{\tilde{\pi}_{\Delta^w}^*} \text{Pic}(\tilde{C}_{\Delta^w}) \xrightarrow{\nu_{\Delta^w}^*} \text{Pic}(C^\nu). \quad (52)$$

Each root \tilde{P}_{Δ^w} on \tilde{C}_{Δ^w} corresponds to a root on the full normalization with a choice of gluings at the nodes that were not blown up. Since there are r^{2g^ν} roots of $\nu_{\Delta^w}^* \tilde{\pi}_{\Delta^w}^*(L)(-\sum_i(u_i p_i + v_i q_i))$ on C^ν and $r^{b_1(\Gamma_C \setminus E(\Delta^w))}$ choices of gluings, every Δ^w is associated to $r^{2g^\nu + b_1(\Gamma_C \setminus E(\Delta^w))}$ limit r th roots. Summing over the $r^{b_1(\Gamma_C)}$ weighted subgraphs gives

$$\sum_{\Delta^w} r^{2g^\nu + b_1(\Gamma_C \setminus E(\Delta^w))} \quad (53)$$

limit r th roots. To get r^{2g} limit r th roots, we need to multiply each summand with a prefactor called the *geometric multiplicity* in [50], namely

$$\mu_{\Delta^w} = r^{b_1(\Gamma_C) - b_1(\Gamma_C \setminus E(\Delta^w))} = r^{|E(\Delta^w)|} = r^{b_1(\Sigma_C)}.$$

One can interpret this geometrically by saying that a single limit root line bundle corresponds to several root bundles on the corresponding smooth, irreducible curve. In [50], μ_{Δ^w} is the

geometric multiplicity of the connected component of the moduli space of limit roots supported at a given limit root (Lemma 4.1.1). Taking the geometric multiplicity into account, we do indeed get r^{2g} limit roots because

$$\sum_{\Delta^w} (r^{2g^\nu + b_1(\Gamma_C \setminus E(\Delta^w))} \cdot \mu_{\Delta^w}) = \sum_{\Delta^w} r^{2g^\nu + b_1(\Gamma_C)} = r^{b_1(\Gamma_C)} \cdot r^{2g^\nu + b_1(\Gamma_C)} = r^{2g}. \quad (54)$$

In [51], only the blow-ups at the full set of nodes were considered, i.e. $E(\Delta^w) = E(\Delta)$. Hence, $\mu_{\Delta^w} = r^{b_1(\Gamma_C)}$ in that case. The first equality of Equation (54) shows that each Δ^w is associated to $r^{2g^\nu + b_1(\Gamma_C)}$ limit roots when the geometric multiplicity is taken into account. Since this quantity does not depend on the weighted subgraph, we will define this specially.

Definition 4.1. The number of limit roots associated to each weighted subgraph Δ^w is

$$\mu := r^{2g^\nu + b_1(\Gamma_C)}. \quad (55)$$

We conclude this section by studying a simple example taken from [50]. To this end, consider two curves C_1, C_2 with general genera g_1, g_2 (marked in dark pink) and assume that they touch in exactly 3 nodes. The goal is to identify all 3rd limit roots of the structure sheaf. Consequently, we look at the following dual graph:



This graph has $b_1(\Gamma_C) = 2$. We list all limit roots in Table 1. In particular, we find a total number of roots:

$$N_{\text{total}} = 1 \cdot r^0 \cdot r^{2g_\nu + 2} + 6 \cdot r^2 \cdot r^{2g_\nu} + 2 \cdot r^2 \cdot r^{2g_\nu} = (1 + 6 + 2) \cdot \mu = 3^{2(2+g_\nu)}. \quad (57)$$

Since $g(C) = 2 + g_\nu = 2 + g_1 + g_2$, this is exactly the expected number.

4.2. Errata, corrections and immediate extensions of earlier work

By taking the geometric multiplicity into account, we can refine the statistics derived in the earlier publication [51]. There, lower bounds $\check{N}_P^{(3)}$ on the number of limit root bundles with $h^0 = 3$ were derived. By taking the geometric multiplicity into account, we can refine these results. Our findings are listed in Table 2. Note that we have grouped the spaces $\Delta_{128}^\circ, \Delta_{130}^\circ, \Delta_{136}^\circ, \Delta_{236}^\circ$ together. This is because the dual graphs are identical for these spaces. We point out a typo in [51] for the result of Δ_{387}° . The correct result is highlighted in green color in Table 2. There is also an incorrect result for Δ_{856}° in this earlier publication. The dual graph of Δ_{856}° is identical to that of Δ_{882}° , so the lower bounds $\check{N}_P^{(3)}$ must agree for both spaces. A detailed check shows that the results for Δ_{856}° coincide with the numbers listed for Δ_{882}° in [51].

This brief study shows that roughly 50% of all limit root bundles are obtained from a full blowup and have exactly three global sections. The largest percentage is found for Δ_{88} (61.1%). In [51], the geometric multiplicity was not taken into account. These earlier counts falsely led us to the conclusion that for the polytope Δ_8 , the largest fraction of full blowup roots with three global sections were found. However, as listed above, the actual percentage is only 57.3% which is strictly smaller than the result for Δ_{88} .

Before we continue, let us point out that the observations from this initial study are subject to the following subtleties. First, there are more limit root bundles, resulting from partial blowups. Second, for physics applications, we are eventually interested in physical roots. We will discuss the first point momentarily and turn to the second in Section 5.


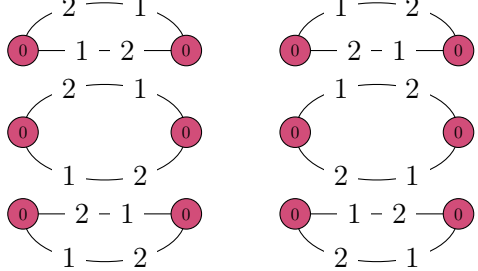
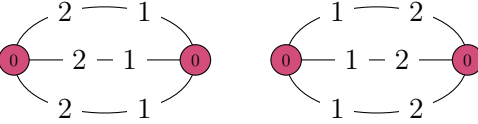
N	Weighted diagram Δ^w	μ_{Δ^w}	N_P
3		r^{2-2}	$r^{(2g_1+2g_2)+2}$
2	inconsistent	–	–
1		r^{2-0}	$r^{(2g_1+2g_2)+0}$
0		r^{2-0}	$r^{(2g_1+2g_2)+0}$

Table 1.: All limit roots on a nodal curve example taken from [50]. The geometric multiplicity is given by $\mu_{\Delta^w} = r^{b_1(\Gamma_C) - b_1(\Gamma_C \setminus E(\Delta^w))}$. The number of nodes left from the blow-up is denoted by N . The number of limit roots is denoted by $N_P = r^{2g_\nu + b_1(\Gamma_C \setminus E(\Delta^w))}$.

4.3. Statistics of partial blowup limit roots in QSM geometries

Let us employ these techniques to the nodal curves relevant for the QSMs. To this end we employ the algorithms available in `gap-4`-package *QSMExplorer*. The latter is part of the `ToricVarieties_project` [36]. Before we list the results, let us discuss the limitations:

1. Not all partial blowups come from tree-like subgraphs. Whenever this is the case, the technology of Section 3 does not apply. Indeed, such configurations matter for the QSM geometries but their number is typically small compared to the tree-like cases. This includes circuits which admit a jump provided that the nodes are moved in special alignment. We will analyze curves of this type in more detail in Section 5. At this point, we cannot treat such curves systematically, but rather rely on a case-by-case study. Therefore, our algorithm merely provides a lower bound in such instances.
2. If the nodal quark-doublet curve contains at least one elliptic curve, then we face the following limitations for partial blowup root bundles. First, if the elliptic curve contains one node that is not blown-up, then the technology of Section 3 does not apply. Otherwise, if there is a $d = 0$ line bundle on an elliptic curve and we are looking for r -th roots, then we know that $r^2 - 1$ of the r^2 roots are guaranteed to have no global sections. The number of global sections on the remaining root depends on whether the original bundle was trivial or not. Distinguishing this is highly non-trivial and definitely goes beyond the topological data considered in our computer scan. Thus, in those cases we provide a lower bound.

If we face one of these two cases, then we can only provide a lower bound to the number of global sections. In particular, in non-generic setups, the actual number of global sections could be strictly larger than this lower bound. Therefore, we will list the roots for which we determine the exact number of global sections and the roots for which we can currently only provide a

		$\check{N}_P^{(3)}$	μ	N_{total}	$\check{N}_P^{(3)} \cdot \mu / N_{\text{total}}$ [%]
$\overline{K}_{B_3}^3 = 6$	Δ_8°	142560	12^3	12^8	57.3
	Δ_4°	11110	12^4	12^8	53.6
	Δ_{134}°	10100	12^4	12^8	48.7
	$\Delta_{128}^\circ, \Delta_{130}^\circ, \Delta_{136}^\circ, \Delta_{236}^\circ$	8910	12^4	12^8	42.0
$\overline{K}_{B_3}^3 = 10$	Δ_{88}°	781.680.888	20^5	20^{12}	61.1
	Δ_{110}°	738.662.983	20^5	20^{12}	57.8
	$\Delta_{272}^\circ, \Delta_{274}^\circ$	736.011.640	20^5	20^{12}	57.5
	Δ_{387}°	733.798.300	20^5	20^{12}	57.3
	$\Delta_{798}^\circ, \Delta_{808}^\circ, \Delta_{810}^\circ, \Delta_{812}^\circ$	690.950.608	20^5	20^{12}	54.0
	Δ_{254}°	35.004.914	20^6	20^{12}	54.7
	Δ_{302}°	34.908.682	20^6	20^{12}	54.7
	Δ_{52}°	34.980.351	20^6	20^{12}	54.7
	Δ_{786}°	32.860.461	20^6	20^{12}	51.3
	Δ_{762}°	32.858.151	20^6	20^{12}	51.3
	Δ_{417}°	32.857.596	20^6	20^{12}	51.3
	Δ_{838}°	32.845.047	20^6	20^{12}	51.3
Δ_{782}°	32.844.379	20^6	20^{12}	51.3	
$\Delta_{377}^\circ, \Delta_{499}^\circ, \Delta_{503}^\circ$	30.846.440	20^6	20^{12}	48.2	
Δ_{1348}°	30.845.702	20^6	20^{12}	48.2	
$\Delta_{882}^\circ, \Delta_{856}^\circ$	30.840.098	20^6	20^{12}	48.2	
Δ_{1340}°	28.954.543	20^6	20^{12}	45.2	
Δ_{1879}°	28.950.852	20^6	20^{12}	45.2	
Δ_{1384}°	27.178.020	20^6	20^{12}	42.5	

Table 2.: The results of [51] listed an incorrect result for Δ_{856}° and displayed a typo for Δ_{387}° . We fix both and refine the earlier findings by use of the geometric multiplicity.

lower bound separately. For Δ_4° with $\mu = 12^4$, our counter finds the following:

N	Percentages		Absolute numbers	
	$h^0 = 3$	$h^0 \geq 3$	$h^0 = 4$	$h^0 \geq 4$
0	53.6		11110	
1	36.7		7601	
2	7.5	0.5	1562	110
3	1.3	0.1	264	11
4		0.3		66
5		0.1		11
7		0.0		1
Σ	99.0	1.0	20537	199

Note that we omit trivial results. Also, the percentages are rounded to one decimal place. Hence, the number 0.0 indicates a non-zero result smaller than 0.045. We observe that $12^4 \cdot (20537 + 199) = 12^8$. Hence, our algorithm indeed enumerated all limit root bundles, in par-

ticular partial blowup limit roots. Therefore, it could tell that at least 99% of all limit roots have exactly three sections on $C_{(\mathbf{3},\mathbf{2})_{1/6}}^\bullet$ irrespective of the complex structure! The remaining percentage of limit roots begs to be investigated in more detail. We will return to this task momentarily in Section 5. Counts similar to Equation (58) are listed in Appendix B. For an overview, we will list the percentages rather than the absolute numbers. For the families of QSM spaces with $\overline{K}_{B_3}^3 = 6$, we summarize our findings in Table 3. Note that E denotes the number of edges and that the nodal quark-doublet curve in Δ_8° contains an elliptic curve. This is the reason why our ignorance is much larger for this curve. The results in Table 3 can be computed in a few minutes on a personal computer. However, for the spaces with $\overline{K}_{B_3}^3 = 10$, the computational challenge increases a lot:

1. The number of ways to conduct partial blowups grows as 2^N with E the number of edges. For $\overline{K}_{B_3}^3 = 6$ spaces, there are at most edges 9 in the dual graph of $C_{(\mathbf{3},\mathbf{2})_{1/6}}^\bullet$. However, for spaces with $\overline{K}_{B_3}^3 = 10$, we can have up to 15 edges. Thus, the number of combinatorial possibilities increases from at most 512 for $\overline{K}_{B_3}^3 = 6$ to up to 32768 for $\overline{K}_{B_3}^3 = 10$.
2. For each of these partial blowups, determining the number of limit root line bundles takes longer since the graph is more complicated.
3. We repeat such a scan for each value of h^0 that we want to find the limit root bundles for. For the spaces with $\overline{K}_{B_3}^3 = 6$, we find all roots after running our algorithm for $h^0 = 3$. However, for $\overline{K}_{B_3}^3 = 10$, we find limit root bundles with $h^0 \in \{3, 4, 5, 6\}$, so that we have to repeat this step up to four times.

In consequence, even on the super-computer `plesken.mathematik.uni-siegen.de`, the computations for the most complicated setups take almost four days. Eventually, this leads to the results summarized in Table 4.

As we can see from Table 3 and Table 4, the biggest limitation for our algorithm is the handling of elliptic curve components. Indeed, whenever at least one $g = 1$ component is present, we can only guarantee that roughly at least 75% of the limit root bundles have $h^0 = 3$. However, whenever no such elliptic curve is present, our ignorance drops significantly and our algorithm finds that at least about 95% have $h^0 = 3$. With an eye towards the F-theory QSMs, it is interesting to wonder if we can lower this ignorance even further. Our immediate focus turns to the polytopes Δ_4° , Δ_{134}° , Δ_{128}° , Δ_{130}° , Δ_{136}° and Δ_{236}° in which we find that at least 99% of all limit root line bundles have $h^0 = 3$. We will study Δ_4 momentarily in Section 5.

Another interesting aspect is to compare our findings to the classical Brill-Noether theory in which one has a continuous space of line bundles and estimates the dimension of the variety of all line bundles with a certain h^0 . This concept does not apply for root bundles since there are only finitely many of them in the first place. To the best of our knowledge, the above tables Table 3 and Table 4 (more details in Appendix B) are the first counts/estimates for such bundles. In this sense, we propose to consider them a first response to the question “what is Brill-Noether theory for limit roots?”. In particular notice from Table 4, that for the QSM setups with $\overline{K}_{B_3}^3 = 10$ we find limit root bundles which always have more than minimal number of global sections.

In the next section, we will study limit roots on circuit-like subgraphs. Since these setups lead to the computation of line bundle cohomology on circuit-like nodal curves, we cannot handle them systematically but rather conduct a case-by-case study. By focusing on Δ_4° , we then find limit roots for which the number of global sections depends on the relative position of the nodes, i.e. depends on the complex structure of this nodal curve. For this reason, we term such

Polytope	E	$h^0 = 3$	$h^0 \geq 3$	$h^0 = 4$	$h^0 \geq 4$
Δ_8°	6	76.4	23.6		
Δ_4°	7	99.0	1.0		
Δ_{134}°	8	99.8	0.2		
$\Delta_{128}^\circ, \Delta_{130}^\circ, \Delta_{136}^\circ, \Delta_{236}^\circ$	9	99.9	0.1		

Table 3.: Statistics of limit roots on $C_{(\mathbf{3},\mathbf{2})_{1/6}}^\bullet$ in all QSM spaces with $\overline{K}_{B_3}^3 = 6$.

Polytope	$h^0 = 3$	$h^0 \geq 3$	$h^0 = 4$	$h^0 \geq 4$	$h^0 = 5$	$h^0 \geq 5$	$h^0 = 6$	$h^0 \geq 6$
Δ_{88}°	74.9	22.1	2.5	0.5	0.0	0.0		
Δ_{110}°	82.4	14.1	3.1	0.4	0.0	0.0		
$\Delta_{272}^\circ, \Delta_{274}^\circ$	78.1	18.0	3.4	0.5	0.0	0.0		
Δ_{387}°	73.8	21.9	3.5	0.7	0.0	0.0		
$\Delta_{798}^\circ, \Delta_{808}^\circ, \Delta_{810}^\circ, \Delta_{812}^\circ$	77.0	17.9	4.4	0.7	0.0	0.0		
Δ_{254}°	95.9	0.5	3.5	0.0	0.0	0.0		
Δ_{52}°	95.3	0.7	3.9	0.0	0.0	0.0		
Δ_{302}°	95.9	0.5	3.5	0.0	0.0	0.0		
Δ_{786}°	94.8	0.3	4.8	0.0	0.0	0.0		
Δ_{762}°	94.8	0.3	4.9	0.0	0.0	0.0		
Δ_{417}°	94.8	0.3	4.8	0.0	0.0	0.0	0.0	
Δ_{838}°	94.7	0.3	5.0	0.0	0.0	0.0		
Δ_{782}°	94.6	0.3	5.0	0.0	0.0	0.0		
$\Delta_{377}^\circ, \Delta_{499}^\circ, \Delta_{503}^\circ$	93.4	0.2	6.2	0.0	0.1	0.0		
Δ_{1348}°	93.7	0.0	6.2	0.0	0.1		0.0	
$\Delta_{882}^\circ, \Delta_{856}^\circ$	93.4	0.3	6.2	0.0	0.1	0.0	0.0	
Δ_{1340}°	92.3	0.0	7.6	0.0	0.1		0.0	
Δ_{1879}°	92.3	0.0	7.5	0.0	0.1		0.0	
Δ_{1384}°	90.9	0.0	8.9	0.0	0.2		0.0	

Table 4.: Statistics of limit roots on $C_{(\mathbf{3},\mathbf{2})_{1/6}}^\bullet$ in selected QSM spaces with $\overline{K}_{B_3}^3 = 10$.

limit roots *jumping-circuits*. In particular, this phenomenon seems to resemble the classical Brill-Noether jump on a smooth, irreducible curve. In the latter case, the points on the curve corresponding to the line bundle divisor in question align such that the Serre dual bundle admits a global section.

5. $\mathcal{O}(10^{11})$ F-theory QSM without vector-like quark-doublets

In this section, we focus on the F-theory QSMs associated to the polytope Δ_4° in the Kreuzer-Skarke database [52]. Specifically, we wish to identify the number of global sections for all limit roots for which our algorithm could only provide a lower bound in Table 3. The upshot of this analysis is that we can identify a condition on the complex structure moduli of those QSM geometries, such that all limit roots on $C_{(\mathbf{3},\mathbf{2})_{1/6}}^\bullet$ have exactly three global sections. This then implies that all physical roots on the smooth, irreducible curve $C_{(\mathbf{3},\mathbf{2})_{1/6}}$ have exactly three global sections. In other words, we can then guarantee that there are no vector-like exotics present.

To this end, we now study all setups in Equation (58) for which only a lower bound is listed.

5.1. Stationary circuits

We begin by looking at two non-resolved nodes. It is not too hard to modify our algorithm to print out the 110 limit roots, for which it can only provided the lower bound $h^0(C^\bullet, P^\bullet) \geq 3$. It turns out that all of them are associated to the following setup:

$$C_1 \quad h^0 = 1 \quad C_2 \quad h^0 = 2 \quad C_3 \quad h^0 = 2 \quad (59)$$

To find out if the lower bound is saturated, we recall that a line bundle on a nodal curve whose irreducible components are all isomorphic to \mathbb{P}^1 is uniquely specified by two pieces of information [65]:

- The degree of the line bundle on each irreducible component.
- Descent data which specifies the gluing conditions at the nodes. The latter corresponds to a number $\lambda \in \mathbb{C}^*$ for each node. In particular, the value of the global sections have to agree at each node up to this factor λ .

So in an ideal world, we would specify the descent data of a line bundle \mathcal{L}^\bullet on a nodal curve C^\bullet , feed this information into the root bundle description of [50] and would end up with the multidegree *and* descent data for each root. In this sense, the information in Equation (59) is incomplete, as it does not detail the descent data. Indeed, we will try simpler. Instead of following the descent data through [50], we will now study all different descent data that we can put on Equation (59). Equivalently, we discuss all line bundles on this nodal curve with the indicated multidegree. The rationale behind this is that we can easily see that all of them admit exactly two global sections on $C_2 \cup C_3$, which is sufficient for our study. The name *stationary circuit* derives from this very observation that *all* of these line bundles have the same number of global sections.

To see that indeed all these line bundles have exactly two global sections on $C_2 \cup C_3$, we pick homogeneous coordinates for C_2, C_3 and parametrize the sections on the curves C_2 and C_3 by $(\alpha_1, \alpha_2, \alpha_3, \alpha_4) \in \mathbb{C}^4$:

Curve	Coordinates	Sections
C_2	$[a : b]$	$\alpha_1 a + \alpha_2 b$
C_3	$[c : d]$	$\alpha_3 c + \alpha_4 d$

(60)

By use of a Möbius transformation, we can assume that the two nodes $C_2 \cap C_3$ are at the following positions:

Label	Coordinates in C_2	Coordinates in C_3
n_1	$[a : b] = [1 : 0]$	$[c : d] = [1 : 0]$
n_2	$[a : b] = [0 : 1]$	$[c : d] = [0 : 1]$

(61)

We now enforce the gluing conditions. At n_1 we demand

$$(\alpha_1 a + \alpha_2 b) ([1 : 0]) = \lambda_1 \cdot (\alpha_3 c + \alpha_4 d) ([1 : 0]), \quad (62)$$

where $\lambda_1 \in \mathbb{C}^*$. Similarly, we enforce at n_2 the gluing by demanding

$$(\alpha_1 a + \alpha_2 b) ([0 : 1]) = \lambda_2 \cdot (\alpha_3 c + \alpha_4 d) ([0 : 1]), \quad (63)$$

where $\lambda_2 \in \mathbb{C}^*$. It is not too hard to see that this is equivalent to

$$\alpha_1 = \lambda_1 \alpha_3, \quad \alpha_2 = \lambda_2 \alpha_4. \quad (64)$$

Hence, the global sections on $C_2 \cup C_3$ are parametrized by $(\alpha_3, \alpha_4) \in \mathbb{C}^2$ via

Curve	Coordinates	Sections
C_2	$[a : b]$	$\lambda_1 \alpha_3 a + \lambda_2 \alpha_4 b$
C_3	$[c : d]$	$\alpha_3 c + \alpha_4 d$

(65)

Hence, irrespective of $\lambda_1, \lambda_2 \in \mathbb{C}^*$, we find exactly two global sections on $C_2 \cup C_3$. Note that we could have rescaled the sections on C_2 such that $\lambda_2 \rightarrow 1$, so that only $\lambda_1 \in \mathbb{C}^*$ appeared in the analysis. We will make use of this simplification in the next section.

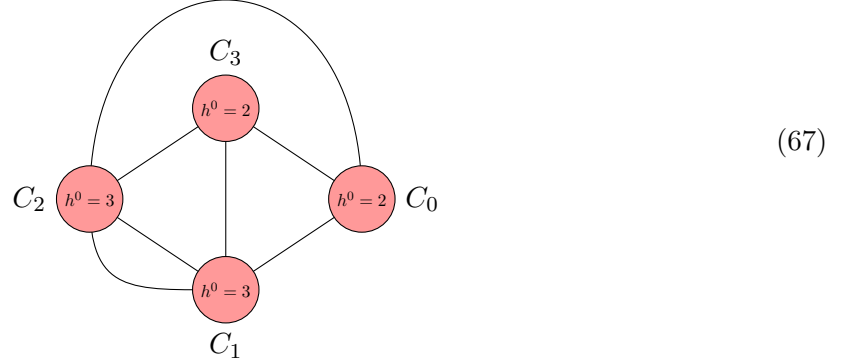
In going back to the setup in Equation (59) we also take C_1 into account. Thereby we find $h^0(C^\bullet, P^\bullet) = 3$. Hence, the lower bound is indeed saturated for this circuit. It is not too hard to repeat this analysis for all circuits with up to five non-resolved nodes. In all of these cases, we find that the lower bound is saturated. We list details in Appendix C and suffice it to note that this improves Equation (58) as follows:

N	Percentages		Absolute numbers	
	$h^0 = 3$	$h^0 \geq 3$	$h^0 = 3$	$h^0 \geq 3$
0	53.6		11110	
1	36.7		7601	
2	8.0		1672	
3	1.3		275	
4	0.3		66	
5	0.1		11	
7		0.0		1
Σ	100.0	0.0	20735	1

(66)

5.2. Jumping circuit

Jump from special node alignment It remains to study the one circuit corresponding to seven remaining nodes:



We parametrize the local sections by $\beta_i \in \mathbb{C}$ and pick homogeneous coordinates of the \mathbb{P}^1 s:

Curve	Coordinates	Sections
C_0	$[u_0 : v_0]$	$\beta_1 u_0 + \beta_2 v_0$
C_1	$[u_1 : v_1]$	$\beta_3 u_1^2 + \beta_4 u_1 v_1 + \beta_5 v_1^2$
C_2	$[u_2 : v_2]$	$\beta_6 u_2^2 + \beta_7 u_2 v_2 + \beta_8 v_2^2$
C_3	$[u_3 : v_3]$	$\beta_9 u_3 + \beta_{10} v_3$

(68)

In the same spirit as in Section 5.1, it is in theory possible to follow the descent data through [50]. Again, this is not necessary for this work and we reserve this task for future investigation. For the time being, we thus again study all descent data for Equation (67), respectively all line bundles on this nodal curves with the displayed multidegree.

Recall that a Möbius transformation allows us to map any three distinct points on a \mathbb{P}^1 to 0, 1 and ∞ . Since there are four nodes on C_1 and C_2 each, a Möbius transformation cannot fix the location of that fourth node. This adds more parameters and allows to tune the location of these nodes. This leads to jumping phenomenon – there is descent data such that the corresponding line bundle jumps from having exactly three global sections to four global sections once the nodes are specially aligned. This mirrors a classical Brill-Noether jump.

While we will not use this effect in the current work, it might be of use in future F-theory MSSM constructions. Let us therefore briefly illustrate these jumps. To this end, we use Möbius transformations and rescalings of the sections on the irreducible components C_i such that the locations of the nodes and the descent data are as follows:

Node	C_0	C_1	C_2	C_3	Descent data
n_1	$[1 : 0]$	$[1 : 0]$			λ_1
n_2	$[1 : 1]$		$[1 : 0]$		1
n_3	$[0 : 1]$			$[1 : 0]$	1
n_4		$[1 : 1]$	$[1 : 1]$		λ_4
n_5		$[0 : 1]$	$[0 : 1]$		λ_5
n_6		$[1 : a]$		$[1 : 1]$	1
n_7			$[1 : b]$	$[0 : 1]$	λ_7

(69)

In this matrix we use $R = \sqrt{\alpha_2^2 - 4\alpha_1\alpha_4}$. For generic parameters $\lambda_1, \lambda_4, \lambda_5, \lambda_7 \in \mathbb{C}^*$, this matrix has $N(A) \cong \mathbb{C}^3$. All 7×7 -minors vanish iff $\lambda_1 = \lambda_4 = \lambda_5 = \lambda_7 = 1$ and

$$N(A) = \text{Span}_{\mathbb{C}} \left(\begin{bmatrix} 0 \\ 0 \\ 0 \\ 1 \\ 0 \\ 0 \\ 1 \\ 0 \\ 0 \\ 0 \end{bmatrix}, \begin{bmatrix} 1 \\ 0 \\ 0 \\ 0 \\ 1 \\ 0 \\ 0 \\ 1 \\ 0 \\ 0 \end{bmatrix}, \begin{bmatrix} 0 \\ 0 \\ 1 \\ 0 \\ 1 \\ 0 \\ 0 \\ 1 \\ 0 \\ 0 \end{bmatrix}, \begin{bmatrix} 0 \\ 1 \\ -\frac{\alpha_1}{\alpha_5} \\ -\frac{\alpha_2}{\alpha_5} \\ -\frac{\alpha_4}{\alpha_5} \\ 0 \\ 0 \\ 0 \\ 0 \\ 1 \end{bmatrix} \right). \quad (79)$$

Hence, $\lambda_1 = \lambda_4 = \lambda_5 = \lambda_7 = 1$ is nothing but the descent data of the canonical bundle. Note that this parametrization differs from Equation (71) since we are now employing the node positions in Equation (77). As a consistency check, recall that we are looking at the nodal curve

$$C^\bullet = V \left(\prod_{i=1}^{28} x_i, s_9 \right). \quad (80)$$

This curve, and also the line bundle in question, remain completely unchanged as we replace s_9 by $\mu \cdot s_9$, where $\mu \in \mathbb{C}^*$ is arbitrary but fixed. Therefore, the null space computed above must be invariant upon rescaling the coefficients of s_9 via $\alpha_i \rightarrow \mu \cdot \alpha_i$. Indeed, this is the case for the null space in Equation (79).

We must now wonder which descent data encodes the physically relevant root. To this end, recall that in following [49], we are solving the root bundle constraint $P_\bullet^{12} = K_{C^\bullet}^{12}$. We found in Section 5.1 that all solutions but the jumping circuit have exactly three global sections. Apparently, $P_\bullet = K_{C^\bullet}$ is a solution and by theory it must always hold $h^0(C^\bullet, K_{C^\bullet}) = 4$. Hence, this solution was not found before and must correspond to the jumping circuit. Therefore, the physically relevant root bundle on this jumping circuit is nothing but the canonical bundle.

We recall that the root bundle conditions are necessary conditions, in that it is not yet clear which of these solutions are obtained top-down from an F-theory gauge potential. Our analysis shows that more than 99.995% of the solutions to these necessary conditions have exactly three global sections. If realized top-down from an F-theory gauge potential, this means that this solution has no vector-like exotics in the representation $C_{(\mathbf{3}, \mathbf{2})_{1/6}}^\bullet$.

5.3. Towards absence of vector-like exotics

Recall that in every QSM geometry, there are three curves with identical topology:

$$C_{(\mathbf{3}, \mathbf{2})_{1/6}} = V(s_3, s_9), \quad C_{(\mathbf{3}, \mathbf{1})_{-2/3}} = V(s_5, s_9), \quad C_{(\mathbf{1}, \mathbf{1})_1} = V(s_1, s_5). \quad (81)$$

Our arguments apply to each of these curves. In focusing on the spaces in $B_3(\Delta_4^\circ)$, let us explicitly parametrize s_1 and s_9 :

$$\begin{aligned}
s_1 = & \alpha_1 \cdot x_0^6 x_4^5 x_5^4 x_6^3 x_7^2 x_8 x_9^4 x_{10}^3 x_{11}^2 x_{12} x_{14}^2 x_{15} x_{17}^4 x_{18}^3 x_{19}^2 x_{20} x_{22}^2 x_{25}^2 x_{26} \\
& + \alpha_2 \cdot x_0^3 x_3^3 x_4^3 x_5^3 x_6^3 x_7^3 x_8^3 x_9^2 x_{10}^2 x_{11}^2 x_{12}^2 x_{13}^2 x_{14} x_{15} x_{16} x_{17}^2 x_{18}^2 x_{19}^2 x_{20}^2 x_{21}^2 x_{22} x_{23} x_{25} x_{26} x_{27} \\
& + \alpha_3 \cdot x_0 x_1 x_2 x_3 x_4 x_5 x_6 x_7 x_8 x_9 x_{10} x_{11} x_{12} x_{13} x_{14} x_{15} x_{16} x_{17} x_{18} \\
& \quad \times x_{19} x_{20} x_{21} x_{22} x_{23} x_{24} x_{25} x_{26} x_{27} x_{28} \\
& + \alpha_4 \cdot x_0^6 x_4 x_5^2 x_6^3 x_7^4 x_8^5 x_{10} x_{11}^2 x_{12}^3 x_{13}^4 x_{15} x_{16}^2 x_{18} x_{19}^2 x_{20}^3 x_{21}^4 x_{23}^2 x_{26} x_{27}^2 \\
& + \alpha_5 \cdot x_0^3 x_9 x_{10} x_{11} x_{12} x_{13} x_{14}^2 x_{15}^2 x_{16}^2 x_{22} x_{23} x_{24}^2 x_{28} \\
& + \alpha_6 \cdot x_1^3 x_{17} x_{18} x_{19} x_{20} x_{21} x_{22} x_{23} x_{24} x_{25}^2 x_{26}^2 x_{27}^2 x_{28}^2, \\
s_9 = & \beta_1 \cdot x_0^6 x_4^5 x_5^4 x_6^3 x_7^2 x_8 x_9^4 x_{10}^3 x_{11}^2 x_{12} x_{14}^2 x_{15} x_{17}^4 x_{18}^3 x_{19}^2 x_{20} x_{22}^2 x_{25}^2 x_{26} \\
& + \beta_2 \cdot x_0^3 x_3^3 x_4^3 x_5^3 x_6^3 x_7^3 x_8^3 x_9^2 x_{10}^2 x_{11}^2 x_{12}^2 x_{13}^2 x_{14} x_{15} x_{16} x_{17}^2 x_{18}^2 x_{19}^2 x_{20}^2 x_{21}^2 x_{22} x_{23} x_{25} x_{26} x_{27} \\
& + \beta_3 \cdot x_0 x_1 x_2 x_3 x_4 x_5 x_6 x_7 x_8 x_9 x_{10} x_{11} x_{12} x_{13} x_{14} x_{15} x_{16} x_{17} x_{18} \\
& \quad \times x_{19} x_{20} x_{21} x_{22} x_{23} x_{24} x_{25} x_{26} x_{27} x_{28} \\
& + \beta_4 \cdot x_0^6 x_4 x_5^2 x_6^3 x_7^4 x_8^5 x_{10} x_{11}^2 x_{12}^3 x_{13}^4 x_{15} x_{16}^2 x_{18} x_{19}^2 x_{20}^3 x_{21}^4 x_{23}^2 x_{26} x_{27}^2 \\
& + \beta_5 \cdot x_0^3 x_9 x_{10} x_{11} x_{12} x_{13} x_{14}^2 x_{15}^2 x_{16}^2 x_{22} x_{23} x_{24}^2 x_{28} \\
& + \beta_6 \cdot x_1^3 x_{17} x_{18} x_{19} x_{20} x_{21} x_{22} x_{23} x_{24} x_{25}^2 x_{26}^2 x_{27}^2 x_{28}^2.
\end{aligned} \tag{82}$$

Now, we demand that

$$\alpha_1, \alpha_4, \alpha_5 \neq 0, \quad \alpha_2^2 \neq 4\alpha_1\alpha_4, \quad \beta_1, \beta_4, \beta_5 \neq 0, \quad \beta_2^2 \neq 4\beta_1\beta_4. \tag{83}$$

Then, by the above arguments, we are guaranteed that for each of the $\mathcal{O}(10^{11})$ toric spaces in $B_3(\Delta_4^\circ)$, more than 99.995% of the limit root bundle on the nodal curves $C_{(\overline{\mathbf{3}}, \mathbf{2})_{1/6}}^\bullet$, $C_{(\overline{\mathbf{3}}, \mathbf{1})_{-2/3}}^\bullet$ and $C_{(\mathbf{1}, \mathbf{1})_1}^\bullet$ which satisfies the necessary condition identified in [49] have exactly three global sections. Let us emphasize that these root bundle conditions are necessary but not sufficient for a physical (i.e. induced from an F-theory gauge potential) root bundle. Hence, the physical roots are special among the ones covered in this article. Since we have found that more than 99.995% of the limit roots in this superset have exactly three sections, this indicates that the chances are good that this carries over to the physical roots in the representations $(\mathbf{3}, \mathbf{2})_{1/6}$, $(\overline{\mathbf{3}}, \mathbf{1})_{-2/3}$ and $(\mathbf{1}, \mathbf{1})_1$.

6. Conclusion and Outlook

Root bundles appear prominently in studies of vector-like spectra of 4d F-theory compactifications. Of particular importance to phenomenology are the Quadrillion F-theory Standard Models (F-theory QSMs) [32]. In this work, we have analyzed a superset of all physical root bundles for the matter representations $(\mathbf{3}, \mathbf{2})_{1/6}$, $(\overline{\mathbf{3}}, \mathbf{1})_{-2/3}$ and $(\mathbf{1}, \mathbf{1})_1$ in $\mathcal{O}(10^{11})$ F-theory QSM geometries. We have found that more than 99.995% of the roots in this superset have exactly three global sections.

We arrived at this finding from a systematic study of a large fraction of QSM geometries. While our results are strongest for the family $B_3(\Delta_4^\circ)$ of toric 3-folds obtained from full, regular, star triangulations of the 4-th polytope in the Kreuzer-Skarke list of 3-dimensional, reflexive polytopes [52], the results for this large fraction of QSM geometries provide statistical evidence

that the absence of the vector-like exotics in the representations $(\mathbf{3}, \mathbf{2})_{1/6}$, $(\bar{\mathbf{3}}, \mathbf{1})_{-2/3}$ and $(\mathbf{1}, \mathbf{1})_1$ is a very likely scenario within the QSMs.

In the QSM geometries, vector-like spectra are counted by the cohomologies of line bundles which are necessarily roots of (twists of certain powers of) the canonical bundle [49]. Such root bundles $P_{\mathbf{R}}$ on the matter curve $C_{\mathbf{R}}$ are by no means unique. Even more, it is not clear exactly which ones are induced top-down from F-theory gauge potentials in the Deligne cohomology. First, on one matter curve, only a subset of all mathematically allowed root bundles could be induced from all physically allowed F-theory gauge potentials. Secondly, it is conceivable that fluxes which induce a specific root bundle on matter curve C_1 , only induce a few selected root bundles on another matter curve C_2 . The study of these questions is involved and currently beyond our abilities. While we hope to return to these questions in future work, in the current work we opted for a local and bottom-up analysis instead. In this sense, we followed the philosophy of the earlier works [49, 51]. The presented study is bottom-up in that we studied *all* mathematically allowed root bundles. In particular, our study covers all root bundles that could possibly be induced from the G_4 -flux and all spin bundles on the matter curve in question. Our study is local in that we focused on one matter curve at a time. Correlations among the vector-like spectra of different matter curves were not taken into account. Hence, we study a set of root bundles on each matter curve, which is a (proper) superset to all physically allowed root bundles. For one family of QSM geometries, we argue that all those roots in this superset have exactly three sections. Consequently, since the physical roots are a subset of the set of roots that we study, the absence of vector-like exotics follows.

A crucial step towards this goal was triangulation independence. Specifically, each family $B_3(\Delta^\circ)$ of toric 3-fold QSM base spaces admits a triangulation independent nodal limit [51]. This observation allows us to probe the vector-like spectra on the entire family $B_3(\Delta^\circ)$ from vector-like spectra on just 5 nodal curves. Another motivation for this deformation is that on smooth, irreducible curves, it is hard to construct root bundles, not to mention count their global sections. On nodal curves however, the construction of all limit root bundles has been detailed in [50]. For the family $B_3(\Delta_4^\circ)$ – associated to the 4-th polytope in the Kreuzer-Skarke list of 3-dimensional polytopes – which consists of $\mathcal{O}(10^{11})$ different toric spaces, we showed that all limit root bundles on the nodal curves $C_{(\mathbf{3}, \mathbf{2})_{1/6}}^\bullet$, $C_{(\bar{\mathbf{3}}, \mathbf{1})_{-2/3}}^\bullet$ and $C_{(\mathbf{1}, \mathbf{1})_1}^\bullet$ have exactly three global sections. By upper semi-continuity, this must hold true on the corresponding smooth, irreducible matter curves in each space of $B_3(\Delta_4^\circ)$. This then implies the absence of vector-like exotics.

Apparently, this argument relies on the ability to compute the cohomologies of *all* limit root bundles. This is exactly the domain of Brill-Noether theory. By following the original work in [50], we find that for some limit roots, this is equivalent to line bundle cohomology on tree-like curves. The remaining limit roots require an understanding of line bundle cohomology on circuit-like curves. We explained this in Section 2. In our applications to the F-theory QSMs, the majority of limit roots arise from tree-like curves with rational irreducible components. Therefore, we presented a computer algorithm that counts line bundle cohomology on such curves in Section 3. The few circuit-like cases are handled by hand.

The reason why there are so few circuits seems related to the fact that we are looking for 12-th and even 20-th roots of the canonical bundle on nodal curves with relatively small Betti numbers, namely 4 and 6. In fact, we observe that lower root indices shift the ratio towards having more circuits. For instance, if instead we were looking at second roots, one should expect equal contributions from tree-like and circuit-like graphs. It would even be conceivable that the circuits would dominate. We reserve a systematic study of line bundle cohomology on circuit-like

curves for future work.

Our algorithm simplifies the pair (C^\bullet, L) of a tree-like, rational, nodal curve and a line bundle L on it by removing components of C^\bullet and adjusting L such that the number of global sections remains unchanged. This simplification eventually terminates and leaves us with a final configuration for which the number of global sections can be read off easily. If we only want to tell if the number of sections is larger than that on a smooth \mathbb{P}^1 , then this algorithm can be optimized further. While this optimization is not directly relevant in order to establish the absence of vector-like exotics in $\mathcal{O}(10^{11})$ QSM geometries, we outlined these steps in Appendix A.

In addition to integrating this algorithm into the algorithm used for [51], we have also taken a combinatorial factor into account. In [50], this factor was introduced as the *geometric multiplicity*. In layman's terms, this multiplicity ensures that we count as many limit root bundles as root bundles on a smooth curve. Alternatively, under a deformation of a smooth to a nodal curve, distinct root bundles on the smooth curve coalesce as we approach the nodal curve. The exact number of distinct roots which coalesce is the geometric multiplicity. In Section 4, we have elaborated in more detail on this factor before pointing out two errors in [51]. The new and refined results were listed in Table 3 and Table 4. The relevant computer algorithms are available in the `gap-4`-package *QSMExplorer* as part of the `ToricVarieties_project` [36]. For convenience of the reader, let us reproduce Table 3 (cf. Appendix B for more details):

Polytope	E	$h^0 = 3$	$h^0 \geq 3$	$h^0 = 4$	$h^0 \geq 4$
Δ_8°	6	76.4	23.6		
Δ_4°	7	99.04	0.96		
Δ_{134}°	8	99.8	0.2		
$\Delta_{128}^\circ, \Delta_{130}^\circ, \Delta_{136}^\circ, \Delta_{236}^\circ$	9	99.9	0.1		

(84)

Hence, by focusing on limit roots on tree-like partial blowups of $C_{(\mathbf{3}, \mathbf{2})_{1/6}}^\bullet$, we have established for the QSM spaces with $\overline{K}_{B_3}^3 = 6$ that are not obtained from FRSTs of Δ_8° , that at least 99% of the limit roots have exactly three global sections. This is a massive improvement compared to [51] in which we merely reached about 60%. Even more, these setups beg for a further investigation of the remaining 1% of the limit roots, which are associated to circuit-like partial blowups.

This is exactly what we have done in Section 5 for the family $B_3(\Delta_4^\circ)$ of QSM spaces obtained from triangulations of the polytope Δ_4° . It turned out that, up to symmetries, only a few line bundles on circuit-like, nodal curves had to be investigated. We found that for some of these circuits, the line bundle cohomology is independent of the relative position of the nodes. We call such circuit-like curves *stationary circuits* (cf. Appendix C for details). These results mirror our finding that for the tree-like blow-up limit roots, the cohomologies are independent of the relative position of the nodes. However, there are special circuits for which such a dependence does exist. In particular, there exists one jumping circuit for the limit roots on $C_{(\mathbf{3}, \mathbf{2})_{1/6}}^\bullet$ in $B_3(\Delta_4^\circ)$. In this case, the number of global sections of line bundles can jump from 3 to 4 as we move the nodes in special alignment. We propose to call such curves *jumping circuits*. It can be speculated that such jumps may be relevant to string model building. We hope to investigate such applications, in particular to F-theory MSSMs, in future works.

To study the jumping circuit for $B_3(\Delta_4^\circ)$ in full detail, we investigated its embedding into all spaces of $B_3(\Delta_4^\circ)$ in Appendix D. This embedding depends on the complex structure moduli

chosen for $C_{(\mathbf{3}, \mathbf{2})_{1/6}}^\bullet$. For the spaces in $B_3(\Delta_4^\circ)$, it holds that

$$\begin{aligned}
C_{(\mathbf{3}, \mathbf{2})_{1/6}}^\bullet &= V \left(\prod_{i=0}^{28} x_i, s_9 \right), \\
s_9 &= \alpha_1 \cdot x_0^6 x_4^5 x_5^4 x_6^3 x_7^2 x_8 x_9^4 x_{10}^3 x_{11}^2 x_{12} x_{14}^2 x_{15} x_{17}^4 x_{18}^3 x_{19}^2 x_{20} x_{22}^2 x_{25}^2 x_{26} \\
&\quad + \alpha_2 \cdot x_0^3 x_3^3 x_4^3 x_5^3 x_6^3 x_7^3 x_8^3 x_9^2 x_{10}^2 x_{11}^2 x_{12}^2 x_{13}^2 x_{14} x_{15} x_{16} x_{17}^2 x_{18}^2 x_{19} \\
&\quad \quad \quad \times x_{20}^2 x_{21}^2 x_{22} x_{23} x_{25} x_{26} x_{27} \\
&\quad + \alpha_3 \cdot x_0 x_1 x_2 x_3 x_4 x_5 x_6 x_7 x_8 x_9 x_{10} x_{11} x_{12} x_{13} x_{14} x_{15} x_{16} x_{17} x_{18} \\
&\quad \quad \quad \times x_{19} x_{20} x_{21} x_{22} x_{23} x_{24} x_{25} x_{26} x_{27} x_{28} \\
&\quad + \alpha_4 \cdot x_3^6 x_4 x_5^2 x_6^3 x_7^4 x_8^5 x_{10} x_{11}^2 x_{12}^3 x_{13}^4 x_{15} x_{16}^2 x_{18} x_{19}^2 x_{20}^3 x_{21}^4 x_{23}^2 x_{26} x_{27}^2 \\
&\quad + \alpha_5 \cdot x_2^3 x_9 x_{10} x_{11} x_{12} x_{13} x_{14}^2 x_{15}^2 x_{16}^2 x_{22} x_{23} x_{24}^2 x_{28} \\
&\quad + \alpha_6 \cdot x_1^3 x_{17} x_{18} x_{19} x_{20} x_{21} x_{22} x_{23} x_{24} x_{25}^2 x_{26}^2 x_{27}^2 x_{28}^2.
\end{aligned} \tag{85}$$

For simplicity, we assumed $\alpha_1, \alpha_4, \alpha_5 \neq 0$ and $\alpha_2^2 \neq 4\alpha_1\alpha_4$. The embedding was then worked out and we found that the global sections on this circuit are encoded by the right null space of

$$A = \begin{bmatrix} \lambda_1 & -\lambda_1 \cdot \frac{\alpha_4}{\alpha_5} & 0 & 0 & -1 & 0 & 0 & 0 & 0 & 0 \\ 1 & 0 & 0 & 0 & 0 & 0 & 0 & -1 & 0 & 0 \\ 0 & 1 & 0 & 0 & 0 & 0 & 0 & 0 & 0 & -1 \\ 0 & 0 & 1 & \frac{-\alpha_2 - R}{2\alpha_4} & \left(\frac{\alpha_2 + R}{2\alpha_4} \right)^2 & -\lambda_4 & -\lambda_4 \left(\frac{-\alpha_2 - R}{2\alpha_4} \right) & -\lambda_4 \left(\frac{\alpha_2 + R}{2\alpha_4} \right)^2 & 0 & 0 \\ 0 & 0 & 1 & \frac{-\alpha_2 + R}{2\alpha_4} & \left(\frac{-\alpha_2 + R}{2\alpha_4} \right)^2 & -\lambda_5 & -\lambda_5 \left(\frac{-\alpha_2 + R}{2\alpha_4} \right) & -\lambda_5 \left(\frac{-\alpha_2 + R}{2\alpha_4} \right)^2 & 0 & 0 \\ 0 & 0 & 1 & 0 & 0 & 0 & 0 & 0 & -1 & \frac{\alpha_1}{\alpha_5} \\ 0 & 0 & 0 & 0 & 0 & 1 & 0 & 0 & -\lambda_7 & 0 \end{bmatrix} \tag{86}$$

In this matrix we use $R = \sqrt{\alpha_2^2 - 4\alpha_1\alpha_4}$. An explicit computation reveals that this right null space is generically of dimension 3. All 7×7 minors of this matrix vanish iff $\lambda_1 = \lambda_4 = \lambda_5 = \lambda_7 = 1$ and the corresponding line bundle then has exactly four sections. Since the multidegrees match those of the canonical bundle on the jumping circuit in Equation (67), we conclude that this very line bundle is nothing but the canonical bundle on this nodal curve. Indeed, we are solving $P_\bullet^{12} = K_{C_\bullet}^{12}$. One solution is apparently $P_\bullet = K_{C_\bullet}$ and by theory $h^0(C_\bullet, K_{C_\bullet}) = 4$. We argued that all other solutions other than the jumping circuit have exactly three global sections. Hence, in this jumping circuit we are interested in K_{C_\bullet} which by theory has to have four global sections. Therefore, we conclude that for the family of toric 3-folds $B_3(\Delta_4^\circ)$, more than 99.995% of the solutions to the necessary root bundle condition – originally derived in [49] – have exactly three global sections. We recall that it is not clear at this point which of these solutions are realized top-down from an F-theory gauge potential. This will likely select a subset of the set of root bundles analyzed in this work. The fact, that more than 99.995% of the roots in this superset have exactly three global sections, indicates that absence of vector-like exotics in the representation $(\mathbf{3}, \mathbf{2})_{1/6}$, $(\bar{\mathbf{3}}, \mathbf{1})_{-2/3}$ and $(\mathbf{1}, \mathbf{1})_1$ is a very likely scenario in the $\mathcal{O}(10^{11})$ QSM geometries $B_3(\Delta_4^\circ)$.

It is, at least in principle, possible to extend this analysis to other QSM spaces. Based on Table 3, one should focus on $B_3(\Delta_{134}^\circ)$, $B_3(\Delta_{128}^\circ)$, $B_3(\Delta_{130}^\circ)$, $B_3(\Delta_{136}^\circ)$, $B_3(\Delta_{236}^\circ)$ next. These geometries and our limit root counts are very similar to those of $B_3(\Delta_4^\circ)$. We should therefore expect similar findings, possibly establishing an even larger class of F-theory Standard Models without vector-like exotics. However, once we turn to spaces with $\overline{K}_{B_3}^3 = 10$, then our argument breaks down. Namely, we can read off from Table 4 that there are root bundles on the canonical nodal matter curves that admit more than three global sections. To understand such setups, one

has to formulate conditions that guarantee that the number of sections remains constant/drops down as one deforms back to a smooth curve. Such conditions will also be vital to guarantee exactly one Higgs pair. It can be speculated that the physics of Yukawa interactions, which informs us how, when and which fields acquire masses upon deformations, will be a good guide towards such conditions. A quest for F-theory MSSM must therefore address this question eventually. We hope to investigate this fascinating and challenging interplay in future works.

As far as the techniques in the current work are concerned, the $\mathcal{O}(10^{11})$ QSM geometries $B_3(\Delta_4^\circ)$ behaved identically. To some extent, this must be seen as very fortunate circumstances. However, many of the intersection numbers – and this applies more generally for all QSM geometries – are triangulation-dependent. This affects the cosmological aspects of these models, including inflation. Namely, as already mentioned in [32], the classical Kähler potential depends on exactly these triangulation-dependent intersection numbers.

While our analysis is streamlined towards the particle phenomenology, specifically the vector-like spectra, of the F-theory QSMs, we were led to establish – what we believe to be the first – computational approaches towards Brill-Noether theory of limit root bundles. The classical Brill-Noether theory concerns a classification of a continuous space of line bundles by their global sections. However, there always exists a finite number N_{total} of root bundles. In this regard, their Brill-Noether theory becomes a question of finding the partition $N_{\text{total}} = N_0 + N_1 + \dots$ in which N_i is the number of root bundles with i global sections. This is exactly how we propose to read our central results in Table 3 and Table 4. Also, we propose to consider a *jumping circuit* as the analogue of a classical Brill-Noether jump.

The ignorances in Table 3 and Table 4 stem from two sources. First, we only provide a lower bound if a node remains on an elliptic curve. For this, one could use theta characteristics to identify a basis of the sections on the elliptic curve in question and then work out the conditions imposed by the gluings at the node. The second limitation arises due to the lack of a systematic treatment of line bundle cohomology on circuit-like nodal curves (with rational or even elliptic) components. In this work, we have treated the relevant cases by hand and proposed to distinguish stationary and jumping circuits. In particular, one could speculate that a circuit of rational curves is jumping if there are at least four nodes on one curve component, owing to the fact that the action of $SL(2, \mathbb{Z})$ can be employed to fix the location of three points. Such a study is reserved for future works and should help to further sharpen our understanding of Brill-Noether theory of limit roots.

Our approach towards Brill-Noether theory of limit root bundles also opens an avenue for a potential machine learning application. Indeed when focusing on (powers of) the canonical bundle, a major part of the information is contained in the dual graph of the nodal curve. For sufficiently simple graphs, our algorithm can – modulo the above-mentioned ignorances – compute an approximation of the Brill-Noether theory of the corresponding limit roots. It would be fascinating to seek a pattern that relates those graphs and the corresponding Brill-Noether approximations (such as Table 3 and Table 4). For a mathematical perspective, this should ideally lead to insights that establish a connection among dual graphs and counts of limit root bundles in a provable manner. With a phenomenological application in mind, one could instead hope to acquire a well-trained algorithm that can estimate the limit root bundles on the Higgs curve, which is currently in most setups beyond our computational abilities. Of course, such counts are then best repeated with conditions that preserve (or explicitly enumerate the defect of) the number of global sections upon deformations, as elaborated upon above.

Finally, it must be mentioned that we have avoided to answer a key question in this program, namely which mathematical roots are induced from an F-theory gauge field in the Deligne cohomology. We anticipate that the answer to that question is involved and have therefore,

decided to analyze the full set of mathematically admissible root bundles instead. In this current work, we have found that in the family $B_3(\Delta_4^\circ)$ of $\mathcal{O}(10^{11})$ different QSM geometries, more than 99.995% of the root bundles in this superset of mathematically admissible root bundles do not have vector-like exotics. This is indicative that absence of vector-like exotics in the representations $(\mathbf{3}, \mathbf{2})_{1/6}$, $(\overline{\mathbf{3}}, \mathbf{1})_{-2/3}$ and $(\mathbf{1}, \mathbf{1})_1$ is a very likely scenario. We reserve a detailed study of the top-down conditions for future work.

Acknowledgement We are grateful to MUYANG LIU for past collaboration, insightful discussions and ongoing collaboration on limit roots on the Higgs curve. The OSCAR computer algebra system was used for key computations in this work, and we thank Lars Kastner and Benjamin Lorenz for valuable discussions. The reliable computations conducted by the supercomputer `plesken.mathematik.uni-siegen.de` allowed us to count limit root bundles. This we truly appreciate. M.B. and M.C. thank the *Ludwig-Maximilians-Universitaet Muenchen* for hospitality during early stages of this project. M.B., R.D. and M.O. are partially supported by the NSF grant DMS 2001673 and by the Simons Foundation Collaboration grant #390287 on “Homological Mirror Symmetry”. M.O. is grateful for the support by the Ph.D. Presidential Fellowship research fund. The work of M.C. is supported by DOE Award DE-SC0013528Y. M.B. and M.C. further acknowledge support by the Simons Foundation Collaboration grant #724069 on “Special Holonomy in Geometry, Analysis and Physics”. M.C. thanks the Slovenian Research Agency No. P1-0306 and the Fay R. and Eugene L. Langberg Chair for support.

A. Speciality

Consider a rational, connected, nodal curve $C := \bigcup_{i \in I} C_i$ and $L \in \text{Pic}(C)$.

Definition A.1. We say that (C, L) with $\deg(L) \geq -1$ is *special* if the following equivalent conditions hold.

- (i) $h^0(C, L)$ jumps (down) under deformation of C ,
- (ii) $h^1(C, L) \neq 0$,
- (iii) $h^0(C, L) \neq \chi(C, L) = \deg(L) + 1$.

Definition A.2. Let $d_i = \deg(L|_{C_i})$. Write $I = I_+ \cup I_-$, where

$$I_- := \{i \in I \mid d_i < 0\}, \quad I_+ := \{i \in I \mid d_i \geq 0\}. \quad (87)$$

Let

$$C_+ := \bigcup_{i \in I_+} C_i, \quad C_- := \bigcup_{i \in I_-} C_i. \quad (88)$$

Note that the curves C_+ , C_- could be disconnected. So, let k_+ and k_- be the numbers of connected components of C_+ and C_- . Let e_i be the intersection number of C_i with C_- and let L_+ be the line bundle on C_+ with $\deg(L_+|_{C_i}) = d_i - e_i$.

Proposition A.3. The pair (C, L) with $\deg(L) \geq -1$ is non-special iff the following conditions hold:

- (i) $h^0(C_+, L_+) = \chi(C_+, L_+)$,
- (ii) $d_i \geq -1$ for all $i \in I$ and $C_i \cap C_j = \emptyset$ for all distinct $i, j \in I_-$.

Proof

Since C is a rational nodal curve, we have the identity

$$\sum_{i \in I_+} e_i = k_+ + k_- - 1. \quad (89)$$

Since Euler characteristics are additive under disjoint union, applying Riemann-Roch to components C_i of C_+ where $g(C_i) = 0$ yields

$$\chi(C_+, L_+) = \deg(L_+) + k_+ = \sum_{i \in I_+} d_i - \sum_{i \in I_+} e_i + k_+. \quad (90)$$

Substituting (90) into the above gives

$$\chi(C_+, L_+) = \sum_{i \in I_+} d_i - k_- + 1 = \deg(L) + 1 - \left(k_- + \sum_{i \in I_-} d_i\right) \geq \chi(C, L), \quad (91)$$

The last inequality follows because $d_i \leq -1$ for all $i \in I_-$ and so,

$$k_- + \sum_{i \in I_-} d_i \leq k_- - |I_-| \leq 0. \quad (92)$$

By Proposition 3.2, $h^0(C, L) = h^0(C_+, L_+)$. Therefore,

$$h^0(C, L) = h^0(C_+, L_+) \geq \chi(C_+, L_+) \geq \chi(C, L). \quad (93)$$

Condition (i) ensures that $h^0(C_+, L_+) = \chi(C_+, L_+)$. Also, $\chi(C_+, L_+) = \chi(C, L)$ iff condition (ii) holds. Indeed, if two curves in C_- intersect, then k_- is strictly less than $|I_-|$. Therefore, the right inequality in Equation (92) is strict. On the other hand, if $d_i < -1$ for some $i \in I_-$, then the left inequality in Equation (92) is strict. Conversely, if condition (ii) holds, then Equation (92) is an equality and $\chi(C_+, L_+) = \chi(C, L)$. \blacksquare

Algorithm 2 ($\deg(L) \geq -1$). Start with (C, L) , where C is a rational, connected, nodal curve and $L \in \text{Pic}(C)$ with $\deg(L) \geq -1$

1. Check condition (ii) of Proposition A.3, which involves the following.
 - (i) Are there any degrees smaller than -1 ? If yes, then (C, L) is special. Otherwise, proceed.
 - (ii) Is I_- trivial? If yes, then (C, L) is not special. Otherwise, proceed.
 - (iii) Do curves with negative degrees intersect? If yes, then (C, L) is special. Otherwise, proceed.
2. Form $I^{(1)} = I_+^{(1)} \cup I_-^{(1)}$, where $d_i = \deg(L|_{C_i})$,

$$I_+^{(1)} = \{i \in I : d_i \geq 0\}, \quad I_-^{(1)} = \{i \in I : d_i < 0\}. \quad (94)$$

If C_i is a curve component of C , then set

$$C_+^{(1)} = \bigcup_{i \in I_+^{(1)}} C_i, \quad C_-^{(1)} = \bigcup_{i \in I_-^{(1)}} C_i. \quad (95)$$

Define a line bundle $L_+^{(1)}$ over $C_+^{(1)}$ such that $\deg(L_+^{(1)}|_{C_i}) = d_i - e_i$ where e_i is the intersection number between C_i and $C_-^{(1)}$.

3. Is $C_+^{(1)} \cap C_-^{(1)} = \emptyset$? If not, feed $(C_+^{(1)}, L_+^{(1)})$ back into step 2 and iterate. Otherwise, proceed.
4. Stop iterating when $C_+^{(n)} \cap C_-^{(n)} = \emptyset$, which means that $(C_+^{(n)}, L_+^{(n)})$ is terminal. Since C has finitely many components, the algorithm will eventually terminate.
5. Check condition (i) of Proposition A.3 by computing $\chi(C, L) = \deg(L) + 1$ and

$$h^0(C_+^{(n)}, L_+^{(n)}) = \sum_{i \in I_+^{(n)}} d_i + k_+(C_+^{(n)}). \quad (96)$$

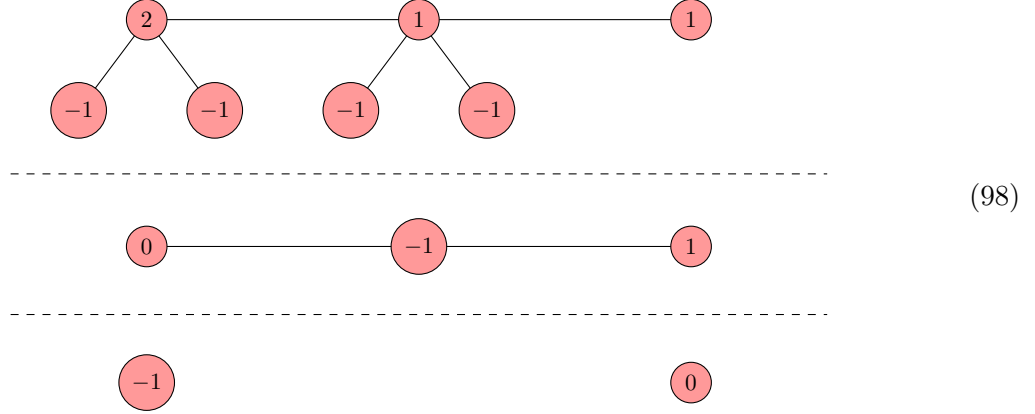
If $h^0(C_+^{(n)}, L_+^{(n)}) \neq \chi(C, L)$, then (C, L) is special. Otherwise, (C, L) is non-special.

This algorithm ultimately seeks to determine if $h^0(C, L) = \chi(C, L)$ by simplifying the curve and checking the conditions of Proposition A.3. Whenever condition (ii) is satisfied in step 1, $\chi(C_+^{(i)}, L_+^{(i)}) = \chi(C_+^{(i+1)}, L_+^{(i+1)})$ by Proposition A.3. In particular, if the algorithm reaches a terminal curve and condition (ii) is satisfied all throughout, then

$$\chi(C, L) = \dots = \chi(C_+^{(n)}, L_+^{(n)}). \quad (97)$$

Thanks to Proposition 3.2, we can use the terminal curve to compute $h^0(C, L) = h^0(C_+^{(n)}, L_+^{(n)})$ in step 5. We check if condition (i) is satisfied by comparing $h^0(C_+^{(n)}, L_+^{(n)})$ with $\chi(C_+^{(n)}, L_+^{(n)})$.

Example A.4. Consider the following pair (C, L) with $\deg(L) = 0$.



Since $I_+^{(2)} \cap I_-^{(2)} = \emptyset$, the algorithm terminates. Since $h^0(C_+^{(2)}, L_+^{(2)}) = 1 = \chi(C, L)$, the curve is non-special.

Definition A.5. The pair (C, L) with $\deg(L) < -1$ is *special* iff $h^0(C, L) > 0$.

This is because $\chi(C, L) = \deg(L) + 1 < 0$.

Algorithm 3 ($\deg(L) < -1$). Start with (C, L) , where C is a rational, connected, nodal curve and $L \in \text{Pic}(C)$ with $\deg(L) < -1$.

1. Form $I^{(1)} = I_+^{(1)} \cup I_-^{(1)}$, where $d_i = \deg(L|_{C_i})$,

$$I_+^{(1)} = \{i \in I : d_i \geq 0\}, \quad I_-^{(1)} = \{i \in I : d_i < 0\}. \quad (99)$$

If C_i is a curve component of C , then set

$$C_+^{(1)} = \bigcup_{i \in I_+^{(1)}} C_i, \quad C_-^{(1)} = \bigcup_{i \in I_-^{(1)}} C_i. \quad (100)$$

Define a line bundle $L_+^{(1)}$ over $C_+^{(1)}$ such that $\deg(L_+^{(1)}|_{C_i}) = d_i - e_i$ where e_i is the intersection number between C_i and $C_-^{(1)}$.

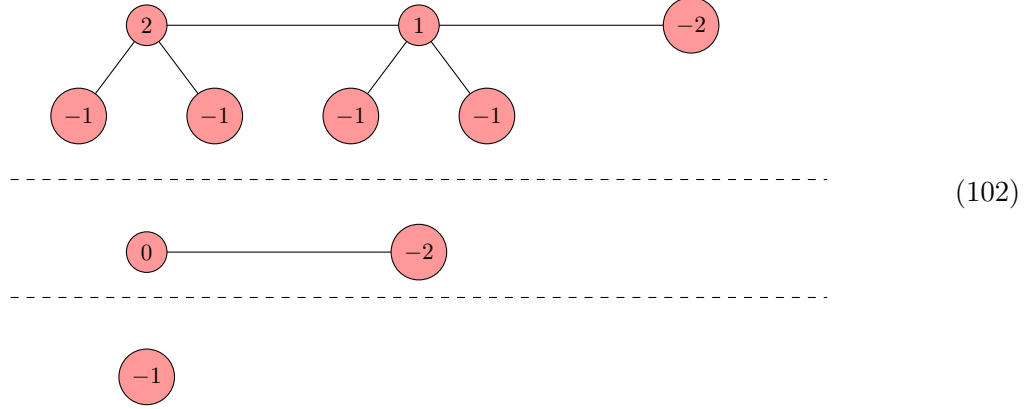
2. After forming $(C_+^{(1)}, L_+^{(1)})$, we perform the following checks:
 - (i) Is $I_+^{(1)} = \emptyset$? If yes, then (C, L) is non-special. Otherwise, proceed.
 - (ii) Is $I_+^{(1)} \cap I_-^{(1)} = \emptyset$? If not, then feed $(C_+^{(1)}, L_+^{(1)})$ into back into Step 2 and iterate. Otherwise proceed.
3. Stop iterating when $C_+^{(n)} \cap C_-^{(n)} = \emptyset$, which means that $(C_+^{(n)}, L_+^{(n)})$ is terminal. Since C has finitely many components, the algorithm will eventually terminate. Compute

$$h^0(C_+^{(n)}, I_+^{(n)}) = \sum_{i \in I_+} d_i + k_+(C_+^{(n)}). \quad (101)$$

4. If $h^0(C_+^{(n)}, I_+^{(n)}) > 0$, then (C, L) is special. If not, then (C, L) is non-special.

This algorithm simplifies (C, L) and allows us to compute $h^0(C, L) = h^0(C_+^{(n)}, L_+^{(n)})$ using the terminal curve thanks to Proposition 3.2.

Example A.6. Consider the following pair (C, L) with $N = 3$ and $\deg(L) = -3$.



Since $I_+^{(2)} \cap I_-^{(2)} = \emptyset$, the algorithm terminates. Since $h^0(C_+^{(2)}, L_+^{(2)}) = 0$, the pair (C, L) is non-special.

We can also formulate an equivalent criterion for determining speciality when $\deg(L) \geq -1$.

Proposition A.7. Let $\deg(L) \geq -1$. Then the following are equivalent:

1. (C, L) is non-special,
2. the restriction of L to every connected subcurve of C has degree ≥ -1 .

Proof

(1) \Rightarrow (2):

Suppose that (C, L) is non-special and there exists a connected subcurve C_{sub} of C such that $\deg(L|_{C_{\text{sub}}}) < -1$. Let $I_{\text{sub}} \subseteq I$ parametrize the components of C_{sub} . Since (C, L) is non-special, $(C_{\text{sub}}, L|_{C_{\text{sub}}})$ satisfies condition (ii) of Proposition A.3 since components of C_{sub} are components of C . So, we have

$$-1 > \deg(L|_{C_{\text{sub}}}) = \sum_{i \in I_{\text{sub}}} d_i \geq \sum_{i \in (I_{\text{sub}})_+} (d_i - e_i) = \deg(L_+|_{(C_{\text{sub}})_+}). \quad (103)$$

The inequality above is strict whenever a component of $(I_{\text{sub}})_-$ intersects more than one component of $(I_{\text{sub}})_+$. Since (C, L) is non-special, $(C_+^{(i)}, L_+^{(i)})$ is non-special for all $i \in \mathbb{N}$ by condition (i) of Proposition A.3. By iterating the argument, we have that $((C_{\text{sub}}^{(i)})_+, (L_{\text{sub}}^{(i)})_+)$ satisfies condition (ii) and

$$-1 > \deg(L|_{C_{\text{sub}}}) \geq \deg(L_+^{(i)}|_{(C_{\text{sub}}^{(i)})_+}) \quad (104)$$

for all $i \in \mathbb{N}$. This includes the terminal pair $((C_{\text{sub}}^{(n)})_+, (L_{\text{sub}}^{(n)})_+)$ for which $(C_{\text{sub}}^{(n)})_+ \cap (C_{\text{sub}}^{(n)})_- = \emptyset$. However, for Equation (104) to hold, the negative degrees must be concentrated in $(I_{\text{sub}}^{(n)})_-$, which violates condition (ii) and contradicts the non-speciality of (C, L) .

(2) \Rightarrow (1):

We first make two simple observations. First, by assumption, $d_i = \deg(L|_{C_i}) \geq -1$. Second, if two components C_i and C_j with degree -1 intersect, then the restriction of L to $C_i \cup C_j$ would have degree $-2 < -1$, which contradicts (2). Hence, no curves with negative degrees intersect.

Recall from Proposition A.3 that (C, L) is non-special iff $d_i \geq -1$, no two components with negative degrees intersect and (C_+, L_+) is non-special. Since we just argued that the first two are satisfied, it remains to show that (C_+, L_+) is non-special.

Consider a connected subcurve C_{sub} of C_+ . Then,

$$\deg(L_+|_{C_{\text{sub}}}) = \sum_{i \in C_{\text{sub}}} (d_i - e_i) = \sum_{i \in \tilde{C}_{\text{sub}}} d_i = \deg(L|_{\tilde{C}_{\text{sub}}}), \quad (105)$$

where \tilde{C}_{sub} is the extension of C_{sub} by all curves in C adjacent to C_{sub} with $d_i = -1$. In particular, \tilde{C}_{sub} is connected. Hence, $\deg(L_+|_{C_{\text{sub}}}) \geq -1$ for all connected subcurves C_{sub} of C_+ by assumption.

By iterating our argument, we conclude that the degree of L_+ on all components in C_+ is greater or equal to -1 . Also, no two components of C_+ with negative degree of L_+ do intersect. Therefore by Proposition A.3, it remains to show that (C_{++}, L_{++}) is non-special.

After sufficiently many iterations, we achieve one of the following configurations $C_+^{(n)}$:

- $(C_+^{(n)})_-$ is disconnected from $(C_+^{(n)})_+$: No components with negative degrees intersect. Hence, $(C_+^{(n)})_-$ is a finite, disjoint union of components, each with $d_i = -1$. So, $h^1(C_+^{(n)}, L_+^{(n)}) = 0$ and $(C_+^{(n)}, L_+^{(n)})$ is non-special.
- $(C_+^{(n)})_- = \emptyset$: Then, $h^1(C_+^{(n)}, L_+^{(n)}) = 0$ and $(C_+^{(n)}, L_+^{(n)})$ is non-special. ■

B. Counts of partial blowup limit roots

In this section we present the detailed counts of limit roots for a number N of remaining nodes. For Δ_8° , there are no limit roots if $N = 4$ or $N = 5$. This repeats for all other spaces. For ease of presentation we omit trivial cases and list absolute numbers of limit roots as multiples of the multiplicity μ introduced in Definition 4.1. Percentages are always rounded to one decimal place. Hence, in the following tables 0.0 indicates a non-zero result smaller than 0.045.

B.1. Spaces with $\overline{K}_{B_3}^3 = 6$

	N	Percentages		Absolute numbers	
		$h^0 = 3$	$h^0 \geq 3$	$h^0 = 3$	$h^0 \geq 3$
$\Delta_8^\circ (\mu = 12^3)$	0	57.3		142560	
	1	19.1	19.1	47520	47520
	2		1.9		4752
	3		2.5		6336
	6		0.1		144
	Σ		76.4	23.6	190080
$\Delta_4^\circ (\mu = 12^4)$	0	53.6		11110	
	1	36.7		7601	
	2	7.5	0.5	1562	110
	3	1.3	0.1	264	11
	4		0.3		66
	5		0.1		11
	7		0.0		1
	Σ		99.0	1.0	20537
$\Delta_{134}^\circ (\mu = 12^4)$	0	48.3		10010	
	1	40.3		8360	
	2	8.6		1782	
	3	2.3		484	
	4	0.3		55	
	5		0.2		44
	8		0.0		1
	Σ		99.8	0.2	20691
$\Delta_{128}^\circ, \Delta_{130}^\circ, \Delta_{136}^\circ, \Delta_{236}^\circ (\mu = 12^4)$	0	43.0		8910	
	1	44.6		9240	
	2	8.0		1650	
	3	3.9		814	
	4	0.3		66	
	5	0.2		33	
	6		0.1		22
	9		0.0		1
	Σ		99.9	0.1	20713

(106)

B.2. Spaces with $\overline{K}_{B_3}^3 = 10$

Table 5.: Percentages

	N	$h^0 = 3$	$h^0 \geq 3$	$h^0 = 4$	$h^0 \geq 4$	$h^0 = 5$	$h^0 \geq 5$	$h^0 = 6$	$h^0 \geq 6$
Δ_{88}°	0	61.1	0.0	2.0		0.0			
	1	12.8	16.2	0.5	0.4		0.0		
	2	1.0	5.2	0.0	0.1				
	3	0.0	0.7		0.0				
	4		0.1						
	5		0.0						
	6		0.0						
	Σ	74.9	22.1	2.5	0.5	0.0	0.0		
Δ_{110}°	0	57.7	0.0	2.2	0.0	0.0			
	1	21.1	9.1	0.9	0.3				
	2	3.3	4.1	0.1	0.1				
	3	0.3	0.8		0.0				
	4	0.0	0.1						
	5		0.0						
	6		0.0						
	Σ	82.4	14.1	3.1	0.4	0.0			
Δ_{272}°	0	57.5	0.0	2.4	0.0	0.0			
	1	17.9	12.2	0.9	0.4	0.0	0.0		
	2	2.4	4.9	0.1	0.1				
	3	0.2	0.9		0.0				
	4	0.0	0.1						
	5		0.0						
	6		0.0						
	Σ	78.1	18.0	3.4	0.5	0.0	0.0		
Δ_{387}°	0	57.3	0.0	2.6		0.0			
	1	14.8	15.2	0.8	0.6	0.0	0.0		
	2	1.6	5.7	0.1	0.1				
	3	0.1	1.0	0.0	0.0				
	4	0.0	0.1						
	5		0.0						
	6		0.0						
	Σ	73.8	21.9	3.5	0.7	0.0	0.0		
Δ_{798}°	0	54.0	0.0	2.9	0.0	0.0			
	1	19.5	11.4	1.3	0.5	0.0	0.0		
Δ_{808}°	2	3.1	5.2	0.2	0.2	0.0	0.0		
	3	0.3	1.1	0.0	0.0				
Δ_{810}°	4	0.0	0.1						
	5	0.0	0.0						
Δ_{812}°	6		0.0						
	Σ	77.0	17.9	4.4	0.7	0.0	0.0		

Percentages – continued on next page

Table 5 – Percentages – continued from previous page

N	$h^0 = 3$	$h^0 \geq 3$	$h^0 = 4$	$h^0 \geq 4$	$h^0 = 5$	$h^0 \geq 5$	$h^0 = 6$	$h^0 \geq 6$
Δ_{254}°	0	54.7		2.2		0.0		
	1	31.8		1.1		0.0		
	2	8.2	0.3	0.2	0.0	0.0	0.0	
	3	1.2	0.2	0.0	0.0			
	4	0.1	0.0	0.0	0.0			
	5	0.0	0.0		0.0			
	6		0.0					
	7		0.0					
	Σ	95.9	0.5	3.5	0.0	0.0	0.0	
Δ_{52}°	0	54.7		2.2		0.0		
	1	31.5		1.3		0.0		
	2	8.0	0.5	0.3	0.0		0.0	
	3	1.1	0.2	0.0	0.0			
	4	0.1	0.1		0.0			
	5	0.0	0.0		0.0			
	6		0.0					
	7		0.0					
	Σ	95.3	0.7	3.9	0.0	0.0	0.0	
Δ_{302}°	0	54.5		2.2		0.0		
	1	32.2		1.1		0.0		
	2	7.9	0.3	0.2	0.0	0.0		
	3	1.2	0.2	0.0	0.0			
	4	0.1	0.0	0.0	0.0			
	5	0.0	0.0		0.0			
	6		0.0					
	7		0.0					
	Σ	95.9	0.5	3.5	0.0	0.0		
Δ_{786}°	0	51.3		2.7		0.0		
	1	32.4		1.7		0.0		
	2	9.3	0.1	0.4	0.0	0.0	0.0	
	3	1.6	0.1	0.0	0.0	0.0	0.0	
	4	0.2	0.0	0.0	0.0			
	5	0.0	0.0	0.0	0.0			
	6	0.0	0.0					
	7		0.0					
	Σ	94.8	0.3	4.8	0.0	0.0	0.0	
Δ_{762}°	0	51.3		2.7		0.0		
	1	32.3		1.7		0.0		
	2	9.3	0.1	0.4	0.0	0.0	0.0	
	3	1.6	0.1	0.1	0.0			
	4	0.2	0.0	0.0	0.0			
	5	0.0	0.0		0.0			
	6	0.0	0.0					
	7		0.0					
	Σ	94.8	0.3	4.9	0.0	0.0	0.0	

Percentages – continued on next page

Table 5 – Percentages – continued from previous page

N	$h^0 = 3$	$h^0 \geq 3$	$h^0 = 4$	$h^0 \geq 4$	$h^0 = 5$	$h^0 \geq 5$	$h^0 = 6$	$h^0 \geq 6$	
Δ_{417}°	0	51.3		2.7		0.0		0.0	
	1	32.4		1.7		0.0			
	2	9.3	0.1	0.4	0.0	0.0	0.0		
	3	1.6	0.1	0.0	0.0	0.0	0.0		
	4	0.2	0.0	0.0	0.0				
	5	0.0	0.0	0.0	0.0				
	6	0.0	0.0						
	7		0.0						
Σ	94.8	0.3	4.8	0.0	0.0	0.0	0.0		
Δ_{838}°	0	51.3		2.7		0.0			
	1	32.3		1.8		0.0			
	2	9.3	0.1	0.5	0.0	0.0	0.0		
	3	1.6	0.1	0.1	0.0		0.0		
	4	0.2	0.0	0.0	0.0				
	5	0.0	0.0		0.0				
	6	0.0	0.0						
	7		0.0						
Σ	94.7	0.3	5.0	0.0	0.0	0.0			
Δ_{782}°	0	51.3		2.7		0.0			
	1	32.3		1.8		0.0			
	2	9.3	0.1	0.5	0.0	0.0	0.0		
	3	1.6	0.1	0.1	0.0		0.0		
	4	0.2	0.0	0.0	0.0				
	5	0.0	0.0		0.0				
	6	0.0	0.0						
	7		0.0						
Σ	94.6	0.3	5.0	0.0	0.0	0.0			
Δ_{377}°	0	48.2		3.1		0.1			
	1	32.7		2.3		0.0			
	2	10.3	0.1	0.7	0.0	0.0	0.0		
	3	2.0	0.1	0.1	0.0	0.0	0.0		
	Δ_{499}°	4	0.2	0.0	0.0	0.0			
		5	0.0	0.0	0.0	0.0			
	Δ_{503}°	6	0.0	0.0					
		7	0.0	0.0					
Σ	93.4	0.2	6.2	0.0	0.1	0.0			
Δ_{1348}°	0	48.2		3.1		0.1		0.0	
	1	32.7		2.3		0.0			
	2	10.4		0.7		0.0			
	3	2.0	0.0	0.1	0.0	0.0			
	4	0.3	0.0	0.0	0.0				
	5	0.0	0.0	0.0	0.0				
	6	0.0	0.0						
	7	0.0	0.0						
Σ	93.7	0.0	6.2	0.0	0.1		0.0		

Percentages – continued on next page

Table 5 – Percentages – continued from previous page

	N	$h^0 = 3$	$h^0 \geq 3$	$h^0 = 4$	$h^0 \geq 4$	$h^0 = 5$	$h^0 \geq 5$	$h^0 = 6$	$h^0 \geq 6$
Δ_{882}°	0	48.2		3.1		0.0		0.0	
	1	32.7		2.3		0.0			
	2	10.3	0.1	0.7	0.0	0.0	0.0		
	3	2.0	0.1	0.1	0.0	0.0	0.0		
	4	0.2	0.0	0.0	0.0				
	5	0.0	0.0	0.0	0.0				
Δ_{856}°	6	0.0	0.0						
	7	0.0	0.0						
	Σ	93.4	0.3	6.2	0.0	0.1	0.0		0.0
Δ_{1340}°	0	45.2		3.5		0.1			0.0
	1	32.9		2.8		0.1			0.0
	2	11.3		1.0		0.0			
	3	2.4	0.0	0.2	0.0	0.0			
	4	0.3	0.0	0.0	0.0				
	5	0.0	0.0	0.0	0.0				
	6	0.0	0.0						
	7	0.0	0.0						
	Σ	92.3	0.0	7.6	0.0	0.1			0.0
Δ_{1879}°	0	45.2		3.5		0.1			0.0
	1	32.9		2.8		0.1			0.0
	2	11.3		1.0		0.0			
	3	2.4	0.0	0.2	0.0	0.0			
	4	0.3	0.0	0.0	0.0				
	5	0.0	0.0	0.0	0.0				
	6	0.0	0.0						
	7	0.0	0.0						
	Σ	92.3	0.0	7.5	0.0	0.1			0.0
Δ_{1384}°	0	42.5		3.8		0.1			0.0
	1	33.0		3.4		0.1			0.0
	2	12.1		1.4		0.0			
	3	2.8		0.3		0.0			
	4	0.4	0.0	0.0	0.0				
	5	0.0	0.0	0.0	0.0				
	6	0.0	0.0						
	7	0.0	0.0						
	Σ	90.9	0.0	8.9	0.0	0.2			0.0

Table 6.: Absolute numbers

	N	$h^0 = 3$	$h^0 \geq 3$	$h^0 = 4$	$h^0 \geq 4$	$h^0 = 5$	$h^0 \geq 5$	$h^0 = 6$	$h^0 \geq 6$
Δ_{88}° $\mu = 20^5$	0	781680888	62712	25196800		106800			
	1	163221088	206886912	5967200	5200000		7200		
	2	13270504	66489896	399200	880400				
	3	504800	9361600		45600				
	4		692000						
	5		24800						
	6		1600						
	Σ	958677280	283519520	31563200	6126000	106800	7200		

Absolute numbers – continued on next page

Table 6 – Absolute numbers – continued from previous page

	N	$h^0 = 3$	$h^0 \geq 3$	$h^0 = 4$	$h^0 \geq 4$	$h^0 = 5$	$h^0 \geq 5$	$h^0 = 6$	$h^0 \geq 6$
Δ_{110}°	$\mu = 20^5$	0	738662983	301017	27732238	5762	168000		
		1	270495495	116866505	10971166	3856834			
		2	41953954	52251246	979978	958822			
		3	3212904	10434296		76800			
		4	83188	930812					
		5		54000					
		6		4000					
Σ		1054408524	180841876	39683382	4898218	168000			
Δ_{272}°	$\mu = 20^5$	0	736011640	131160	30428570	2230	196800		
		1	229717974	156098026	11338671	5229729	2000	31200	
		2	31225880	62229320	1224000	1388800			
		3	2052498	11425902		105600			
		4	43200	1064800					
		5		49600					
		6		2400					
Σ		999051192	231001208	42991241	6726359	198800	31200		
Δ_{387}°	$\mu = 20^5$	0	733798300	59300	32742000		306000		
		1	189788940	194187060	10830000	7116000	72000	36000	
		2	20364840	73241160	1224000	1596000			
		3	1134000	12170000	60000	120000			
		4	34000	1074000					
		5		44400					
		6		2000					
Σ		945120080	280777920	44856000	8832000	378000	36000		
Δ_{798}°	$\mu = 20^5$	0	690950608	123792	37074570	2230	469600		
		1	250171050	146465350	16720271	6645729	128800	54400	
		2	40113524	66594076	2840800	2065600	400	1600	
		3	3586377	13878823	147600	211200			
		4	157600	1506400					
		5	2400	80800					
		6		6400					
Σ		984981559	228655641	56783241	8924759	598800	56000		
Δ_{254}°	$\mu = 20^6$	0	35004914		1396842		9258		
		1	20350604		706580		1822		
		2	5220580	194384	129078	6010	94	4	
		3	759982	111668	11322	2098			
		4	60688	27286	360	276			
		5	2616	3238					
		6		274					
Σ		61399384	336860	2244182	8396	11174	4		
Δ_{52}°	$\mu = 20^6$	0	34980351		1438026		9794		
		1	20149232		862358		1408		
		2	5110469	292371	173179	10368			54
		3	715533	149594	10409	5304			
		4	52346	33342		597			
		5	1308	3817					
		6		127					
Σ		61009239	479255	2483972	16278	11202	54		

Absolute numbers – continued on next page

Table 6 – *Absolute numbers – continued from previous page*

	N	$h^0 = 3$	$h^0 \geq 3$	$h^0 = 4$	$h^0 \geq 4$	$h^0 = 5$	$h^0 \geq 5$	$h^0 = 6$	$h^0 \geq 6$
Δ_{302}°	$\mu = 20^6$	0	34908682		1396458		6388		
		1	20592434		715731		4874		
		2	5055454	194096	121628	5960	320		
		3	741181	118536	11182	2346			
		4	85844	25418	744	174			
		5	6776	4922		39			
		6		786					
		7		27					
	Σ	61390371	343785	2245743	8519	11582			
Δ_{786}°	$\mu = 20^6$	0	32860461		1719897		19661		
		1	20719735		1076991		6835		
		2	5976644	91108	265865	3978	667	13	
		3	1029259	60313	31227	2121	14	11	
		4	106187	17559	1575	264			
		5	6217	2758	18	18			
		6	238	331					
		7		35					
	Σ	60698741	172104	3095573	6381	27177	24		
Δ_{762}°	$\mu = 20^6$	0	32858151		1722871		18984		
		1	20703000		1093360		6702		
		2	5962907	91385	281675	3935	262	18	
		3	1020651	63981	33392	2526			
		4	105082	19543	1338	567			
		5	6182	3022		30			
		6	160	258					
		7		18					
	Σ	60656133	178207	3132636	7058	25948	18		
Δ_{417}°	$\mu = 20^6$	0	32857596		1723530		18545		77
		1	20722495		1074066		7982		
		2	5980745	90711	260581	4102	880	15	
		3	1024325	66272	30773	2116	14	5	
		4	104665	19054	1548	333			
		5	6204	2749	18	6			
		6	242	320					
		7		31					
	Σ	60696272	179137	3090516	6557	27421	20	77	
Δ_{838}°	$\mu = 20^6$	0	32845047		1739918		20615		
		1	20641615		1137880		9155		
		2	5963926	90449	290774	4354	692	25	
		3	1015475	66705	36569	2288		13	
		4	104650	18640	1686	324			
		5	5772	2871		27			
		6	146	354					
		7		30					
	Σ	60576631	179049	3206827	6993	30462	38		

Absolute numbers – continued on next page

Table 6 – Absolute numbers – continued from previous page

	N	$h^0 = 3$	$h^0 \geq 3$	$h^0 = 4$	$h^0 \geq 4$	$h^0 = 5$	$h^0 \geq 5$	$h^0 = 6$	$h^0 \geq 6$
Δ_{782}°	$\mu = 20^6$	0	32844379		1740840		20654		
		1	20644971		1134088		8228		
		2	5953958	91168	302751	4189	563	16	
		3	1015304	64607	36518	2664		22	
		4	105016	18859	1431	489			
		5	5831	2976		30			
		6	120	303					
		7		25					
Σ		60569579	177938	3215628	7372	29445	38		
Δ_{377}°	$\mu = 20^6$	0	30846440		1997602		34270		
		1	20949495		1457977		17032		
		2	6576718	85540	450756	4812	2094	24	
		3	1265969	50759	69181	3007	50	34	
		4	153456	15220	4308	576			
		5	10846	2811	48	63			
		6	616	240					
		7	16	40					
Σ		59803556	154610	3979872	8458	53446	58		
Δ_{1348}°	$\mu = 20^6$	0	30845702		2000040		33043		54
		1	20949103		1455999		17509		
		2	6682151		437511		2633		
		3	1304785	14941	67651	478	140		
		4	160502	8102	4788	93			
		5	12234	1508	96	3			
		6	646	223					
		7	28	37					
Σ		59955151	24811	3966085	574	53325		54	
Δ_{882}°	$\mu = 20^6$	0	30840098		2005760		31362		308
		1	20954897		1454627		18060		
		2	6582752	84392	439884	5174	3280	26	
		3	1259073	62243	66781	3463	50	10	
		4	150706	17636	4170	768			
		5	10700	2707	48	57			
		6	544	372					
		7	16	36					
Σ		59798786	167386	3971270	9462	52752	36	308	
Δ_{1340}°	$\mu = 20^6$	0	28954543		2237908		49877		216
		1	21074384		1820659		33865		46
		2	7243577		642014		6961		
		3	1554653	4776	121250	186	625		
		4	217875	3851	10569	105			
		5	19271	1008	321	6			
		6	1232	104					
		7	88	30					
Σ		59065623	9769	4832721	297	91328		262	

Absolute numbers – continued on next page

Table 6 – *Absolute numbers – continued from previous page*

	N	$h^0 = 3$	$h^0 \geq 3$	$h^0 = 4$	$h^0 \geq 4$	$h^0 = 5$	$h^0 \geq 5$	$h^0 = 6$	$h^0 \geq 6$
$\Delta_{1879}^\circ \quad \mu = 20^6$	0	28950852		2242073		48482		370	
	1	21078338		1819768		33768		92	
	2	7243403		636926		7878			
	3	1554736	9494	118700	396	754			
	4	215750	5782	10320	243				
	5	18880	1142	312	24				
	6	1266	143						
	7	84	24						
Σ	59063309	16585	4828099	663	90882		462		
$\Delta_{1384}^\circ \quad \mu = 20^6$	0	27178020		2439920		68270		540	
	1	21092430		2184225		56190		230	
	2	7757630		870520		15010			
	3	1806325		193330		2170			
	4	280930	1330	21060	30				
	5	27970	610	930	15				
	6	2060	40						
	7	200	15						
Σ	58145565	1995	5709985	45	141640		770		

C. Stationary circuits in $\mathcal{O}(10^{11})$ F-theory QSMs

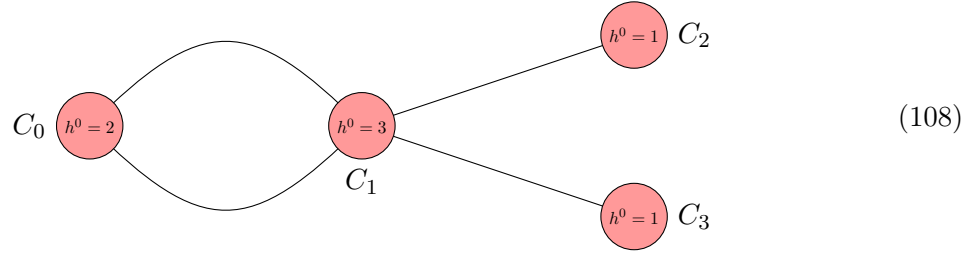
In this section, we count the global sections on the stationary circuits encountered when enumerating the limit roots for the nodal quark-doublet curve in the family of QSM base spaces $B_3(\Delta_4^\circ)$. For this we always encounter nodal curves whose reducible components are smooth rational curves. In the following, we display their dual graphs. The line bundle in question is listed implicitly, by stating the number of sections on each irreducible component. The goal is to argue that for all these configuration, the number of global sections is exactly three.

Three non-resolved nodes Up to symmetry, we are looking at the following setup:

$$\begin{array}{c}
 \begin{array}{ccc}
 C_1 & & C_2 \\
 \circ & \text{---} & \circ \\
 h^0 = 2 & & h^0 = 2
 \end{array} \\
 \\
 \begin{array}{ccc}
 C_3 & & \\
 \circ & \text{---} & \\
 h^0 = 1 & & \\
 \\
 C_0 & & \\
 \circ & & \\
 h^0 = 1 & &
 \end{array}
 \end{array}
 \tag{107}$$

As explained in Section 5.1, there are exactly two global sections on the circuit $C_1 \cup C_2$. On the tree-like curve $C_3 \cup C_4$, there exists exactly one global section by the technology described in Section 3. Hence, we conclude $h^0(C^\bullet, P^\bullet) = 3$.

Four non-resolved nodes Up to symmetry, there are two configurations. The first one is:

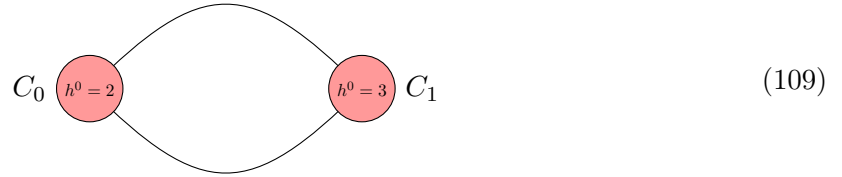


To determine the number of global sections, we recall that a line bundle on a nodal curve whose irreducible components are all isomorphic to \mathbb{P}^1 is uniquely specified by two pieces of information [65]:

- The degree of the line bundle on each irreducible component.
- The descent data, which corresponds to a number $\lambda \in \mathbb{C}^*$ for each node. In particular, the values of the global sections agree at each node up to this factor λ .

Hence, the information displayed above does not specify the descent data. Rather, this diagram encodes an infinite family of line bundles. Our claim is that every line bundle in this family has exactly three global sections.

To see this, we first notice that the (constant) sections on C_2 and C_3 are uniquely fixed by the gluing condition at the nodes $C_1 \cap C_2$ and $C_1 \cap C_3$, respectively. For this reason, we can focus on the following simpler configuration:



We pick local coordinates and parametrize the local sections by $(\alpha_1, \dots, \alpha_5) \in \mathbb{C}^5$:

Curve	Coordinates	Sections
C_0	$[a : b]$	$\alpha_1 a + \alpha_2 b$
C_1	$[c : d]$	$\alpha_3 c^2 + \alpha_4 cd + \alpha_5 d^2$

(110)

By use of a Möbius transformation, the nodes are located at the following positions:

Label	C_0	C_1	Descent data
n_1	$[a : b] = [1 : 0]$	$[c : d] = [1 : 0]$	1
n_2	$[a : b] = [0 : 1]$	$[c : d] = [0 : 1]$	λ

(111)

Upon rescaling of the local sections, we can assume that the gluing conditions are

$$(\alpha_1 a + \alpha_2 b) ([1 : 0]) = (\alpha_3 c^2 + \alpha_4 cd + \alpha_5 d^2) ([1 : 0]) , \quad (112)$$

$$(\alpha_1 a + \alpha_2 b) ([0 : 1]) = \lambda \cdot (\alpha_3 c^2 + \alpha_4 cd + \alpha_5 d^2) ([0 : 1]) , \quad (113)$$

where $\lambda \in \mathbb{C}^*$. This is equivalent to

$$\alpha_1 = \alpha_3, \quad \alpha_2 = \lambda\alpha_5. \quad (114)$$

Hence, the global sections are parameterized by $(\alpha_3, \alpha_4, \alpha_5) \in \mathbb{C}^3$:

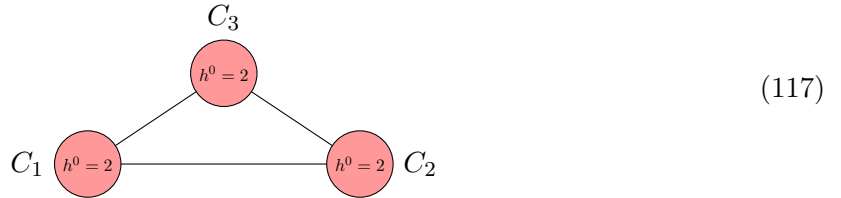
Curve	Coordinates	Sections
C_0	$[a : b]$	$\alpha_3 a + \lambda\alpha_5 b$
C_1	$[c : d]$	$\alpha_3 c^2 + \alpha_4 cd + \alpha_5 d^2$

(115)

In particular, $h^0(C^\bullet, P^\bullet) = 3$. We now turn to the second configuration:



Just as above, we can ignore C_4 and instead focus on the following simpler configuration:



We pick homogeneous coordinates and parametrize the local sections by $(\alpha_1, \dots, \alpha_6) \in \mathbb{C}^6$:

Curve	Coordinates	Sections
C_1	$[a : b]$	$\alpha_1 a + \alpha_2 b$
C_2	$[c : d]$	$\alpha_3 c + \alpha_4 d$
C_3	$[e : f]$	$\alpha_5 e + \alpha_6 f$

(118)

The three nodes are placed, by use of a Möbius transformation, at the following positions:

Label	C_1	C_2	C_3	Descent data
n_1	$[a : b] = [1 : 0]$	$[c : d] = [1 : 0]$		1
n_2	$[a : b] = [0 : 1]$		$[e : f] = [1 : 0]$	1
n_3		$[c : d] = [0 : 1]$	$[e : f] = [0 : 1]$	$\lambda \in \mathbb{C}^*$

(119)

Note that upon a suitable rescaling of the sections on C_2 and C_3 , we can ensure gluing conditions as listed above. Hence, the three gluing conditions are:

$$\alpha_1 = \alpha_3, \quad \alpha_2 = \alpha_5, \quad \alpha_4 = \lambda\alpha_6. \quad (120)$$

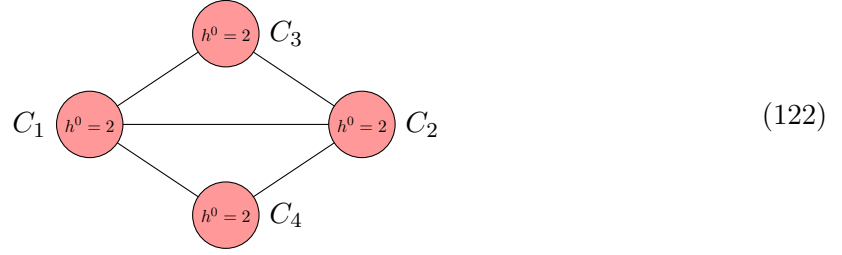
Thus, the global sections are always parametrized by $(\alpha_3, \alpha_5, \alpha_6) \in \mathbb{C}^3$ via:

Curve	Coordinates	Sections
C_1	$[a : b]$	$\alpha_3 a + \alpha_5 b$
C_2	$[c : d]$	$\alpha_3 c + \lambda\alpha_6 d$
C_3	$[e : f]$	$\alpha_5 e + \alpha_6 f$

(121)

In particular, we find $h^0(C^\bullet, P^\bullet) = 3$.

Five non-resolved nodes Up to symmetry, there is only one configuration:



From the previous case study, we know that the triangle $C_1 - C_2 - C_3$ has exactly three global sections. The values of these sections at $C_1 \cap C_4$ and $C_2 \cap C_4$ uniquely fix the sections on C_4 (cf. lemma 7 in [49]) and $h^0(C^\bullet, P^\bullet) = 3$.

D. Jumping circuit in $\mathcal{O}(10^{11})$ F-theory QSMs

In this section we study the location of the nodes of the nodal quark-doublet curve $C_{(\mathbf{3}, \mathbf{2})_{1/6}}^\bullet$ which was originally introduced in [49]. Specifically, we will argue that, in terms of suitable local homogeneous coordinates, the location of these nodes is the same for all QSM geometries associated to the 3-dimensional, reflexive polytope Δ_4° in the Kreuzer-Skarke database [52]. Explicitly, this polytope is given by

$$\Delta_4^\circ = \text{Conv} \left\{ \begin{bmatrix} -1 \\ -1 \\ -1 \end{bmatrix}, \begin{bmatrix} 2 \\ -1 \\ -1 \end{bmatrix}, \begin{bmatrix} -1 \\ 2 \\ -1 \end{bmatrix}, \begin{bmatrix} -1 \\ -1 \\ 5 \end{bmatrix} \right\} \subseteq \mathbb{R}^3. \quad (123)$$

More background information on the constructions can be found e.g. in [32, 51, 53, 62]. This leads to a family $B_3(\Delta_4^\circ)$ of smooth, projective toric varieties. It can be estimated that $B_3(\Delta_4^\circ)$ consists of 3×10^{11} toric spaces [53].

Recall that the nodal quark-doublet curve $C_{(\mathbf{3}, \mathbf{2})_{1/6}}^\bullet$ is given by [49]:

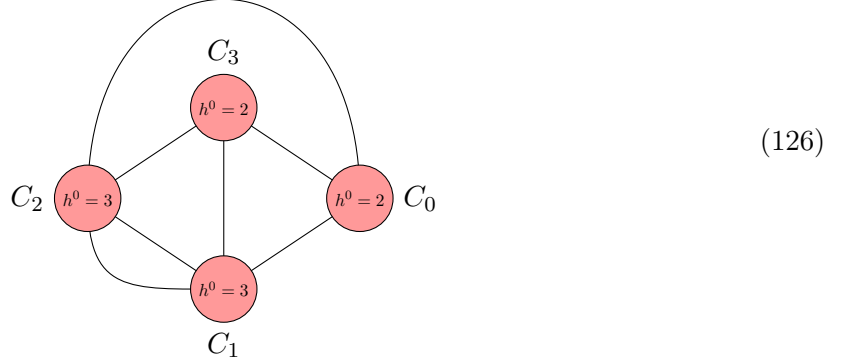
$$C_{(\mathbf{3}, \mathbf{2})_{1/6}}^\bullet = V \left(\prod_{i=0}^{28} x_i, s_9 \right) \subseteq B_3. \quad (124)$$

In this expression $s_9 \in H^0(X_\Sigma, \overline{K}_{X_\Sigma}) \cong \mathbb{C}^6$ and will argue momentarily that

$$\begin{aligned} s_9 = & \alpha_1 \cdot x_0^6 x_4^5 x_5^4 x_6^3 x_7^2 x_8 x_9^4 x_{10}^3 x_{11}^2 x_{12} x_{14}^2 x_{15} x_{17}^4 x_{18}^3 x_{19}^2 x_{20} x_{22}^2 x_{25}^2 x_{26} \\ & + \alpha_2 \cdot x_0^3 x_3^3 x_4^3 x_5^3 x_6^3 x_7^3 x_8^3 x_9^2 x_{10}^2 x_{11}^2 x_{12}^2 x_{13}^2 x_{14} x_{15} x_{16} x_{17}^2 x_{18}^2 x_{19}^2 x_{20}^2 x_{21}^2 x_{22} x_{23} x_{25} x_{26} x_{27} \\ & + \alpha_3 \cdot x_0 x_1 x_2 x_3 x_4 x_5 x_6 x_7 x_8 x_9 x_{10} x_{11} x_{12} x_{13} x_{14} x_{15} x_{16} x_{17} x_{18} \\ & \quad \times x_{19} x_{20} x_{21} x_{22} x_{23} x_{24} x_{25} x_{26} x_{27} x_{28} \\ & + \alpha_4 \cdot x_3^6 x_4 x_5^2 x_6^3 x_7^4 x_8^5 x_{10} x_{11}^2 x_{12}^3 x_{13}^4 x_{15} x_{16}^2 x_{18} x_{19}^2 x_{20}^3 x_{21}^4 x_{23}^2 x_{26} x_{27}^2 \\ & + \alpha_5 \cdot x_2^3 x_9 x_{10} x_{11} x_{12} x_{13} x_{14}^2 x_{15}^2 x_{16}^2 x_{22} x_{23} x_{24}^2 x_{28} \\ & + \alpha_6 \cdot x_1^3 x_{17} x_{18} x_{19} x_{20} x_{21} x_{22} x_{23} x_{24} x_{25}^2 x_{26}^2 x_{27}^2 x_{28}^2, \end{aligned} \quad (125)$$

where x_i are the homogeneous coordinates of $X_\Sigma \in B_3(\Delta_4^\circ)$. The parameters $\alpha_i \in \mathbb{C}$ provide a (possibly redundant) parametrization of the complex structure moduli of $C_{(\mathbf{3}, \mathbf{2})_{1/6}}^\bullet$. As explained

in Section 2.5, to count limit roots we can always pass to a simplified nodal curve by removing circuits. The dual graph of this simplified curve is for all spaces $X_\Sigma \in B_3(\Delta_4^\circ)$ given by:



The irreducible components C_i displayed in Equation (126) are given by $C_i = V(x_i, s_9)$. We conduct a detailed study of this curve under the simplifying assumption

$$\alpha_4 \neq 0, \quad \alpha_2^2 \neq 4\alpha_1\alpha_4, \quad (127)$$

We will identify homogeneous coordinates $[u_i : v_i]$ of C_i and show that the location of the nodes of the circuit Equation (126) are independent of the FRSTs of Δ_4° . More explicitly, we will argue that for all $X_\Sigma \in B_3(\Delta_4^\circ)$, the location of these nodes is then given as follows:

Label	Superset	Coordinates in first curve	Coordinates in second curve
n_1	$C_0 \cap C_1$	$[u_0 : v_0] = [\alpha_5 : -\alpha_4]$	$[u_1 : v_1] = [0 : 1]$
n_2	$C_0 \cap C_2$	$[u_0 : v_0] = [1 : 0]$	$[u_2 : v_2] = [0 : 1]$
n_3	$C_0 \cap C_3$	$[u_0 : v_0] = [0 : 1]$	$[u_3 : v_3] = [0 : 1]$
n_4	$C_1 \cap C_2$	$\left[1 : \frac{-\alpha_2 - \sqrt{\alpha_2^2 - 4\alpha_1\alpha_4}}{2\alpha_4} \right]$	$\left[1 : \frac{-\alpha_2 - \sqrt{\alpha_2^2 - 4\alpha_1\alpha_4}}{2\alpha_4} \right]$
n_5	$C_1 \cap C_2$	$\left[1 : \frac{\alpha_2 - \sqrt{\alpha_2^2 - 4\alpha_1\alpha_4}}{2\alpha_4} \right]$	$\left[1 : \frac{\alpha_2 - \sqrt{\alpha_2^2 - 4\alpha_1\alpha_4}}{2\alpha_4} \right]$
n_6	$C_1 \cap C_3$	$[u_1 : v_1] = [1 : 0]$	$[u_3 : v_3] = [\alpha_5 : -\alpha_1]$
n_7	$C_2 \cap C_3$	$[u_2 : v_2] = [1 : 0]$	$[u_3 : v_3] = [1 : 0]$

(128)

D.1. Ray generators

For every $X_\Sigma \in B_3(\Delta_4^\circ)$, the ray generators/toric divisors are one-to-one to the non-trivial lattice points of the polytope

$$\Delta_4^\circ = \text{Conv} \left\{ \begin{bmatrix} -1 \\ -1 \\ -1 \end{bmatrix}, \begin{bmatrix} 2 \\ -1 \\ -1 \end{bmatrix}, \begin{bmatrix} -1 \\ 2 \\ -1 \end{bmatrix}, \begin{bmatrix} -1 \\ -1 \\ 5 \end{bmatrix} \right\}. \quad (129)$$

This polytope has exactly 29 non-trivial lattice points and we make the following assignment of homogeneous variables:

Ray	Lattice points	Variable	Ray	Lattice points	Variable
r_0	$[-1, -1, -1]$	x_0	r_{15}	$[-1, 1, 0]$	x_{15}
r_1	$[2, -1, -1]$	x_1	r_{16}	$[-1, 1, 1]$	x_{16}
r_2	$[-1, 2, -1]$	x_2	r_{17}	$[0, -1, -1]$	x_{17}
r_3	$[-1, -1, 5]$	x_3	r_{18}	$[0, -1, 0]$	x_{18}
r_4	$[-1, -1, 0]$	x_4	r_{19}	$[0, -1, 1]$	x_{19}
r_5	$[-1, -1, 1]$	x_5	r_{20}	$[0, -1, 2]$	x_{20}
r_6	$[-1, -1, 2]$	x_6	r_{21}	$[0, -1, 3]$	x_{21}
r_7	$[-1, -1, 3]$	x_7	r_{22}	$[0, 0, -1]$	x_{22}
r_8	$[-1, -1, 4]$	x_8	r_{23}	$[0, 0, 1]$	x_{23}
r_9	$[-1, 0, -1]$	x_9	r_{24}	$[0, 1, -1]$	x_{24}
r_{10}	$[-1, 0, 0]$	x_{10}	r_{25}	$[1, -1, -1]$	x_{25}
r_{11}	$[-1, 0, 1]$	x_{11}	r_{26}	$[1, -1, 0]$	x_{26}
r_{12}	$[-1, 0, 2]$	x_{12}	r_{27}	$[1, -1, 1]$	x_{27}
r_{13}	$[-1, 0, 3]$	x_{13}	r_{28}	$[1, 0, -1]$	x_{28}
r_{14}	$[-1, 1, -1]$	x_{14}			

(130)

These rays are same for every FRST of Δ_4° . Furthermore, since we construct projective toric varieties X_Σ , they have no torus-factor. Hence, we have the following short-exact sequence:

$$0 \rightarrow M \rightarrow \text{Div}_T(X_\Sigma) \rightarrow \text{Cl}(X_\Sigma). \quad (131)$$

The first map in this sequence is given by $A \in \mathbb{M}(29 \times 3, \mathbb{Z})$ with rows given by the rays in Equation (130). Hence, $\text{Div}_T(X_\Sigma) \rightarrow \text{Cl}(X_\Sigma)$ is the cokernel of A . The latter defines the grading of the Cox ring. Hence, for all FRSTs of Δ_4° , the grading of the Cox ring is the same. Specifically, we can take the Cox ring $S = \mathbb{C}[x_0, \dots, x_{28}]$ to be \mathbb{Z}^{26} -graded via

x_0	x_1	x_2	x_3	x_4	x_5	x_6	x_7	x_8	x_9	x_{10}	x_{11}	x_{12}	x_{13}	x_{14}	x_{15}	x_{16}	x_{17}	x_{18}	x_{19}	x_{20}	x_{21}	x_{22}	x_{23}	x_{24}	x_{25}	x_{26}	x_{27}	x_{28}	
26	-21	-14	-6	-27																									
3	-3	-2	-1	-3																									
7	-6	-4	-2	-8	1																								
11	-9	-6	-3	-12		1																							
15	-12	-8	-4	-16			1																						
19	-15	-10	-5	-20				1																					
8	-7	-5	-2	-9					1																				
12	-10	-7	-3	-13						1																			
16	-13	-9	-4	-17							1																		
20	-16	-11	-5	-21								1																	
24	-19	-13	-6	-25									1																
17	-14	-10	-4	-18										1															
21	-17	-12	-5	-22											1														
25	-20	-14	-6	-26												1													
-13	10	7	3	13													1												
-9	7	5	2	9														1											
-5	4	3	1	5															1										
-1	1	1	1	1																1									
3	-2	-1	-1	-3																	1								
-4	3	2	1	4																		1							
4	-3	-2	-1	-4																			1						
5	-4	-3	-1	-5																				1					
-25	20	14	6	26																					1				
-21	17	12	5	22																						1			
-17	14	10	4	18																							1		
-16	13	9	4	17																								1	

(132)

From this it follows that for every FRST of Δ_4° , we can express $s \in H^0(B_3, \overline{K}_{B_3})$ as in Equation (125). The coefficients $\alpha_i \in \mathbb{C}$ used in the expansion of s provide a (possibly redundant) description of the complex structure moduli of the nodal curve in question. Therefore, these parameters will play a crucial role in the following analysis.

D.2. Vanishing intersections and approximation of Stanley-Reisner ideal

There are many FRSTs of the lattice points in Δ_4° . To approximate them, we follow [53] and compute FRTs of the four facets of Δ_4° :

$$\begin{aligned} f_1 &= \text{Conv} \{r_0, r_1, r_2\}, & f_2 &= \text{Conv} \{r_0, r_1, r_3\}, \\ f_3 &= \text{Conv} \{r_0, r_2, r_3\}, & f_4 &= \text{Conv} \{r_1, r_2, r_3\}. \end{aligned} \quad (133)$$

These have 10, 16, 16 and 10 lattice points respectively. Hence, for the facets the FRTs can be computed relatively quickly. It then follows that every FRST of Δ_4° is the “union” of an FRT of each of its facets. Crucially though, such a “union” need not yield a regular triangulation. In this sense, the FRTs of the facets approximate the FRSTs of Δ_4° .

Triangulations of the facets

The software TOPCOM [66] can enumerate the FRTs of f_1 .² By adding the origin, we obtain fans which define toric varieties. By computing the intersection of the Stanley-Reisner ideals of these toric varieties, we find the ideal I_1 of those elements common to all Stanley-Reisner ideals. All of these tasks can be achieved very efficiently with the computer algebra system OSCAR [68,69]. Explicitly, we run the following code in Julia [70]:

```
# (0) Load Oscar
using Oscar;

# (1) Define the polytope
f1 = convex_hull( [-1 -1 -1; 2 -1 -1; -1 2 -1]);

# (2) Set variable names of our choice
vars_dict = Dict()
vars_dict[matrix(ZZ, [-1 -1 -1])] = "x0";
vars_dict[matrix(ZZ, [2 -1 -1])] = "x1";
vars_dict[matrix(ZZ, [-1 2 -1])] = "x2";
vars_dict[matrix(ZZ, [-1 0 -1])] = "x9";
vars_dict[matrix(ZZ, [-1 1 -1])] = "x14";
vars_dict[matrix(ZZ, [0 -1 -1])] = "x17";
vars_dict[matrix(ZZ, [0 0 -1])] = "x22";
vars_dict[matrix(ZZ, [0 1 -1])] = "x24";
vars_dict[matrix(ZZ, [1 -1 -1])] = "x25";
vars_dict[matrix(ZZ, [1 0 -1])] = "x28";

#(3) Form point set to be triangulated
points = lattice_points(f1);
d = ambient_dim(f1)
pts = vcat(zero_matrix(ZZ, 1, d), matrix(ZZ, transpose(reduce(hcat, points))));

#(4) Triangulate the points
trias = star_triangulations(pts; full=true, regular=true);
trias = [[c[k]-1 for k in 2:length(c)] for c in t for t in trias];

#(5) Compute rays of all toric varieties
fan_rays = matrix(ZZ, points);

#(6) Construct ring which contains all Stanley-Reisner ideals
max_cones = IncidenceMatrix(vcat(trias[1]));
pmfan = Polymake.fan.PolyhedralFan(RAYS=fan_rays, MAXIMAL_CONES=max_cones);
variety = NormalToricVariety(PolyhedralFan{fmpq}(pmfan));
my_vars = [vars_dict[fan_rays[i,:]] for i in 1:nrows(fan_rays)];
```

²Recently, parallel enumerations of triangulations were investigated in [67]. This can lead to significant performance improvements. A computer implementation is available at <https://polymake.org/doku.php/mptopcom>.

```

set_coordinate_names(variety, my_vars);
R = cox_ring(variety);

#(7) Compute all Stanley-Reisner ideals
sr_ideals_julia = [];
for n in 1:length(trias)
    id = stanley_reisner_ideal(R, SimplicialComplex(trias[n]));
    push!(sr_ideals_julia, id);
end;

#(8) Finally intersect all ideals
common_sr_ideal = reduce(intersect, sr_ideals_julia);

```

This identifies 79 FRTs for f_1 and leads to

$$\begin{aligned}
I_1 = \langle & x_{24}x_1, x_{17}x_1, x_2x_1, x_0x_1, x_2x_{28}, x_9x_{28}, x_{14}x_{25}, x_0x_{25}, x_{17}x_{24}, x_9x_2, x_0x_2, x_0x_{14}, \\
& x_9x_{14}x_1, x_0x_{24}x_{28}, x_{14}x_{17}x_{28}, x_9x_{24}x_{25}, x_2x_{17}x_{25}, \\
& x_{22}x_{25}x_{28}x_1, x_{14}x_{22}x_{28}x_1, x_9x_{22}x_{25}x_1, x_{22}x_{24}x_{25}x_{28}, x_{17}x_{22}x_{25}x_{28}, x_{14}x_{22}x_{24}x_{28}, \\
& x_0x_{17}x_{22}x_{28}, x_2x_{22}x_{24}x_{25}, x_9x_{17}x_{22}x_{25}, x_{14}x_2x_{22}x_{24}, x_9x_{14}x_{22}x_{24}, x_0x_9x_{22}x_{24}, \\
& x_{14}x_2x_{17}x_{22}, x_9x_{14}x_{17}x_{22}, x_0x_9x_{17}x_{22} \rangle.
\end{aligned} \tag{134}$$

Similarly, we find 14295, 14295 and 79 FRTs for f_2, f_3, f_4 . Hence, an upper bound for the FRSTs of Δ_4° is $79^2 \times 14295^2 \sim 1.275 \times 10^{12}$ which matches the result in [53]. By repeating the above ideal intersection code for f_2 we find

$$\begin{aligned}
I_2 = \langle & x_{21}x_1, x_{19}x_1, x_{17}x_1, x_3x_1, x_6x_1, x_0x_1, x_{25}x_{27}, x_3x_{27}, x_7x_{27}, x_5x_{27}, x_0x_{27}, x_8x_{26}, \\
& x_6x_{26}, x_4x_{26}, x_3x_{25}, x_7x_{25}, x_5x_{25}, x_0x_{25}, x_{19}x_{21}, x_{18}x_{21}, x_{17}x_{21}, x_{18}x_{20}, x_{17}x_{20}, \\
& x_{17}x_{19}, x_7x_3, x_6x_3, x_5x_3, x_4x_3, x_0x_3, x_6x_8, x_5x_8, x_4x_8, x_0x_8, x_5x_7, x_4x_7, x_0x_7, \\
& x_4x_6, x_0x_6, x_0x_5, x_{18}x_{27}x_1, x_4x_{27}x_1, x_{20}x_{25}x_1, x_8x_{25}x_1, x_5x_{20}x_1, x_4x_{20}x_1, \\
& x_8x_{18}x_1, x_7x_{18}x_1, x_7x_8x_1, x_4x_5x_1, x_6x_{21}x_{27}, x_4x_{21}x_{27}, x_4x_{20}x_{27}, x_8x_{19}x_{27}, \\
& x_8x_{18}x_{27}, x_6x_{18}x_{27}, x_8x_{17}x_{27}, x_6x_{17}x_{27}, x_4x_{17}x_{27}, x_7x_{21}x_{26}, x_5x_{21}x_{26}, x_0x_{21}x_{26}, \\
& x_5x_{20}x_{26}, x_0x_{20}x_{26}, x_3x_{19}x_{26}, x_0x_{19}x_{26}, x_3x_{18}x_{26}, x_7x_{18}x_{26}, x_3x_{17}x_{26}, x_7x_{17}x_{26}, \\
& x_5x_{17}x_{26}, x_8x_{21}x_{25}, x_6x_{21}x_{25}, x_4x_{21}x_{25}, x_6x_{20}x_{25}, x_4x_{20}x_{25}, x_4x_{19}x_{25}, x_8x_{18}x_{25}, \\
& x_8x_{17}x_{25}, x_6x_{17}x_{25}, x_{20}x_{26}x_{27}x_1, x_8x_{20}x_{27}x_1, x_{18}x_{25}x_{26}x_1, x_7x_{20}x_{26}x_1, \\
& x_5x_{18}x_{26}x_1, x_4x_{18}x_{25}x_1, x_{20}x_{21}x_{26}x_{27}, x_{19}x_{20}x_{26}x_{27}, x_{18}x_{19}x_{26}x_{27}, x_{17}x_{18}x_{26}x_{27}, \\
& x_8x_{20}x_{21}x_{27}, x_6x_{19}x_{20}x_{27}, x_4x_{18}x_{19}x_{27}, x_{20}x_{21}x_{25}x_{26}, x_{19}x_{20}x_{25}x_{26}, x_{18}x_{19}x_{25}x_{26}, \\
& x_{17}x_{18}x_{25}x_{26}, x_3x_{20}x_{21}x_{26}, x_7x_{19}x_{20}x_{26}, x_5x_{18}x_{19}x_{26}, x_0x_{17}x_{18}x_{26}, x_8x_{19}x_{20}x_{25}, \\
& x_6x_{18}x_{19}x_{25}, x_4x_{17}x_{18}x_{25}, x_8x_3x_{20}x_{21}, x_7x_8x_{20}x_{21}, x_6x_7x_{20}x_{21}, x_5x_6x_{20}x_{21}, \\
& x_4x_5x_{20}x_{21}, x_0x_4x_{20}x_{21}, x_8x_3x_{19}x_{20}, x_7x_8x_{19}x_{20}, x_6x_7x_{19}x_{20}, x_5x_6x_{19}x_{20}, \\
& x_4x_5x_{19}x_{20}, x_0x_4x_{19}x_{20}, x_8x_3x_{18}x_{19}, x_7x_8x_{18}x_{19}, x_6x_7x_{18}x_{19}, x_5x_6x_{18}x_{19}, \\
& x_4x_5x_{18}x_{19}, x_0x_4x_{18}x_{19}, x_8x_3x_{17}x_{18}, x_7x_8x_{17}x_{18}, x_6x_7x_{17}x_{18}, x_5x_6x_{17}x_{18}, \\
& x_4x_5x_{17}x_{18}, x_0x_4x_{17}x_{18} \rangle.
\end{aligned} \tag{135}$$

We would now like to conclude that $I_1 + I_2 \subseteq I_{\text{SR}}(X_\Sigma)$. There is a minor caveat to this. Suppose that $r_i, r_j \in f_1 \cap f_2$. If $x_i x_j \in I_1$, this means that there is never a triangle in the FRTs of f_1 with r_i and r_j as vertices. However, this is not necessarily the case in f_2 , in which case $x_i x_j \notin I_2$. So, we have to look for such discrepancies and then correct for them. Note that

$f_1 \cap f_2 = \{r_0, r_1, r_{17}, r_{25}\} \leftrightarrow \{x_0, x_1, x_{17}, x_{25}\}$. The relevant generators of I_1 are $x_0x_1, x_0x_{25}, x_1x_{17}$. All are contained in I_2 , so no adjustment is necessary.

By the same logic we find from f_3 :

$$\begin{aligned}
I_3 = \langle & x_{13}x_2, x_{11}x_2, x_9x_2, x_3x_2, x_6x_2, x_0x_2, x_{14}x_{16}, x_3x_{16}, x_7x_{16}, x_5x_{16}, x_0x_{16}, x_8x_{15}, \\
& x_6x_{15}, x_4x_{15}, x_3x_{14}, x_7x_{14}, x_5x_{14}, x_0x_{14}, x_{11}x_{13}, x_{10}x_{13}, x_9x_{13}, x_{10}x_{12}, x_9x_{12}, \\
& x_9x_{11}, x_7x_3, x_6x_3, x_5x_3, x_4x_3, x_0x_3, x_6x_8, x_5x_8, x_4x_8, x_0x_8, x_5x_7, x_4x_7, x_0x_7, \\
& x_4x_6, x_0x_6, x_0x_5, x_{10}x_{16}x_2, x_4x_{16}x_2, x_{12}x_{14}x_2, x_8x_{14}x_2, x_5x_{12}x_2, x_4x_{12}x_2, \\
& x_8x_{10}x_2, x_7x_{10}x_2, x_7x_8x_2, x_4x_5x_2, x_6x_{13}x_{16}, x_4x_{13}x_{16}, x_4x_{12}x_{16}, x_8x_{11}x_{16}, \\
& x_8x_{10}x_{16}, x_6x_{10}x_{16}, x_8x_9x_{16}, x_6x_9x_{16}, x_4x_9x_{16}, x_7x_{13}x_{15}, x_5x_{13}x_{15}, x_0x_{13}x_{15}, \\
& x_5x_{12}x_{15}, x_0x_{12}x_{15}, x_3x_{11}x_{15}, x_0x_{11}x_{15}, x_3x_{10}x_{15}, x_7x_{10}x_{15}, x_3x_9x_{15}, x_7x_9x_{15}, \\
& x_5x_9x_{15}, x_8x_{13}x_{14}, x_6x_{13}x_{14}, x_4x_{13}x_{14}, x_6x_{12}x_{14}, x_4x_{12}x_{14}, x_4x_{11}x_{14}, x_8x_{10}x_{14}, \\
& x_8x_9x_{14}, x_6x_9x_{14}, x_{12}x_{15}x_{16}x_2, x_8x_{12}x_{16}x_2, x_{10}x_{14}x_{15}x_2, x_7x_{12}x_{15}x_2, \\
& x_5x_{10}x_{15}x_2, x_4x_{10}x_{14}x_2, x_{12}x_{13}x_{15}x_{16}, x_{11}x_{12}x_{15}x_{16}, x_{10}x_{11}x_{15}x_{16}, \\
& x_9x_{10}x_{15}x_{16}, x_8x_{12}x_{13}x_{16}, x_6x_{11}x_{12}x_{16}, x_4x_{10}x_{11}x_{16}, x_{12}x_{13}x_{14}x_{15}, \\
& x_{11}x_{12}x_{14}x_{15}, x_{10}x_{11}x_{14}x_{15}, x_9x_{10}x_{14}x_{15}, x_3x_{12}x_{13}x_{15}, x_7x_{11}x_{12}x_{15}, \\
& x_5x_{10}x_{11}x_{15}, x_0x_9x_{10}x_{15}, x_8x_{11}x_{12}x_{14}, x_6x_{10}x_{11}x_{14}, x_4x_9x_{10}x_{14}, \\
& x_8x_3x_{12}x_{13}, x_7x_8x_{12}x_{13}, x_6x_7x_{12}x_{13}, x_5x_6x_{12}x_{13}, x_4x_5x_{12}x_{13}, x_0x_4x_{12}x_{13}, \\
& x_8x_3x_{11}x_{12}, x_7x_8x_{11}x_{12}, x_6x_7x_{11}x_{12}, x_5x_6x_{11}x_{12}, x_4x_5x_{11}x_{12}, x_0x_4x_{11}x_{12}, \\
& x_8x_3x_{10}x_{11}, x_7x_8x_{10}x_{11}, x_6x_7x_{10}x_{11}, x_5x_6x_{10}x_{11}, x_4x_5x_{10}x_{11}, x_0x_4x_{10}x_{11}, \\
& x_8x_3x_9x_{10}, x_7x_8x_9x_{10}, x_6x_7x_9x_{10}, x_5x_6x_9x_{10}, x_4x_5x_9x_{10}, x_0x_4x_9x_{10} \rangle.
\end{aligned} \tag{136}$$

Finally, f_4 leads to

$$\begin{aligned}
I_4 = \langle & x_{24}x_1, x_{21}x_1, x_2x_1, x_3x_1, x_2x_{28}, x_{13}x_{28}, x_{16}x_{27}, x_3x_{27}, x_{21}x_{24}, x_{13}x_2, x_3x_2, x_3x_{16}, \\
& x_{13}x_{16}x_1, x_3x_{24}x_{28}, x_{16}x_{21}x_{28}, x_{13}x_{24}x_{27}, x_2x_{21}x_{27}, x_{23}x_{27}x_{28}x_1, x_{16}x_{23}x_{28}x_1, \\
& x_{13}x_{23}x_{27}x_1, x_{23}x_{24}x_{27}x_{28}, x_{21}x_{23}x_{27}x_{28}, x_{16}x_{23}x_{24}x_{28}, x_3x_{21}x_{23}x_{28}, x_2x_{23}x_{24}x_{27}, \\
& x_{13}x_{21}x_{23}x_{27}, x_{16}x_2x_{23}x_{24}, x_{13}x_{16}x_{23}x_{24}, x_3x_{13}x_{23}x_{24}, x_{16}x_2x_{21}x_{23}, x_{13}x_{16}x_{21}x_{23}, \\
& x_3x_{13}x_{21}x_{23} \rangle.
\end{aligned} \tag{137}$$

There are no discrepancies as mentioned above. Therefore, it follows that for every FRST of Δ_4° it holds $I_1 + I_2 + I_3 + I_4 \subseteq I_{\text{SR}}(X_\Sigma)$.

Interplay of different facets

We can improve this statement further. Namely, $r_i \in f_1$ and $r_j \in f_2$ cannot appear as vertices of a cone of Σ unless $r_i, r_j \in f_1 \cap f_2$. Put differently, if $r_i \in f_1 \setminus f_2$ and $r_j \in f_2 \setminus f_1$, then $x_i x_j \in I_{\text{SR}}(X_\Sigma)$. Hence we notice:

$$\begin{aligned}
& \{r_0, r_1, r_2, r_9, r_{14}, r_{17}, r_{22}, r_{24}, r_{25}, r_{28}\} \subseteq f_1, \\
& \{r_0, r_1, r_3, r_4, r_5, r_6, r_7, r_8, r_{17}, r_{18}, r_{19}, r_{20}, r_{21}, r_{25}, r_{26}, r_{27}\} \subseteq f_2, \\
& \{r_0, r_2, r_3, r_4, r_5, r_6, r_7, r_8, r_9, r_{10}, r_{11}, r_{12}, r_{13}, r_{14}, r_{15}, r_{16}\} \subseteq f_3, \\
& \{r_1, r_2, r_3, r_{13}, r_{16}, r_{21}, r_{23}, r_{24}, r_{27}, r_{28}\} \subseteq f_4.
\end{aligned} \tag{138}$$

Therefore, the above argument implies that for each FRST of Δ_4° , we have $I_5 \subseteq I_{\text{SR}}(X_\Sigma)$ where

$$\begin{aligned}
I_5 = \langle & x_0x_{23}, x_4x_{22}, x_4x_{23}, x_4x_{24}, x_4x_{28}, x_5x_{22}, x_5x_{23}, x_5x_{24}, x_5x_{28}, x_6x_{22}, x_6x_{23}, \\
& x_6x_{24}, x_6x_{28}, x_7x_{22}, x_7x_{23}, x_7x_{24}, x_7x_{28}, x_8x_{22}, x_8x_{23}, x_8x_{24}, x_8x_{28}, x_9x_{22}, \\
& x_9x_{18}, x_9x_{19}, x_9x_{20}, x_9x_{21}, x_9x_{23}, x_9x_{26}, x_9x_{27}, x_{10}x_{17}, x_{10}x_{18}, x_{10}x_{19}, x_{10}x_{20}, \\
& x_{10}x_{21}, x_{10}x_{22}, x_{10}x_{23}, x_{10}x_{24}, x_{10}x_{25}, x_{10}x_{26}, x_{10}x_{27}, x_{10}x_{28}, x_{10}x_{31}, x_{11}x_{17}, \\
& x_{11}x_{18}, x_{11}x_{19}, x_{11}x_{20}, x_{11}x_{21}, x_{11}x_{22}, x_{11}x_{23}, x_{11}x_{24}, x_{11}x_{25}, x_{11}x_{26}, x_{11}x_{27}, \\
& x_{11}x_{28}, x_{11}x_{31}, x_{12}x_{17}, x_{12}x_{18}, x_{12}x_{19}, x_{12}x_{20}, x_{12}x_{21}, x_{12}x_{22}, x_{12}x_{23}, x_{12}x_{24}, \\
& x_{12}x_{25}, x_{12}x_{26}, x_{12}x_{27}, x_{12}x_{28}, x_{12}x_{31}, x_{13}x_{17}, x_{13}x_{18}, x_{13}x_{19}, x_{13}x_{20}, x_{13}x_{22}, \\
& x_{13}x_{25}, x_{13}x_{26}, x_{14}x_{18}, x_{14}x_{19}, x_{14}x_{20}, x_{14}x_{21}, x_{14}x_{23}, x_{14}x_{26}, x_{14}x_{27}, x_{15}x_{17}, \\
& x_{15}x_{18}, x_{15}x_{19}, x_{15}x_{20}, x_{15}x_{21}, x_{15}x_{22}, x_{15}x_{23}, x_{15}x_{24}, x_{15}x_{25}, x_{15}x_{26}, x_{15}x_{27}, \\
& x_{15}x_{28}, x_{15}x_{31}, x_{16}x_{17}, x_{16}x_{18}, x_{16}x_{19}, x_{16}x_{20}, x_{16}x_{22}, x_{16}x_{25}, x_{16}x_{26}, x_{2x_{18}}, \\
& x_{2x_{19}}, x_{2x_{20}}, x_{2x_{26}}, x_{17x_{23}}, x_{18x_{22}}, x_{18x_{23}}, x_{18x_{24}}, x_{18x_{28}}, x_{19x_{22}}, x_{19x_{23}}, \\
& x_{19x_{24}}, x_{19x_{28}}, x_{20x_{22}}, x_{20x_{23}}, x_{20x_{24}}, x_{20x_{28}}, x_{21x_{22}}, x_{22x_{23}}, x_{22x_{26}}, x_{22x_{27}}, \\
& x_{23x_{25}}, x_{23x_{26}}, x_{24x_{26}}, x_{26x_{28}} \rangle. \tag{139}
\end{aligned}$$

Consequently, for every FRST, it follows that

$$I_1 + I_2 + I_3 + I_4 + I_5 \subseteq I_{\text{SR}}(X_\Sigma). \tag{140}$$

This argument can of course be extended to three and four rays. For our purposes, it will be sufficient to notice that this includes $I_6 \subseteq I_{\text{SR}}(X_\Sigma)$ where

$$\begin{aligned}
I_6 = \langle & x_0x_{13}x_{24}, x_3x_9x_{24}, x_9x_{13}x_{24}, x_{13}x_{14}x_{24}, x_3x_{17}x_{28}, x_0x_{21}x_{28}, x_{17}x_{27}x_{28}, x_{21}x_{25}x_{28}, \\
& x_{21}x_0x_9, x_{21}x_0x_{28}, x_4x_9x_{17}, x_1x_9x_4, x_1x_9x_5, x_1x_9x_6, x_1x_9x_7, x_1x_9x_8, x_1x_9x_{16}, \\
& x_1x_{13}x_4, x_1x_{13}x_5, x_1x_{13}x_6, x_1x_{13}x_7, x_1x_{13}x_8, x_1x_{13}x_{14}, x_1x_{14}x_4, x_1x_{14}x_6, \\
& x_1x_{14}x_8, x_1x_{16}x_4, x_1x_{16}x_6, x_1x_{16}x_8, x_1x_{28}x_4, x_1x_{28}x_5, x_1x_{28}x_6, x_1x_{28}x_7, x_1x_{28}x_8, \\
& x_2x_{25}x_4, x_2x_{25}x_8, x_2x_{25}x_{21}, x_2x_{21}x_4, x_2x_{21}x_5, x_2x_{21}x_7, x_2x_{21}x_8, x_2x_{17}x_4, x_2x_{17}x_5, \\
& x_2x_{17}x_7, x_2x_{17}x_8, x_2x_{17}x_{27}, x_2x_{27}x_4, x_2x_{27}x_8, x_2x_{24}x_4, x_2x_{24}x_5, x_2x_{24}x_7, \\
& x_2x_{24}x_8, x_3x_9x_{17}, x_3x_9x_{24}, x_3x_{17}x_{13}, x_3x_{17}x_{28}, x_3x_{8x_{24}}, x_3x_{8x_{28}}, x_8x_{13}x_{21}, \\
& x_0x_{24}x_{28}x_3, x_0x_{24}x_{28}x_{16}, x_0x_{24}x_{28}x_{27}, x_3x_{24}x_{28}x_{14}, x_3x_{24}x_{28}x_{25}, x_{14}x_{24}x_{28}x_{16}, \\
& x_{14}x_{24}x_{28}x_{27} \rangle. \tag{141}
\end{aligned}$$

Vanishing intersections from facet interiors

The following homogeneous coordinates correspond to facet interior points of Δ_4° :

$$I_7 = \{x_{10}, x_{11}, x_{12}, x_{15}, x_{18}, x_{19}, x_{20}, x_{22}, x_{23}, x_{26}\}. \tag{142}$$

Therefore, $V(z, s) = \emptyset$ for all $z \in I_7$ [51].

D.3. The nodal curve

The components

In [51] we argued that the structure of the canonical nodal quark-doublet curve is independent of the FRST. Specifically, we have

$$C_{(\mathbf{3},\mathbf{2})_{1/6}}^\bullet = V\left(\prod_{i=0}^{28} x_i, s_9\right) \subseteq B_3. \quad (143)$$

By taking I_7 into account, it follows that C^\bullet has the following 17 irreducible components (each a smooth \mathbb{P}^1 for generic $s \in H^0(B_3, \overline{K}_{B_3})$):

$$\begin{aligned} C_0^\bullet &= V(x_0, s_9) & C_1^\bullet &= V(x_1, s_9) & C_2^\bullet &= V(x_2, s_9) & C_3^\bullet &= V(x_3, s_9) \\ C_4^\bullet &= V(x_4, s_9) & C_5^\bullet &= V(x_5, s_9) & C_6^\bullet &= V(x_6, s_9) & C_7^\bullet &= V(x_7, s_9) \\ C_8^\bullet &= V(x_8, s_9) & C_9^\bullet &= V(x_9, s_9) & C_{13}^\bullet &= V(x_{13}, s_9) & C_{14}^\bullet &= V(x_{14}, s_9) \\ C_{16}^\bullet &= V(x_{16}, s_9) & C_{17}^\bullet &= V(x_{17}, s_9) & C_{21}^\bullet &= V(x_{21}, s_9) & C_{25}^\bullet &= V(x_{25}, s_9) \\ C_{27}^\bullet &= V(x_{27}, s_9) & & & & & & \end{aligned} \quad (144)$$

In addition, $C_{24}^\bullet = V(x_{24}, s_9)$ and $C_{28}^\bullet = V(x_{28}, s_9)$ are reducible (cf. [51] and references therein):

$$C_{24}^\bullet = V(x_{24}, s_9) = C_{24,0}^\bullet \cup C_{24,1}^\bullet, \quad C_{28}^\bullet = V(x_{28}, s_9) = C_{28,0}^\bullet \cup C_{28,1}^\bullet. \quad (145)$$

We now wish to identify the dual graph and the location of the intersection points of the components of C^\bullet . In order to analyze $C_{24}^\bullet, C_{28}^\bullet$ efficiently, we employ the simplifying assumption

$$\alpha_4 \neq 0. \quad (146)$$

We will see momentarily, that this allows to express $C_{24,0}^\bullet, C_{24,1}^\bullet, C_{28,0}^\bullet, C_{28,1}^\bullet$ in terms of

$$\tilde{\alpha}_1 = \frac{\alpha_2 + \sqrt{\alpha_2^2 - 4\alpha_1\alpha_4}}{2\alpha_4}, \quad \tilde{\alpha}_3 = \frac{\alpha_2 - \sqrt{\alpha_2^2 - 4\alpha_1\alpha_4}}{2\alpha_4}. \quad (147)$$

With that said, we will now discuss various vanishing sets and their intersections. Eventually, we wish to identify homogeneous coordinates of $C_0^\bullet, C_1^\bullet, C_2^\bullet, C_3^\bullet$.

Details of C_{24}^\bullet and C_{28}^\bullet

Recall that $C_{24}^\bullet = V(x_{24}, s_9)$. By recalling $I_1 + I_2 + I_3 + I_4 + I_5 + I_6 \subseteq I_{\text{SR}}(X_\Sigma)$, we note that $x_1, x_4, x_5, x_6, x_7, x_8, x_{10}, x_{11}, x_{12}, x_{15}, x_{17}, x_{18}, x_{19}, x_{20}, x_{21}, x_{26}$ cannot vanish on C_{24}^\bullet . Let us set these variables temporarily to 1. Then we see

$$C_{24}^\bullet = V(x_{24}, \alpha_1 z_1^2 + \alpha_2 z_1 z_2 + \alpha_4 z_2^2), \quad z_1 = x_0^3 x_9^2 x_{14} x_{22} x_{25}, \quad z_2 = x_3^3 x_{13}^2 x_{16} x_{23} x_{27}. \quad (148)$$

Provided that $\alpha_4 \neq 0$ – this is where we use our simplifying assumption – we can write

$$\begin{aligned} \alpha_1 z_1^2 + \alpha_2 z_1 z_2 + \alpha_4 z_2^2 &= \alpha_4 \cdot \left(z_2 + \frac{\alpha_2 + \sqrt{\alpha_2^2 - 4\alpha_1\alpha_4}}{2\alpha_4} \cdot z_1 \right) \\ &\quad \times \left(z_2 + \frac{\alpha_2 - \sqrt{\alpha_2^2 - 4\alpha_1\alpha_4}}{2\alpha_4} \cdot z_1 \right) \\ &= (z_2 + \tilde{\alpha}_1 z_1)(z_2 + \tilde{\alpha}_3 z_1). \end{aligned} \quad (149)$$

We use this result to identify the two irreducible components of C_{24}^\bullet . To express these components economically and homogeneously, we define

$$d_1 = x_0^3 x_4^2 x_5 x_9^2 x_{10} x_{17}^2 x_{18} x_{22} x_{25}, \quad d_2 = x_3^3 x_7 x_8^2 x_{12} x_{13}^2 x_{20} x_{21}^2 x_{23} x_{27}. \quad (150)$$

By taking into account that $I_1 + I_2 + I_3 + I_4 + I_5 + I_6 \subseteq I_{\text{SR}}(X_\Sigma)$ and that $V(z, s) = \emptyset$ for all $z \in I_7$ it then follows that $d_1, d_2 \neq 0$ on C_{24}^\bullet . We set

$$S_{24} = \{0, 1, 2, 3, \dots, 28\} \setminus \{x_2, x_{14}, x_{16}, x_{24}, x_{28}\}. \quad (151)$$

Then we have $C_{24}^\bullet = C_{24,0}^\bullet \cup C_{24,1}^\bullet$ and

$$C_{24,0}^\bullet = \left\{ x \in X_\Sigma \left| x_{24} = 0, x_{16} = -\tilde{\alpha}_1 \cdot \frac{d_1 x_{14}}{d_2}, x_i \neq 0 \forall i \in S_{24} \right. \right\}, \quad (152)$$

$$C_{24,1}^\bullet = \left\{ x \in X_\Sigma \left| x_{24} = 0, x_{16} = -\tilde{\alpha}_3 \cdot \frac{d_1 x_{14}}{d_2}, x_i \neq 0 \forall i \in S_{24} \right. \right\}. \quad (153)$$

Notice that $x_2 x_{28} \in I_1$, so that $C_{24,0}^\bullet, C_{24,1}^\bullet \cong \mathbb{P}_{[x_2: x_{28}]}^1$. Similarly, we set

$$S_{28} = \{0, 1, 2, 3, \dots, 28\} \setminus \{x_1, x_{14}, x_{16}, x_{24}, x_{28}\}. \quad (154)$$

Then we have $C_{28}^\bullet = C_{28,0}^\bullet \cup C_{28,1}^\bullet$ and

$$C_{28,0}^\bullet = \left\{ x \in X_\Sigma \left| x_{28} = 0, x_{16} = -\tilde{\alpha}_1 \cdot \frac{d_1 x_{14}}{d_2}, x_i \neq 0 \forall i \in S_{28} \right. \right\}, \quad (155)$$

$$C_{28,1}^\bullet = \left\{ x \in X_\Sigma \left| x_{28} = 0, x_{16} = -\tilde{\alpha}_3 \cdot \frac{d_1 x_{14}}{d_2}, x_i \neq 0 \forall i \in S_{28} \right. \right\}. \quad (156)$$

Notice that $x_1 x_{24} \in I_1$, so that $C_{28,0}^\bullet, C_{28,1}^\bullet \cong \mathbb{P}_{[x_1: x_{24}]}^1$. We can now look at the intersection of $C_{24,0}^\bullet$ and $C_{28,1}^\bullet$. If we write this non-homogeneous, then

$$C_{24,0}^\bullet \cap C_{28,1}^\bullet = V(x_{24}, x_{28}, x_{16} = -\tilde{\alpha}_1 = -\tilde{\alpha}_3). \quad (157)$$

This has a solution iff $\tilde{\alpha}_1 = \tilde{\alpha}_3$. By use of Equation (147), we can see that this is equivalent to

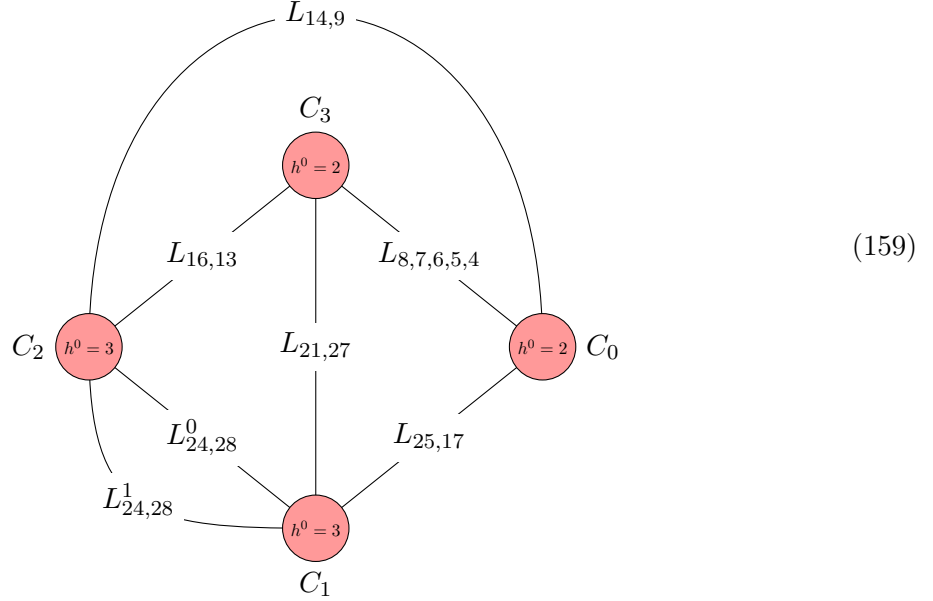
$$0 = \sqrt{\alpha_2^2 - 4\alpha_1\alpha_4}. \quad (158)$$

Hence, as long as we ensure $\alpha_2^2 \neq 4\alpha_1\alpha_4$, we have $C_{24,0}^\bullet \cap C_{28,1}^\bullet = \emptyset$. Similarly, this condition ensures $C_{24,1}^\bullet \cap C_{28,0}^\bullet = \emptyset$. At the same time, it then follows that $C_{24,0}^\bullet \cap C_{28,0}^\bullet$ and $C_{24,1}^\bullet \cap C_{28,1}^\bullet$ are both non-empty and consist of exactly one point.

Simplifying the nodal curve by removing chains

By repeating this exercise, it is not too hard to verify that the dual graph of C^\bullet is given in Equation (159). Here, L_{i_1, \dots, i_k} represents a chain of k genus zero curves C_{i_j} such that C_{i_j} and $C_{i_{j+1}}$ intersect each other at a single node. As a dual graph, L_{i_1, \dots, i_k} is a string of red vertices. The chain is ordered so that C_{i_1} intersects the \mathbb{P}^1 on the left and C_{i_k} intersects the \mathbb{P}^1 on the

right. For $L_{21,27}$, we have that C_{21} intersects C_3 while C_{27} intersects C_1 .



As argued in [51] and Section 2.5, we can simplify the counting task by looking at a simplified nodal curve. The dual graph of this simplified curve is obtained by replacing each of the chains T_{ij} in Equation (159) by a single edge. This leads to a nodal curve with components $C_0^\bullet, C_1^\bullet, C_2^\bullet, C_3^\bullet$ whose dual graph is exactly the jumping circuit in Equation (126). The position of the nodes on this simplified nodal curve are as follows:

Label	Superset	Coordinates in first curve	Coordinates in second curve
n_1	$C_0^\bullet \cap C_1^\bullet$	$V(x_0, x_{17}, s)$	$V(x_1, x_{25}, s)$
n_2	$C_0^\bullet \cap C_2^\bullet$	$V(x_0, x_9, s)$	$V(x_2, x_{14}, s)$
n_3	$C_0^\bullet \cap C_3^\bullet$	$V(x_0, x_4, s)$	$V(x_3, x_8, s)$
n_4	$C_1^\bullet \cap C_2^\bullet$	$C_{28,0}^\bullet \cap C_1^\bullet$	$C_{24,0}^\bullet \cap C_2^\bullet$
n_5	$C_1^\bullet \cap C_2^\bullet$	$C_{28,1}^\bullet \cap C_1^\bullet$	$C_{24,1}^\bullet \cap C_2^\bullet$
n_6	$C_1^\bullet \cap C_3^\bullet$	$V(x_1, x_{27}, s)$	$V(x_3, x_{21}, s)$
n_7	$C_2^\bullet \cap C_3^\bullet$	$V(x_2, x_{16}, s)$	$V(x_3, x_{13}, s)$

(160)

D.4. The location of the nodes

Nodes on C_0^\bullet

Recall that $C_0^\bullet = V(x_0, s)$. We define

$$\begin{aligned}
 g_1 &= x_5^2 x_6^3 x_7^4 x_8^5 x_3^6 x_{10} x_{11}^2 x_{12}^3 x_{13}^4 x_{15} x_{16}^2 x_{18} x_{19}^2 x_{20}^3 x_{21}^4 x_{23} x_{26} x_{27}^2, \\
 g_2 &= x_{10} x_{11} x_{12} x_{13} x_{14}^2 x_{15}^2 x_{16}^2 x_2^3 x_{22} x_{24}^2 x_{28}, \\
 g_3 &= x_1^3 x_{18} x_{19} x_{20} x_{21} x_{22} x_{24}^2 x_{25}^2 x_{26}^2 x_{27}^2 x_{28}.
 \end{aligned}$$

(161)

By use of $I_1 + I_2 + I_3 + I_4 + I_5 + I_6 \subseteq I_{\text{SR}}(X_\Sigma)$ and that $V(z, s) = \emptyset$ for all $z \in I_7$, it follows that $g_1, g_2, g_3 \neq 0$ on C_0^\bullet and that we can write

$$C_0^\bullet = V\left(x_0, \alpha_4 \left(\frac{g_1 x_4}{g_3}\right) + \alpha_5 \left(\frac{g_2 x_9}{g_3}\right) + \alpha_6 x_{17}\right), \quad (162)$$

$$1 \cong (0, \dots, 0, 1, 0, \dots, 0) = w\left(\frac{g_1 x_4}{g_3}\right) = w\left(\frac{g_2 x_9}{g_3}\right) = w(x_{17}). \quad (163)$$

Since $x_4 x_9 x_{17} \in I_6 \subseteq I_{\text{SR}}(X_\Sigma)$, we can consider C_0^\bullet as hypersurface in $\mathbb{P}_{[x_4:x_9:x_{17}]}^2$. In particular, the following map is well-defined

$$\varphi: \mathbb{P}_{[u:v]}^1 \rightarrow C_0^\bullet, [u:v] \mapsto \left[\frac{g_1 x_4}{g_3} = u : \frac{g_2 x_9}{g_3} = v : x_{17} = -\frac{\alpha_4 u + \alpha_5 v}{\alpha_6}\right]. \quad (164)$$

This establishes $C_0^\bullet \cong \mathbb{P}_{[u:v]}^1$ with $\left[\frac{g_1 x_4}{g_3} : \frac{g_2 x_9}{g_3}\right] = [u_0 : v_0]$ as homogeneous coordinates of C_0^\bullet . In terms of $[u_0 : v_0]$, the locations of the nodes on C adjacent to C_0^\bullet are as follows:

$$n_1 = \left[1 : -\frac{\alpha_4}{\alpha_5}\right], \quad n_2 = [1 : 0], \quad n_3 = [0 : 1]. \quad (165)$$

We want to emphasize that it is important to represent the node n_1 as $\left[1 : -\frac{\alpha_4}{\alpha_5}\right]$ for the computation of the global sections. To see this, recall that we are looking at the nodal curve

$$C^\bullet = V\left(\prod_{i=1}^{28} x_i, s_9\right). \quad (166)$$

Apparently, this curve remains the same if we replace s_9 by $\lambda \cdot s_9$, where $\lambda \in \mathbb{C}^*$ is arbitrary but fixed. Consequently, the location of the nodes must remain unchanged upon rescaling the coefficients α_i of s_9 , i.e. upon

$$\alpha_i \rightarrow \lambda \cdot \alpha_i, \quad \lambda \in \mathbb{C}^*. \quad (167)$$

This scale invariance must also be true for the number of global sections on C^\bullet , which we will eventually compute from the right nullspace of a \mathbb{C} -valued matrix. To “inform“ this matrix about the scale invariance, it is imperative to use the complex numbers 1 and $-\frac{\alpha_4}{\alpha_5}$ (or 1 and $-\frac{\alpha_5}{\alpha_4}$) as coordinates for the node n_1 .

Nodes on C_1^\bullet

We define

$$\begin{aligned} g_4 &= x_0^6 x_4^5 x_5^4 x_6^3 x_7^2 x_8 x_9^4 x_{10}^2 x_{11} x_{14}^2 x_{17}^4 x_{18}^3 x_{19}^2 x_{20} x_{22}^2, \\ g_5 &= x_0^3 x_4^3 x_5^3 x_6^3 x_7^3 x_8^3 x_9^2 x_{10} x_{11} x_{12} x_{13}^2 x_{14} x_{16} x_{17}^2 x_{18}^2 x_{19}^2 x_{20}^2 x_{21}^2 x_{22} x_{23} x_3^3, \\ g_6 &= x_4 x_5^2 x_6^3 x_7^4 x_8^5 x_{11} x_{12}^2 x_{13}^4 x_{16}^2 x_{18} x_{19}^3 x_{20}^4 x_{21}^2 x_{23}^6, \\ g_7 &= x_2^3 x_9 x_{13} x_{14}^2 x_{15} x_{16}^2 x_{22} x_{23} x_{24}^2. \end{aligned} \quad (168)$$

By use of $I_1 + I_2 + I_3 + I_4 + I_5 + I_6 \subseteq I_{\text{SR}}(X_\Sigma)$ and that $V(z, s) = \emptyset$ for all $z \in I_7$, it follows that $g_4, g_5, g_6, g_7 \neq 0$ on C_1^\bullet and that we can write

$$C_1^\bullet = V\left(x_1, \alpha_1 x_{25}^2 + \alpha_2 x_{25} \cdot \frac{g_5 \cdot x_{27}}{g_4} + \alpha_4 \cdot \frac{g_6 x_{27}^2}{g_4} + \alpha_5 \cdot \frac{g_7 x_{28}}{g_4 x_{26}}\right). \quad (169)$$

An explicit computation shows that $g_4g_6 - g_5^2 = 0$. Consequently,

$$C_1^\bullet = V \left(x_1, \alpha_1 x_{25}^2 + \alpha_2 x_{25} \cdot \frac{g_5 \cdot x_{27}}{g_4} + \alpha_4 \cdot \left(\frac{g_5 \cdot x_{27}}{g_4} \right)^2 + \alpha_5 \cdot \frac{g_7 x_{28}}{g_4 x_{26}} \right). \quad (170)$$

We notice that

$$w(x_{25}) = w \left(\frac{g_5 x_{27}}{g_4} \right) = w \left(\frac{g_7 x_{28}}{g_4 x_{26}} \right) = (0, \dots, 0, 1, 0, \dots, 0) \cong 1. \quad (171)$$

Also $x_{25}x_{27} \in I_2$. Therefore, the following map is well-defined:

$$\varphi: \mathbb{P}_{[u:v]}^1 \rightarrow C_1^\bullet, [u:v] \mapsto \left[x_{25} = u : \frac{g_5 x_{27}}{g_4} = v : \frac{g_7 x_{28}}{g_4 x_{26}} = -\frac{\alpha_1 u^2 + \alpha_2 uv + \alpha_4 v^2}{\alpha_5} \right]. \quad (172)$$

This establishes $C_1^\bullet \cong \mathbb{P}_{[u:v]}^1$ and allows us to pick $[x_{25} : \frac{g_5 x_{27}}{g_4}] \equiv [u_1 : v_1]$ as its homogeneous coordinates. In terms of these coordinates, the location of the nodes n_1, n_4, n_5, n_6 are:

Node	Coordinates on C_1^\bullet	
n_1	$[0 : 1]$	
n_4	$[1 : -\widetilde{\alpha}_1] = \left[1 : \frac{-\alpha_2 - \sqrt{\alpha_2^2 - 4\alpha_1\alpha_4}}{2\alpha_4} \right]$	(173)
n_5	$[1 : -\widetilde{\alpha}_3] = \left[1 : \frac{\alpha_2 - \sqrt{\alpha_2^2 - 4\alpha_1\alpha_4}}{2\alpha_4} \right]$	
n_6	$[1 : 0]$	

Nodes on C_2^\bullet

We define

$$\begin{aligned} g_8 &= x_0^6 x_4^5 x_5^4 x_6^3 x_7^2 x_8 x_9^4 x_{10}^3 x_{11}^2 x_{12} x_{17}^4 x_{18}^2 x_{19} x_{22}^2 x_{25}^2, \\ g_9 &= x_0^3 x_3^3 x_4^3 x_5^3 x_6^3 x_7^3 x_8^3 x_9^2 x_{10}^2 x_{11}^2 x_{12}^2 x_{13}^2 x_{17}^2 x_{18} x_{19} x_{20} x_{21}^2 x_{22} x_{23} x_{25} x_{27}, \\ g_{10} &= x_3^6 x_4 x_5^2 x_6^3 x_7^4 x_8^5 x_{10} x_{11}^2 x_{12}^3 x_{13}^4 x_{19} x_{20}^4 x_{21}^2 x_{23}^2 x_{27}^2, \\ g_{11} &= x_1^3 x_{17} x_{21} x_{22} x_{23} x_{25}^2 x_{26} x_{27}^2 x_{28}^2. \end{aligned} \quad (174)$$

By use of $I_1 + I_2 + I_3 + I_4 + I_5 + I_6 \subseteq I_{\text{SR}}(X_\Sigma)$ and that $V(z, s) = \emptyset$ for all $z \in I_7$, it follows that $g_8, g_9, g_{10}, g_{11} \neq 0$ on C_2^\bullet and that we can write

$$C_2^\bullet = V \left(x_2, \alpha_1 x_{14}^2 + \alpha_2 \cdot x_{14} \cdot \frac{g_9 x_{16}}{g_8} + \alpha_4 \cdot \frac{g_{10} x_{16}^2}{g_8} + \alpha_6 \cdot \frac{g_{11} x_{24}}{g_8 x_{15}} \right). \quad (175)$$

An explicit computation shows that $g_8 g_{10} - g_9^2 = 0$. Hence, we have

$$C_2^\bullet = V \left(x_2, \alpha_1 x_{14}^2 + \alpha_2 \cdot x_{14} \cdot \frac{g_9 x_{16}}{g_8} + \alpha_4 \cdot \left(\frac{g_9 x_{16}}{g_8} \right)^2 + \alpha_6 \cdot \frac{g_{11} x_{24}}{g_8 x_{15}} \right). \quad (176)$$

We notice that

$$w(x_{14}) = w \left(\frac{g_9 x_{16}}{g_8} \right) = w \left(\frac{g_{11} x_{24}}{g_8 x_{15}} \right) = (0, \dots, 0, 1, 0, \dots, 0) \cong 1. \quad (177)$$

Notice that $x_{14}x_{16} \in I_3$. Therefore, the following map is well-defined:

$$\varphi: \mathbb{P}_{[u:v]}^1 \rightarrow C_2^\bullet, [u : v] \mapsto \left[x_{14} = u : \frac{g_9 x_{16}}{g_8} = v : \frac{x_{24}}{x_{15}} = -\frac{\alpha_1 u^2 + \alpha_2 uv + \alpha_4 v^2}{\alpha_6} \right]. \quad (178)$$

This establishes $C_2^\bullet \cong \mathbb{P}_{[u:v]}^1$ and allows us to pick $[x_{14} : \frac{g_9 x_{16}}{g_8}] \equiv [u_2 : v_2]$ as its homogeneous coordinates. In terms of these coordinates, the location of the nodes n_2, n_4, n_5 and n_7 are:

Node	Coordinates on C_2^\bullet	
n_2	$[0 : 1]$	
n_4	$[1 : -\widetilde{\alpha}_1] = \left[1 : \frac{-\alpha_2 - \sqrt{\alpha_2^2 - 4\alpha_1\alpha_4}}{2\alpha_4} \right]$	(179)
n_5	$[1 : -\widetilde{\alpha}_3] = \left[1 : \frac{\alpha_2 - \sqrt{\alpha_2^2 - 4\alpha_1\alpha_4}}{2\alpha_4} \right]$	
n_7	$[1 : 0]$	

Nodes on C_3^\bullet

We first define

$$\begin{aligned} g_{12} &= x_0^6 x_4^5 x_5^4 x_6^3 x_7^2 x_9^4 x_{10}^3 x_{11}^2 x_{12} x_{14}^2 x_{15} x_{17}^4 x_{18}^3 x_{19}^2 x_{20} x_{22}^2 x_{25}^2 x_{26}, \\ g_{13} &= x_9 x_{10} x_{11} x_{12} x_{14}^2 x_{15}^2 x_{16}^2 x_{22}^2 x_{23} x_{24}^2 x_{28}, \\ g_{14} &= x_1^3 x_{17} x_{18} x_{19} x_{20} x_{22} x_{23} x_{24} x_{25}^2 x_{26}^2 x_{27}^2 x_{28}^2. \end{aligned} \quad (180)$$

By use of $I_1 + I_2 + I_3 + I_4 + I_5 + I_6 \subseteq I_{\text{SR}}(X_\Sigma)$ and that $V(z, s) = \emptyset$ for all $z \in I_7$, it follows that $g_{12}, g_{13}, g_{14} \neq 0$ on C_3^\bullet and that we can write

$$C_3^\bullet = V \left(x_3, \alpha_1 \cdot \frac{g_{12} x_8}{g_{14}} + \alpha_5 \cdot \frac{g_{13} x_{13}}{g_{14}} + \alpha_6 \cdot x_{21} \right), \quad (181)$$

$$w \left(\frac{g_{12} x_8}{g_{14}} \right) = w \left(\frac{g_{13} x_{13}}{g_{14}} \right) = w(x_{21}) = (0, \dots, 0, 1, 0, \dots, 0) \cong 1. \quad (182)$$

Since $x_8 x_{13} x_{21} \in I_6$, we can think of C_3^\bullet as hypersurface in $\mathbb{P}_{[x_8 : x_{13} : x_{21}]}^2$. Alternatively, the following map is well-defined:

$$\varphi: \mathbb{P}_{[u:v]}^1 \rightarrow C_3^\bullet, [u : v] \mapsto \left[\frac{g_{12} x_8}{g_{14}} = u : \frac{g_{13} x_{13}}{g_{14}} = v : x_{21} = -\frac{\alpha_1 u + \alpha_5 v}{\alpha_6} \right]. \quad (183)$$

This establishes $C_3^\bullet \cong \mathbb{P}_{[u:v]}^1$ and identifies $[\frac{g_{12} x_8}{g_{14}} : \frac{g_{13} x_{13}}{g_{14}}] = [u_3 : v_3]$ as its homogeneous coordinates. The locations of the nodes are

$$n_3 = [0 : 1], \quad n_6 = \left[1 : -\frac{\alpha_1}{\alpha_5} \right], \quad n_7 = [1 : 0]. \quad (184)$$

References

- [1] P. Candelas and Gary T. Horowitz and Andrew Strominger and Edward Witten, *Vacuum configurations for superstrings*, *Nuclear Physics B* **258** (1985) 46–74. 3
- [2] Brian R. Greene and Kelley H. Kirklín and Paul J. Miron and Graham G. Ross, *A superstring-inspired standard model*, *Physics Letters B* **180** (1986) 69–76. 3

- [3] Braun, Volker and He, Yang-Hui and Ovrut, Burt A. and Pantev, Tony, *A heterotic standard model*, *Physics Letters B* **618** (Jul, 2005) 252–258. 3
- [4] Bouchard, Vincent and Donagi, Ron, *An $SU(5)$ heterotic standard model*, *Physics Letters B* **633** (Feb, 2006) 783–791. 3
- [5] Bouchard, Vincent and Cvetič, Mirjam and Donagi, Ron, *Tri-linear couplings in an heterotic minimal supersymmetric Standard Model*, *Nuclear Physics B* **745** (Jun, 2006) 62–83. 3
- [6] L. B. Anderson, J. Gray, Y.-H. He and A. Lukas, *Exploring Positive Monad Bundles And A New Heterotic Standard Model*, *JHEP* **02** (2010) 054, [0911.1569]. 3
- [7] L. B. Anderson, J. Gray, A. Lukas and E. Palti, *Two Hundred Heterotic Standard Models on Smooth Calabi-Yau Threefolds*, *Phys. Rev.* **D84** (2011) 106005, [1106.4804]. 3
- [8] L. B. Anderson, J. Gray, A. Lukas and E. Palti, *Heterotic line bundle standard models*, *Journal of High Energy Physics* **2012** (Jun, 2012) . 3
- [9] M. Berkooz, M. R. Douglas and R. G. Leigh, *Branes intersecting at angles*, *Nuclear Physics B* **480** (Nov, 1996) 265–278. 3
- [10] G. Aldazabal, S. Franco, L. E. Ibáñez, R. Rabadan and A. M. Uranga, *$D=4$ chiral string compactifications from intersecting branes*, *Journal of Mathematical Physics* **42** (Jul, 2001) 3103–3126. 3
- [11] G. Aldazabal, S. Franco, L. E. Ibáñez, R. Rabadan and A. M. Uranga, *Intersecting brane worlds*, *JHEP* **02** (2001) 047, [hep-ph/0011132]. 3
- [12] L. E. Ibáñez, F. Marchesano and R. Rabadan, *Getting just the standard model at intersecting branes*, *Journal of High Energy Physics* **2001** (Nov, 2001) 002–002. 3
- [13] R. Blumenhagen, B. Kors, D. Lüst and T. Ott, *The Standard Model from stable intersecting brane world orbifolds*, *Nuclear Physics B* **616** (Nov, 2001) 3–33. 3
- [14] Cvetič, Mirjam and Shiu, Gary and Uranga, Angel M., *Three family supersymmetric standard - like models from intersecting brane worlds*, *Phys. Rev. Lett.* **87** (2001) 201801, [hep-th/0107143]. 3
- [15] M. Cvetič, G. Shiu and A. M. Uranga, *Chiral four-dimensional $N=1$ supersymmetric type IIA orientifolds from intersecting $D6$ -branes*, *Nuclear Physics B* **615** (Nov, 2001) 3–32. 3
- [16] R. Blumenhagen, M. Cvetič, P. Langacker and G. Shiu, *Toward realistic intersecting D -brane models*, *Annual Review of Nuclear and Particle Science* **55** (Dec, 2005) 71–139. 3
- [17] Gómez, Tomás L. and Lukic, Sergio and Sols, Ignacio, *Constraining the Kähler Moduli in the Heterotic Standard Model*, *Communications in Mathematical Physics* **276** (Sep, 2007) 1–21. 3
- [18] V. Bouchard and R. Donagi, *On heterotic model constraints*, *Journal of High Energy Physics* **2008** (Aug, 2008) 060–060. 3
- [19] Vafa, Cumrun, *Evidence for F -theory*, *Nuclear Physics B* **469** (Jun, 1996) 403–415. 3

- [20] Morrison, David R. and Vafa, Cumrun, *Compactifications of F-theory on Calabi-Yau threefolds (II)*, *Nuclear Physics B* **476** (Sep, 1996) 437–469. 3
- [21] Morrison, David R. and Vafa, Cumrun, *Compactifications of F-theory on Calabi-Yau threefolds. (I)*, *Nuclear Physics B* **473** (Aug, 1996) 74–92. 3
- [22] M. Cvetič, J. Halverson, G. Shiu and W. Taylor, *Snowmass White Paper: String Theory and Particle Physics*, 2204.01742. 3
- [23] T. W. Grimm and H. Hayashi, *F-theory fluxes, chirality and Chern-Simons theories*, *Journal of High Energy Physics* **2012** (Mar, 2012) . 3
- [24] S. Krause, C. Mayrhofer and T. Weigand, *Gauge Fluxes in F-theory and Type IIB Orientifolds*, *Journal of High Energy Physics* **2012** (Aug, 2012) . 3
- [25] Braun, Volker and Grimm, Thomas W. and Keitel, Jan, *Geometric Engineering in Toric F-Theory and GUTs with U(1) Gauge Factors*, *JHEP* **12** (2013) 069, [1306.0577]. 3
- [26] M. Cvetič, A. Grassi, D. Klevers and H. Piragua, *Chiral four-dimensional F-theory compactifications with SU(5) and multiple U(1)-factors*, *JHEP* **04** (2014) 010, [1306.3987]. 3
- [27] M. Cvetič, D. Klevers, D. K. M. Peña, P.-K. Oehlmann and J. Reuter, *Three-Family Particle Physics Models from Global F-theory Compactifications*, *JHEP* **08** (2015) 087, [1503.02068]. 3
- [28] L. Lin, C. Mayrhofer, O. Till and T. Weigand, *Fluxes in F-theory Compactifications on Genus-One Fibrations*, *JHEP* **01** (2016) 098, [1508.00162]. 3
- [29] L. Lin and T. Weigand, *G₄-flux and standard model vacua in F-theory*, *Nuclear Physics B* **913** (Dec, 2016) 209–247. 3
- [30] Krause, Sven and Mayrhofer, Christoph and Weigand, Timo, *G₄-flux, chiral matter and singularity resolution in F-theory compactifications*, *Nuclear Physics B* **858** (May, 2012) 1–47. 3
- [31] M. Cvetič, L. Lin, M. Liu and P.-K. Oehlmann, *An F-theory Realization of the Chiral MSSM with Z₂-Parity*, *JHEP* **09** (2018) 089, [1807.01320]. 3
- [32] M. Cvetič, J. Halverson, L. Lin, M. Liu and J. Tian, *Quadrillion F-Theory Compactifications with the Exact Chiral Spectrum of the Standard Model*, *Phys. Rev. Lett.* **123** (2019) 101601, [1903.00009]. 3, 4, 7, 8, 9, 32, 36, 54
- [33] Bies, Martin and Mayrhofer, Christoph and Pehle, Christian and Weigand, Timo, *Chow groups, Deligne cohomology and massless matter in F-theory*, 1402.5144. 3, 4, 7
- [34] M. Bies, C. Mayrhofer and T. Weigand, *Gauge Backgrounds and Zero-Mode Counting in F-Theory*, *JHEP* **11** (2017) 081, [1706.04616]. 3, 4, 7
- [35] M. Bies, *Cohomologies of coherent sheaves and massless spectra in F-theory*. PhD thesis, Heidelberg U., 2, 2018. 1802.08860. 10.11588/heidok.00024045. 3, 4, 7

- [36] The Toric Varieties project authors, “The `ToricVarieties` project.”
https://github.com/homalg-project/ToricVarieties_project, 2019–2022.
 4, 6, 22, 34
- [37] D. R. Grayson and M. E. Stillman, “Macaulay2, a software system for research in algebraic geometry.” <http://www.math.uiuc.edu/Macaulay2/>. 4
- [38] The Sage Developers, “Sagemath, the Sage Mathematics Software System (Version 8.5).”
<http://www.sagemath.org>, 2018. 4
- [39] J. Carifio, J. Halverson, D. Krioukov and B. D. Nelson, *Machine Learning in the String Landscape*, *Journal of High Energy Physics* **09** (2017) 157. 4
- [40] J. Halverson, B. Nelson and F. Ruehle, *Branes with Brains: Exploring String Vacua with Deep Reinforcement Learning*, *Journal of High Energy Physics* **06** (2019) 003. 4
- [41] S. Abel, A. Constantin, T. R. Harvey and A. Lukas, *String Model Building, Reinforcement Learning and Genetic Algorithms*, in *Nankai Symposium on Mathematical Dialogues: In celebration of S.S.Chern’s 110th anniversary*, 11, 2021. 2111.07333. 4
- [42] F. Ruehle, *Data science applications to string theory*, *Phys. Rept.* **839** (2020) 1–117. 4
- [43] M. Bies, M. Cvetič, R. Donagi, L. Lin, M. Liu and F. Ruehle, *Machine Learning and Algebraic Approaches towards Complete Matter Spectra in 4d F-theory*, *JHEP* **01** (2021) 196, [2007.00009]. 4
- [44] M. Bies, M. Cvetič, R. Donagi, L. Lin, M. Liu and F. Ruehle, “Database.”
<https://github.com/Learning-line-bundle-cohomology>, 2020. 4
- [45] Brill, Alexander and Noether, Max, *Ueber die algebraischen Functionen und ihre Anwendung in der Geometrie*, *Mathematische Annalen* **7** (1874) 269–310. 4
- [46] D. Eisenbud, M. Green and J. Harris, *Cayley-Bacharach theorems and conjectures*, *Bulletin of the American Mathematical Society* **33** (jul, 1996) 295–325. 4
- [47] Watari, Taizan, *Vector-like pairs and Brill–Noether theory*, *Physics Letters B* **762** (Nov, 2016) 145–150. 4
- [48] P. Jefferson, W. Taylor and A. P. Turner, *Chiral matter multiplicities and resolution-independent structure in 4D F-theory models*, 2108.07810. 4, 7
- [49] M. Bies, M. Cvetič, R. Donagi, M. Liu and M. Ong, *Root bundles and towards exact matter spectra of F-theory MSSMs*, *JHEP* **09** (2021) 076, [2102.10115]. 4, 5, 6, 8, 9, 11, 12, 31, 32, 33, 35, 54
- [50] Lucia Caporaso and Cinzia Casagrande and Maurizio Cornalba, *Moduli of Roots of Line Bundles on Curves*, *Transactions of the American Mathematical Society* **359** (2007) 3733–3768. 5, 6, 8, 11, 12, 19, 20, 21, 22, 26, 28, 33, 34
- [51] M. Bies, M. Cvetič and M. Liu, *Statistics of limit root bundles relevant for exact matter spectra of F-theory MSSMs*, *Phys. Rev. D* **104** (2021) L061903, [2104.08297]. 5, 6, 8, 9, 10, 11, 12, 21, 23, 33, 34, 54, 60, 61, 63

- [52] M. Kreuzer and H. Skarke, *Classification of reflexive polyhedra in three-dimensions*, *Adv. Theor. Math. Phys.* **2** (1998) 853–871. 5, 6, 9, 11, 25, 32, 54
- [53] J. Halverson and J. Tian, *Cost of seven-brane gauge symmetry in a quadrillion F-theory compactifications*, *Phys. Rev. D* **95** (2017) 026005, [1610.08864]. 5, 11, 54, 57, 58
- [54] V. V. Batyrev, *Dual polyhedra and mirror symmetry for Calabi-Yau hypersurfaces in toric varieties*, *J. Alg. Geom.* **3** (1994) 493–545. 5, 9, 10
- [55] E. Pervvalov and H. Skarke, *Enhanced gauged symmetry in type II and F theory compactifications: Dynkin diagrams from polyhedra*, *Nuclear Physics B* **505** (Nov, 1997) 679–700. 5, 10
- [56] Cox, D.A. and Katz, S., *Mirror Symmetry and Algebraic Geometry*. Mathematical surveys and monographs. American Mathematical Society, 1999. 5, 9, 10
- [57] F. Rohsiepe, *Lattice polarized toric K3 surfaces*, hep-th/0409290. 5, 10
- [58] A. P. Braun, C. Long, L. McAllister, M. Stillman and B. Sung, *The Hodge Numbers of Divisors of Calabi-Yau Threefold Hypersurfaces*, 1712.04946. 5
- [59] E. Witten, *On flux quantization in M theory and the effective action*, *J. Geom. Phys.* **22** (1997) 1–13. 7
- [60] A. Collinucci and R. Savelli, *On Flux Quantization in F-Theory*, *Journal of High Energy Physics* **02** (2012) 015, [1011.6388]. 7
- [61] T. Weigand, *F-theory, PoS TASI2017* (2018) 016, [1806.01854]. 7
- [62] Jesús A. De Loera and Jörg Rambau and Francisco Santos, *Triangulations*. Graduate studies in mathematics. Springer, Heidelberg Dordrecht London New York, 2010, 10.1007/978-3-642-12971-1. 9, 54
- [63] D. Cox, J. Little and H. Schenck, *Toric Varieties*. Graduate studies in mathematics. American Mathematical Soc., 2011, 10.1090/gsm/124. 9
- [64] M. Kreuzer, *Toric geometry and Calabi-Yau compactifications*, *Ukr. J. Phys.* **55** (2010) 613–625. 10
- [65] Harris, J. and Morrison, I., *Moduli of Curves*. Graduate Texts in Mathematics. Springer New York, 2006. 26, 52
- [66] Rambau, Jörg, *TOPCOM: Triangulations of Point Configurations and Oriented Matroids*, *Proceedings of the International Congress of Mathematical Software* (2002) . 57
- [67] Jordan, Charles and Joswig, Michael and Kastner, Lars, *Parallel Enumeration of Triangulations*, *The Electronic Journal of Combinatorics* (2018) . 57
- [68] “OSCAR – Open Source Computer Algebra Research system, Version 0.8.0-DEV.” <https://oscar.computeralgebra.de>, 2022. 57
- [69] Eder, Christian and Decker, Wolfram and Fieker, Claus and Horn, Max and Joswig, Michael, ed., *The OSCAR book*. 2024. 57
- [70] Bezanson, Jeff and Edelman, Alan and Karpinski, Stefan and Shah, Viral B, *Julia: A fresh approach to numerical computing*, *SIAM Review* **59** (2017) 65–98. 57